



Q-SORT
is funded by the EU

Grant Agreement
no. 766970

Q-SORT/DIP
International Conference
on Electron Beam Shaping
in Space and Time

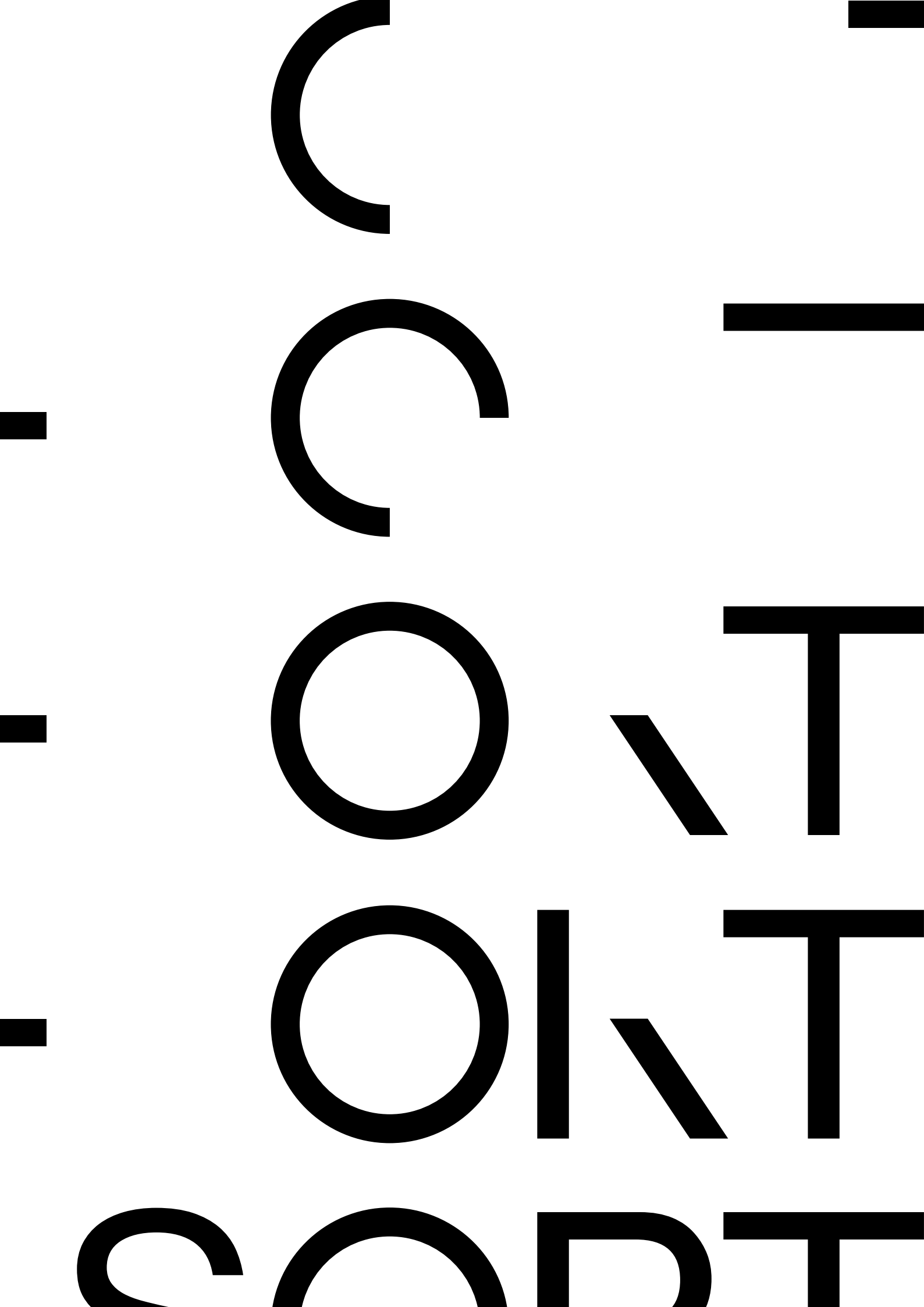
Sunday 27 – Wednesday 30
May 2018

Forschungszentrum Jülich
Germany

Table of contents

| | |
|--------------------------|-----|
| Conference programme | 7 |
| List of talk abstracts | 17 |
| Q-SORT Science Bash | 107 |
| List of poster abstracts | 111 |
| List of participants | 129 |

Conference programme



Sunday 27 May

PGI, Building 04.8, 1st Floor,
Room 142-143
Forschungszentrum Jülich
Wilhelm-Johnen-Strasse
52428 Jülich

15:00 – 15:15

Welcome

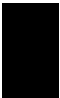
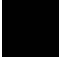

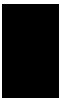
15:15 – 18:00










Pre-Conference Wikipedia Edit-a-Thon

Monday 28 May

Zentralbibliothek
(Building 04.7)
Forschungszentrum Jülich
Wilhelm-Johnen-Strasse
52428 Jülich

| | | |
|---------------|---|--|
| 08:30 – 09:30 | | Registration |
| 09:30 – 09:45 | | Welcome and Institutional Delegates |
| 09:45 – 10:45 |  | Session A. <i>Low Dose Methods</i> Chair: Rafal Dunin-Borkowski, Forschungszentrum Jülich (Germany) |
| 09:45 – 10:00 | A1 | <i>Low-dose cryo electron ptychography via non-convex Bayesian optimization</i> Philipp Pelz, Max Planck Institute (Germany) |
| 10:00 – 10:15 | A2 | <i>Production of arbitrary phase apertures for electron ptychography beams</i> Wouter Van den Broek, Humboldt University of Berlin (Germany) |
| 10:15 – 10:30 | A3 | <i>Next generation sample preparation for fully automated cryo-EM analysis of macromolecular structures and cells</i> Peter Peters, Maastricht University (The Netherlands) |
| 10:30 – 10:45 |  | Remote demonstration from the microscope |
| 10:45 – 11:15 |  | Coffee Break |
| 11:15 – 12:45 |  | Session B. <i>EMCD, Plasmons and Quantum Phenomena</i> Chair: Stefano Frabboni, University of Modena and Reggio Emilia (Italy) |
| 11:15 – 11:30 | B1 | <i>Measuring the phase and transverse fields of plasmonic excitations</i> Giulio Guzzinati, University of Antwerp (Belgium) |
| 11:30 – 11:45 | B2 | <i>Atomic scale imaging of magnetic circular dichroism by achromatic spatially-resolved electron energy-loss magnetic chiral dichroism</i> Xiaoyan Zhong, Tsinghua University (PRC) |
| 11:45 – 12:00 | B3 | <i>Theoretical study of the interaction between phase-shaped electrons and surface plasmon modes</i> Hugo Lourenço-Martins, University of Paris-Sud (France) |
| 12:00 – 12:15 | B4 | <i>Investigating the proximity of magnetic dichroic signal by atomic sized electron vortex and aberrated beam.</i> Devendra Negi, Uppsala University (Sweden) |
| 12:15 – 12:30 | B5 | <i>The cubic phase in quantum mechanics and hydrodynamics</i> Matthias Zimmermann, Ulm University (Germany) |

| | | |
|---------------|---|--|
| 12:30 – 12:45 | B6 | <i>The Cubic Phases of Wave packets in Linear Potential</i> Georgi Gary Rozenman, Tel Aviv University (Israel) |
| 12:45 – 13:45 |  | Lunch Break |
| 13:45 – 14:00 |  | Invited Speaker - Q-SORT Webinar Chair: Wolfgang Schleich, Ulm University (Germany) |
| 13:45 – 14:45 |  | <i>Low-damage multi-pass electron microscopy</i> Mark Kasevich, Stanford University (USA) |
| 14:45 – 16:00 |  | Session C. <i>QEM and quantum phenomena</i> Chair: Wolfgang Schleich, Ulm University (Germany) |
| 14:45 – 15:00 | C1 | <i>Optical multi-pass microscopy</i> Thomas Juffmann, University of Vienna (Austria) |
| 15:00 – 15:15 | C2 | <i>A 10keV Multi-Pass Electron Microscope</i> Stewart Koppell, Stanford University (USA) |
| 15:15 – 15:30 | C3 | <i>Aberration-Corrected Quantum Electron Microscopy</i> Marco Turchetti, Massachusetts Institute of Technology (USA) |
| 15:30 – 15:45 | C4 | <i>Simulated Quantum Electron Microscope Images</i> Yuri Van Staaden, Delft University of Technology (The Netherlands) |
| 15:45 – 16:00 | C5 | <i>A design for combining multi-pass and OAM sorter for dose effective magnetic measurements</i> Vincenzo Grillo, National Research Council (Italy) |
| 16:00 – 16:30 |  | Coffee Break |
| 16:30 – 18:15 |  | Round Table: <i>Quantum concepts in electron microscopy</i> Chair: Vincenzo Grillo, National Research Council (Italy) Special Seminar: Wolfgang Schleich, Ulm University (Germany) |
| 19:00 |  | Social Dinner Steakhaus El Toro, Große Rurstraße 34, 52428 Jülich |

Tuesday 29 May

Zentralbibliothek
(Building 04.7)
Forschungszentrum Jülich
Wilhelm-Johnen-Strasse
52428 Jülich

08:30 – 09:30

Registration

09:00 – 10:15



Session D. *UTEM-Time shaping*

Chair: Avraham Gover, Tel Aviv University (Israel)

09:00 – 09:15

D1 *Ultrafast Transmission Electron Microscopy with High-Coherence Electron Pulses*
Tyler Harvey, University of Göttingen (Germany)

09:15 – 09:30

D2 *meV Resolution in Laser-Assisted Energy-Filtered Transmission Electron Microscopy*
Enrico Pomarico, École polytechnique fédérale de Lausanne (Switzerland)

09:30 – 09:45

D3 *Temporal manipulation of sub-relativistic electron beams using light and matter*
Roy Shiloh, Friedrich-Alexander University (Germany)

09:45 – 10:00

D4 *Attosecond coherent control of a free-electron wave-function via semi-infinite light fields and plasmon polaritons*
Giovanni Maria Vanacore, École polytechnique fédérale de Lausanne (Switzerland)

10:00 – 10:15

D5 *The ultrafast and ultracold electron source*
Jim Franssen, Eindhoven University (The Netherlands)

10:15 – 10:45



Coffee Break

10:45 – 12:00



Session E. *Light-electron interaction*

Chair: Ido Kaminer, Technion – Israel Institute of Technology (Israel)

10:45 – 11:15

E1 *History-Dependent Radiative Interaction of Single Electron Quantum Wavepacket*
Avraham Gover, Tel Aviv University (Israel)

11:15 – 11:30

E2 *Tailoring the Spectral and Angular Response of Smith-Purcell Radiation*
Roei Remez, Tel Aviv University (Israel)

11:30 – 11:45

E3 *Spontaneous and Stimulated Radiative emission of modulated free-electron quantum wavepackets - QED Analysis*
Yiming Pan, Tel Aviv University (Israel)





11:45 – 12:00

E4 *Electron-light interaction in Wigner phase space*
Peter Kling, Ulm University (Germany)

12:00 – 13:30



Lunch Break

| | | |
|---------------|---|--|
| 13:15 – 14:15 |  | <p>Q-SORT Science Bash Schlosskapelle</p> <p>Gymnasium Zitadelle In der Zitadelle, 52428 Jülich</p> <p>Speaker: Peter Peters Title: <i>Beauty and benefits of nanobiology</i></p> |
| 13:30 – 14:45 |  | <p>Session F. <i>Phase plates and beam shaping</i> Chair: Ady Arie, Tel Aviv University (Israel)</p> |
| 13:30 – 13:45 | | <p>F1 <i>Experimental realization of a cylindrical quantum basis set for bandwidth-limited two dimensional electron wavefronts</i> Jun Yuan, University of York (United Kingdom)</p> |
| 13:45 – 14:00 | | <p>F2 <i>Analysis of non-diffractive electron Bessel beams for potential application in electron microscopy</i> Simon Hettler, Karlsruhe Institute of Technology (Germany)</p> |
| 14:00 – 14:15 | | <p>F3 <i>Refractive wavefront shaping with a sculpted thin film enables aberration-corrected imaging on uncorrected electron microscopes</i> Peng-Han Lu, Forschungszentrum Jülich (Germany)</p> |
| 14:15 – 14:30 | | <p>F4 <i>Diffractive Guiding Using Slits</i> Moritz Carmesin, Helmholtz-Zentrum Dresden-Rossendorf (Germany)</p> |
| 14:30 – 14:45 | | <p>F5 <i>Generation of non-diffracting Bessel beams with amorphous carbon phase masks</i> Lukas Grünewald, Karlsruhe Institute of Technology (Germany)</p> |
| 14:45 – 15:45 |  | <p>Invited Speaker - Q-SORT Webinar Chair: Ady Arie, Tel Aviv University (Israel)</p> <p><i>Shaping electron wavepackets with light; Shaping light with electron wavepackets</i> Ido Kaminer, Technion – Israel Institute of Technology (Israel)</p> |
| 15:45 – 16:00 |  | Coffee Break |
| 16:00 – 18:00 | | Session P. Poster and Exhibitors |
| 19:00 |  | <p>Social Dinner Im Alten Zollhaus, Friedlandstraße 22, 52064 Aachen</p> |

Tuesday 29 May

Poster session

Zentralbibliothek
(Building 04.7)
Forschungszentrum Jülich
Wilhelm-Johnen-Strasse
52428 Jülich

- P1 *Holography in Scanning Transmission Electron Microscopy*
Harvey, T.R.; Ophus, C.; Yasin, F.S.; Chess, J.J.; Pierce, J.S.; McMorran, B.J.
- P2 *Maximizing contrast in cryo-transmission electron microscopy with physical phase plates*
Obermair, M.; Hettler, S.; Hsieh, C.; Marko, M., Gerthsen, D.
- P3 *The ultimate direct-electron detector and neural network*
van Schayck P.; van Genderen E.,; Boulanger E.M.H.; Roussel L., Peters P.; Ravelli R.
- P4 *Realization of the Feynman-Young thought experiment:
Controlled electron interference in Fraunhofer and image space*
Tavabi A.H.; Boothroyd C.B.; Yücelen E.; Frabboni S.; Gazzadi G.C.; Dunin-Borkowski R.E.; Pozzi G.
- P5 *MEMS fabrication processes for Tunable Amperometric Phase Plate devices*
Balboni, R.; Roncaglia, A.
- P6 *Fabrication of an e-beam OAM sorter via Electron Beam Lithography*
Rosi, P.; Medici, G.; Menozzi, C.; Venturi F.; Gazzadi, G.C.; Frabboni S.; Grillo, V.
- P7 *A Numerical Analysis of Interaction-Free Measurement for Low-Dose Imaging
Using Conditional Sample Re-illumination*
Agarwal, A.; Goyal, V.; Berggren, K. K.
- P8 TBD

Wednesday 30 May

Zentralbibliothek
(Building 04.7)
Forschungszentrum Jülich
Wilhelm-Johnen-Strasse
52428 Jülich

| | | |
|---------------|---|--|
| 08:30 – 09:00 | | Registration |
| 09:00 – 10:45 |  | <i>Session H. Programmable phase plates and beam shaping</i> Chair: Johan Verbeeck, University of Antwerp (Belgium) |
| 09:00 – 09:15 | H1 | <i>Nanoelectromechanical systems on a Si-on-insulator chip to act on the phase of the electron wave-field inside a transmission electron microscope</i> Martial Duchamp, Nanyang Technological University (Singapore) |
| 09:15 – 09:30 | H2 | <i>Recent developments in the design and implementation of phase plates for electrons</i> Marco Beleggia, Technical University of Denmark (Denmark) |
| 09:30 – 09:45 | H3 | <i>Dynamic generation of electron vortices to probe magnetic information in a (S)TEM</i> Armand Béché, University of Antwerp (Belgium) |
| 09:45 – 10:00 | H4 | <i>Electron Mode Conversion and Vortex Generation</i> Christian Kramberger, TU Wien (Austria) |
| 10:00 – 10:15 | H5 | <i>Electrostatic Aharonov-Bohm effect: a tunable electron vortex beam generator</i> Amir H. Tavabi, Forschungszentrum Jülich (Germany) |
| 10:15 – 10:30 | H6 | <i>A setup for electron wave front manipulation using patterned electrostatic mirrors</i> Maurice Krielaart, Delft University of Technology (The Netherlands) |
| 10:30 – 10:45 | H7 | <i>Imaging through a multimode fibre using modal correction and time of flight to give 3D images</i> Daan Stellinga, University of Glasgow (United Kingdom) |
| 10:30 – 11:00 |  | Coffee Break |
| 11:00 – 12:00 |  | <i>Invited Speaker - Q-SORT Webinar</i> Chair: Ido Kaminer, Technion – Israel Institute of Technology (Israel) <i>Programmable phase plates for electrons</i> Johan Verbeeck, University of Antwerp (Belgium) |
| 12:00 – 12:15 |  | Concluding Remarks |
| 12:15 – 13:00 |  | Lunch |

List of talk abstracts (by presenting author)

Dynamic generation of electron vortices to probe magnetic information in a (S)TEM

A. Béché¹ and J. Verbeeck¹

¹EMAT, University of Antwerp, Groenenborgerlaan 171, 2020 Antwerp, Belgium

E-mail: armand.beche@uantwerpen.be

Introduction

Electron vortex beams are a subset of electron beams which are attaining growing interest since their experimental production in transmission electron microscopes less than a decade ago [1,2]. Electron vortex beams are of particular interest due to their azimuthally varying phase which makes them carry orbital angular momentum (OAM) as well as a quantized magnetic moment. These properties make vortex beams able to rotate nanoparticles [3] or characterize chiral crystals [4].

In the present case, the potential of mapping magnetic information down to the atomic scale by using electron vortex beams is investigated. Indeed, theoretical studies predict electron magnetic chiral dichroism (EMCD) to arise when atomic columns of magnetic materials are illuminated with atomic sized electron vortices [5]. Such beams were proven to be achievable in state-of-the-art scanning transmission electron microscopes (STEM) [6]. However, due to the weak nature of the EMCD signal, holographic gratings and static magnetic rod apertures are not ideal for this task as they require changing the experimental conditions in order to shift the sign of the vortex beam.

Here, we investigate the creation of dynamic electron vortex beams to prevent such experimental limitations. We first discuss the feasibility of building micron scale solenoids followed by experimental results.

Experimental realisation

One of the most versatile approaches towards the creation of dynamic electron vortices in TEM instruments consists of creating small solenoids. Indeed, similarly to a long single domain ferromagnetic rod [7], the end of a small solenoid can be placed over a small TEM condenser aperture to create electron vortex beams. However, requirements to obtain an electron vortex beam of high quality in a TEM impose an upper limit to the aperture size of about 50 μm in diameter due to a limited coherence length. The solenoid should appear thin and long in comparison to this aperture, which puts a limit on the diameter of a few microns at most, with a total length superior to a few tens of microns.

These size constraints already allow estimating the possibility to generate an electron beam of OAM $m=1$. This requires a magnetic flux of $2\phi_q$, where $\phi_q = h/2e$ is the magnetic quantum flux, h the Planck constant and e the electron charge. The magnetic flux inside the solenoid is approximately given by:

$$\phi = BS = \mu_0 NIS, \quad (1)$$

with B the magnetic flux density, S the section of the solenoid, μ_0 the magnetic permeability in vacuum, N the winding density and I the electric current in the solenoid. Following equation

(1), it is possible to estimate the necessary electrical current, taking the hypothesis that each winding can be $1\text{ }\mu\text{m}$ apart, and that the solenoid has a diameter of $5\text{ }\mu\text{m}$ leading to $I \approx 0.2\text{ mA}$. Quite surprisingly, it requires a rather high current to generate an OAM $m=1$ at this small scale, as the current density reaches almost 9 A.mm^{-2} for a wire section of $1\text{ }\mu\text{m}^2$. As a comparison, the maximum current density allowed in electrical wiring copper cables is 10.6 A.mm^{-2} . This estimate shows that a micron sized solenoid is unlikely to provide electron vortex beams of high vorticity, especially in continuous operation before melting due to Joule losses. However, hope remains for small value OAM vortex beams.

In order to test this idea, a focused ion beam (FIB) instrument provides the required spatial resolution and has sufficient flexibility to create such device. As the current density in the solenoid is expected to be quite large, all metals grown by FIB induced deposition have to be excluded. Indeed, such materials present a much larger resistivity than pure metals and would cause too much Joule losses. Moreover, as one of the solenoid extremities has to hang over the center of the condenser aperture, the return current line has to be designed in a way that it does not block the electron beam.

In order to accomodate for all these constraints, a micro solenoid was designed with a silicon core of square section ($3 \times 3\text{ }\mu\text{m}^2$), with in its center a gold wire of approximately 500 nm in diameter acting as the return wire. This part was then sputter coated by a $1\text{ }\mu\text{m}$ thick layer of gold. In order to contact the internal return wire, a small part of the gold coating was milled away by FIB at one extremity of the rod. Afterwards, the solenoid coils were FIB patterned into the remaining gold coating by rotating the core four times and repeating the tedious milling process. The solenoid was finally moved to the aperture with a nanomanipulator. The aperture consists of a $40\text{ }\mu\text{m}$ diameter hole in a gold back coated SiN membrane, and contacted using gold beams in the FIB. The resulting device is displayed in Figure 1a.

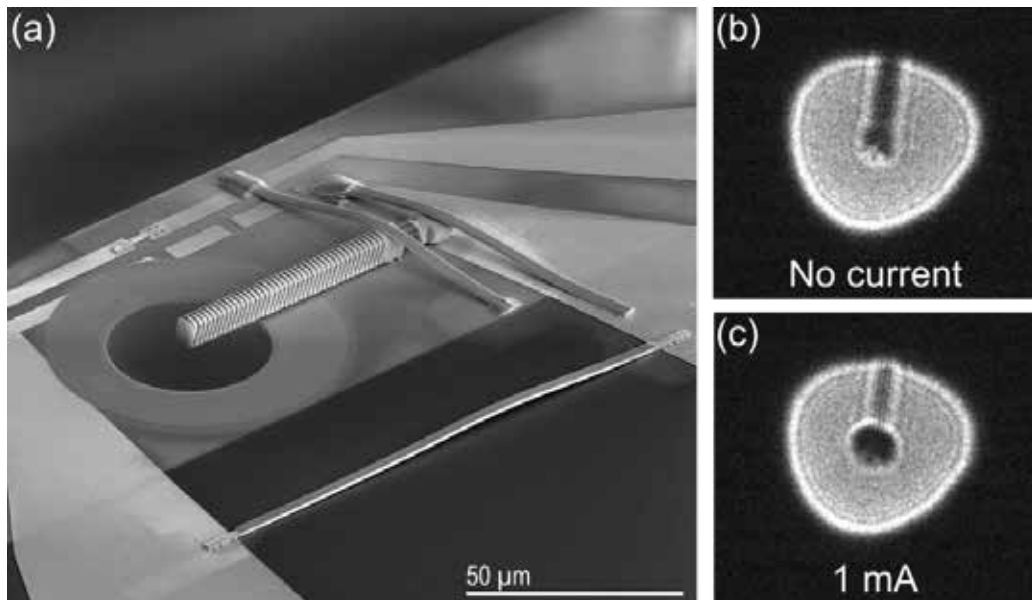


Figure 1: (a) SEM view of the micron scale solenoid over a $40\text{ }\mu\text{m}$ aperture. (b) Far field intensity pattern of the aperture without current flowing through the solenoid. (c) Same image with 1 mA current.

Results and discussion

In order to assess the performance of the device, the solenoid was introduced into a slightly modified Dens Solutions Wildfire S3 holder to allow electrical connections, before being introduced in a FEI Titan³ microscope operating in Lorentz mode. In the far field of the aperture, displayed in Fig. 1b with a slight defocus of -400 nm, one can recognize the shadow image of the solenoid. The bright contrast in the middle of the beam is due to slight amount of charging at the tip of the solenoid. By increasing the current into the solenoid to a value of 1 mA, as displayed in Fig. 1c, a dark core appears in the middle of the beam, surrounded by a closed ring of constructive interference, typical for an electron vortex beam. This last picture demonstrates the potential of such solenoid in generating electron vortex beams.

Some drawbacks remain, especially regarding the maximal current sustainable for the device. During our tests, the current was increased to 2 mA to obtain larger OAM beams, and the device melted due to Joule losses. However, micron scale solenoids seem to hold promise as very efficient and versatile devices to create tunable electron vortices of low OAM.

Acknowledgments

A.B. and J.V. acknowledge funding from the European Research Council under the 7th Framework Program (FP7), ERC Starting Grant No. 278510 VORTEX.

References

- [1] M. Uchida & A. Tonomura, *Nature* **464**, 737-739 (2010)
- [2] J. Verbeeck, H. Tian & P. Schattschneider, *Nature* **467**, 301-304 (2010)
- [3] J. Verbeeck, H. Tian and G. Van Tendeloo, *Advanced Materials* **25**, 1114-1117 (2013)
- [4] R. Juchtmans, A. Béché, M. Batuk, A. Abakumov and J. Verbeeck, *Physical Review B* **91**, 094112 (2015)
- [5] J. Rusz and S. Bhowmick, *PRL* **111**, 105504 (2013)
- [6] A. Béché, R. Juchtmans and J. Verbeeck, *Ultramicroscopy* **178**, 12-19 (2017)
- [7] A. Béché, R. Van Boxem, G. Van Tendeloo and J. Verbeeck, *Nature Physics* **10**, 26-29 (2014)

Recent developments in the design and implementation of phase plates for electrons

M. Beleggia¹

¹*DTU Danchip Cen, Technical University of Denmark, 2800 Kgs. Lyngby, Denmark
E-mail: mb@cen.dtu.dk*

Shaping the electron wave function with the purpose of enhancing phase contrast can be accomplished by phase plates based on electric or magnetic fields. Amongst the many new designs proposed recently in the literature, two appear particularly noteworthy: the Tunable Ampere Phase Plate (TAPP) [1], and the Hole Free Phase Plate (HFPP) [2], also known as Volta [3]. The phase shift between the low- q and the high- q regions of the object spectrum, necessary to produce phase contrast in absence of defocus or apertures in the transfer function, arises from a localized vertical current segment in the TAPP and from a localized charge in the HFPP. The vertical current segment of the TAPP generates a curling magnetic induction around it, whose vector potential is parallel to the current and the beam, thereby producing a phase shift inversely proportional to the distance from the center of the current-carrying wire (see Fig. 1). The localized charge in the HFPP is beam-induced, and generates a local electric field which also produces a phase shift that decays with distance.

Both designs offer unique advantages over conventional Zernike-type setups. The current in the TAPP device can be adjusted continuously, which permits the modulation of the phase shift in magnitude and sign. Being made of a conductive element, it is less prone to charging artifacts, even with the high current density of the direct beam tails impinging on it. Even if some charge arises due to oxidation or contamination of the wire, the specific spatial profile of the phase shift, coincident of that of an electric point charge, makes it possible to compensate the artifact by tuning the current. On the other hand, the wire itself is opaque to electrons, and cuts a portion of the diffracted wave producing Foucault-type contrast that may affect the resulting phase contrast. A discussion of the TAPP performance related to size and positioning of the device with respect to the direct beam center will be the first topic of this presentation.

The charge distribution established on the HFPP film is located underneath the diffracted intensities, and has a spatial extent that depends on the beam profile. Consequently, there is no need to position the HFPP, which can be conveniently operated. On the other hand, the amount of charge, how it distributes over the film, and even whether it is positive or negative, and therefore the magnitude, sign, and spatial profile of the HFPP phase shift, are not yet parameters that we have learned how to control. The sign of the charge on the HFPP is a particularly puzzling aspect [4]. While secondary electron emission appears as the most intuitive mechanism for building up a charge distribution on an irradiated thin film, evidence is accumulating on the HFPP providing a negative phase shift, which can arise only from either thickness removal or negative charge accumulation. A hypothesis was formulated recently on

how a negative HFPP shift may arise in certain circumstances [5], which will be the second topic of this presentation (see Fig. 2).



Fig. 1 Left: SEM view of part of the TAPP device; the central segment of the wire is positioned parallel to the electron beam, and current is injected into it after establishing electrical contact. Center: contour map of the TAPP phase shift; the asymmetry of the contours is due to the perturbed reference wave, but does not affect the operation of the device. Right: calculated TAPP phase shift superimposed to the shadow of the wire and to the spectrum of a phase object corresponding to a biomolecular complex.

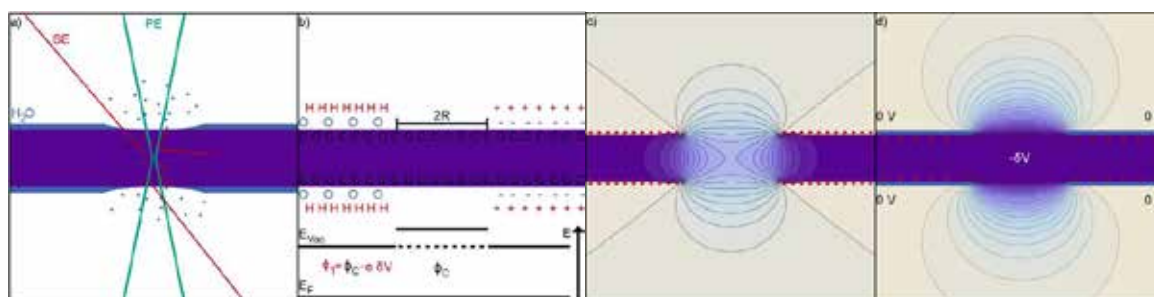


Fig. 2 (a) Some of the secondaries generated by e-beam irradiation of a thin film can initiate the desorption of adsorbed water molecules (blue) from the film surfaces. (b) The adsorbed water layer forms a dipole with the positive hydrogen end pointing towards vacuum. The water layer effectively reduces the work function by an amount δV proportional to the dipole moment of a water molecule. (c) Electrostatic potential distribution for two interrupted dipole layers (red arrows) in empty space *without* carbon film. The potential range is between the step $-\delta V$ (purple) caused by the dipole layer and 0 V (white). (d) Potential distribution between $-\delta V$ (purple) and 0 V (white) for an interrupted water layer on the surface of a carbon thin film (purple). Adapted from Fig. 8 in Ref. [5] with permission.

While neither the TAPP nor the HFPP require sophisticated nanofabrication techniques, shaping the electron wave with purposes other than phase contrast generally relies heavily on them. For example, the “hologram” phase plates used to generate vortex beams are often made lithographically, and their ultimate performance is limited by the spatial resolution and quality of the patterns achieved. We have recently introduced a new concept in e-beam lithography where the role of the resist is assumed by a frozen layer of organic molecules

condensed in-situ within the instrument later used for patterning [6] (see Fig. 3). Choosing compounds that are volatile at ambient temperature makes it possible to bypass entirely the whole pattern development procedure that requires chemicals and ex-situ processing [7]. In fact, e-beam irradiation of these compounds turns them into a solid residue with dimensions comparable to the beam size, so that upon raising the temperature the non-irradiated portion of the frozen layer evaporates away naturally. The technique bears similarities with Focused Electron Beam Induced Deposition, the main differences being that absorption/desorption and diffusion of molecules are not relevant parameters, so that the patterns are sharper and form much more quickly throughout the entire thickness of the frozen layer. The third and final topic of this presentation will be an introduction to e-beam lithography with organic ice resists, and a discussion of the perspective of using it to create complex phase plates that would enhance our ability of manipulating and shaping the electron wave.

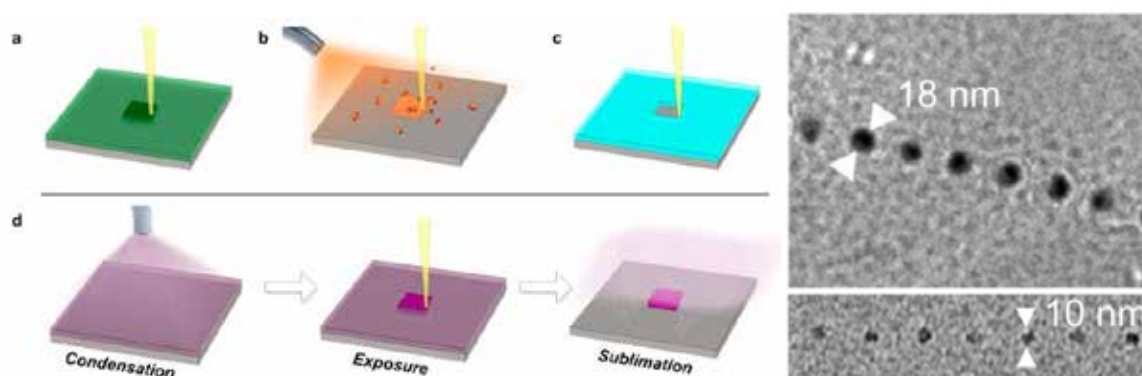


Fig. 3 Organic Ice Resist patterning compared to other e-beam based techniques: (a) EBL, (b) FEBID, (c) Ice Lithography, and (d) OIR: a vapor of a simple organic compound is first condensed onto the cooled sample to form a uniform layer. Its interaction with the e-beam modifies locally its chemical composition, resulting in a nonvolatile product. When the sample is heated to room temperature, the unexposed OIR sublimates while the exposed patterns are stable, enabling ambient downstream processing. On the right: an example of OIR-patterned (nonane) dot arrays on a 5-nm thick SiN membrane. The whole process from condensation of the OIR to imaging of the exposure products was carried out in-situ in an environmental TEM operated at 80 kV. Figure adapted from Ref. [6] with permission.

References

- [1] A. Tavabi et al., Sci. Rep., in press (2018)
- [2] M. Malac et al., Ultramicrosc. **118**, 77 (2012)
- [3] R. Danev et al., Proc. Nat. Acad. Sci. **111**, 15635 (2014)
- [4] M. Malac et al., Micron **100**, 10 (2017)
- [5] S. Hettler et al., Ultramicrosc. **184**, 252 (2018)
- [6] W. Tiddi et al., Nanolett. **17**, 7886 (2017)
- [7] W. Tiddi et al., M. Eng. **192**, 38 (2018)

Diffraction Guiding Using Slits

Moritz Carmesin^{1,2}, Maxim A. Efremov¹, Dror Weisman³, Ady Arie³, Wolfgang P. Schleich^{1,4}

¹ *Institut für Quantenphysik and Center for Integrated Quantum Science and Technology (IQST),
Universität Ulm, 89081 Ulm, Germany*

² *Abteilung Laser-Teilchenbeschleunigung, Helmholtz Zentrum Dresden Rossendorf, 01328 Dresden,
Germany*

³ *Department of Physical Electronics, Faculty of Engineering, Tel-Aviv University, Tel-Aviv 69978,
Israel*

⁴ *Hagler Institute for Advanced Study, Institute for Quantum Science and Engineering (IQSE), and
Texas A&M AgriLife Research, Texas A&M University, College Station, TX 77843-4242, USA
e-mail: moritz.carmesin@uni-ulm.de*

Introduction

Diffraction focusing [1] just by amplitude modulation, e. g. by a single slit, is a novel technique to focus waves. In contrast to the usual approach to focus a wave, the phase is not modulated like for instance with a lens. Recently [2] the effect has been experimentally exploited for matter waves in two dimensions.

We developed the concept of diffraction focusing and propose a new concept: diffraction guiding. Here the aim is to guide a wave over a given distance employing the focusing effect of single slits while minimizing the loss of wave intensity. We present the optimal arrangement of one dimensional (1D) single slits in order to guide a matter wave (e. g. surface plasmons) in 2D over a given distance.

Methods & Results

We plan to use surface polariton plasmons to realize the diffraction guiding. Perpendicular to the incoupled wave we place several, partially absorbing slits. In such a setup we study the propagation of different transversal profiles, in particular the eigenmode of the system.

In parallel to the experiment we also develop a theoretical model. For the case of fully absorbing slits, we have developed a simple 1D model, which allows to determine the eigenmodes and eigenvalues. In order to go beyond the simple mode we solve numerically the 2D Schrödinger equation for a complex valued potential which models the slits with realistic values for absorption, reflection and transmission. The result of such a simulation is shown in Figure 1.

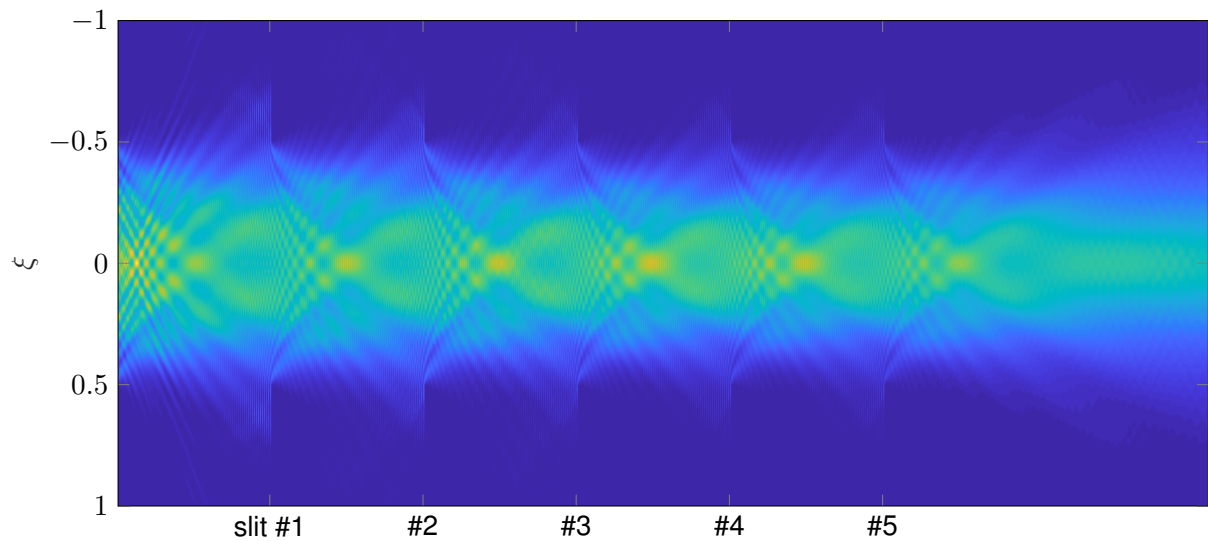


Figure 1: Numerical simulation of the transversal distribution at the peak of an eigenmode wave packet propagating through 5 slits. The absorption and reflection at the slit are each about 50%.

Outlook

We are going to compare the theoretical predictions to the experimental data. Furthermore, we will consider more complex setups, e. g. bent wave guides.

References

- [1] W. B. Case, E. Sadurni, and W. P. Schleich. “A diffractive mechanism of focusing”. In: *Optics Express* 20.25 (2012), pp. 27253–27262.
- [2] Dror Weisman et al. “Diffractive Focusing of Waves in Time and in Space”. In: *Phys. Rev. Lett.* 118 (15 Apr. 2017), p. 154301.

Nanoelectromechanical systems on a Si-on-insulator chip to act on the phase of the electron wave-field inside a transmission electron microscope

M. Duchamp^{1, 2}, O. Girard^{3, 4}, G. Pozzi⁵, H. Soltner⁶, F. Winkler², R. Speen², R.E. Dunin-Borkowski² and D. Cooper^{3, 4}

¹ *School of Materials Science and Engineering, Nanyang Technological University, 50 Nanyang Avenue, Singapore 639798, Singapore*

² *Ernst Ruska-Centre for Microscopy and Spectroscopy with Electrons (ER-C), Forschungszentrum Jülich, 52425 Jülich, Germany*

³ *Université Grenoble Alpes, 38000 Grenoble, France*

⁴ *CEA, LETI, MINATEC Campus, 38054 Grenoble, France*

⁵ *Department of Physics and Astronomy, University of Bologna, viale B. Pichat 6/2, 40127 Bologna, Italy*

⁶ *Central Institute of Engineering, Electronics and Analytics (ZEA-1), Forschungszentrum Jülich, 52425 Jülich, Germany*

E-mail: mduchamp@ntu.edu.sg

For various applications, the electron wave-field propagating through the electron column in a transmission electron microscope (TEM) needs to be spatially tuned at the sub-micrometer scale [1,2]. It is currently performed using macroscopic electron-optics elements such as aberration-correctors or focus ion beam (FIB) processed structures [3,4]. These approaches are time consuming and/or expensive to fabricate. An alternative approach is to use semiconductor processing technology to fabrication devices which act on the electron wave-field through sub-micrometer electrostatic poles. Nanoelectromechanical systems (NEMS) are a class of devices which integrate mechanical functionality on the nanoscale fabricated using semiconductor processing technology. Their nanometer dimensions lead to low mass, high mechanical resonance frequencies and strong electrostatic fields.

Off-axis electron holography allows both the amplitude and the phase shift of an electron wave-field propagating through a specimen in a TEM to be recovered. The technique requires the use of an electron biprism to deflect an object wave and a reference wave to form an interference pattern. Most implementations of the technique rely on the deflection of electrons that have passed through the specimen towards a vacuum reference electron wave using a Möllenstedt–Düker electron biprism, which normally takes the form of a sub-micrometer-diameter metal or metal-coated quartz wire [5,6] that is located close to a conjugate image plane in the microscope (in an aperture holder). Despite considerable progress in many aspects of instrumentation for electron microscopy, little has been done to improve the design and manufacture of electron biprisms.

Here, we present an approach to fabricate fine electron biprisms with rectangular cross-sections using NEMS technology. A dedicated chip holder which was designed, machined and used to test the biprism in the selected area (SA) aperture plane of a Philips CM20 FEG TEM. We also performed electrostatic calculations and preliminary experiments demonstrate that such biprisms promise improved performance for electron holography experiments. The holograms obtained with this setup have as an overlap width of 45 nm, an interference fringe spacing of 0.2 nm and an interference fringe contrast of 16% for 27 V applied to the

rectangular biprism [7,8]. We will also present a proof-of-concept of a dedicated chip holder to be inserted in the condenser system of a Jeol ARM200F probe corrected TEM.

References

- [1] G. Guzzinati, L. Clark, A. Béché, R. Juchtmans, R. Van Boxem, M. Mazilu, J. Verbeeck, *Ultramicroscopy*. **151**, 85 (2015)
- [2] J. Verbeeck, G. Guzzinati, L. Clark, R. Juchtmans, R. Van Boxem, H. Tian, A. Béché, A. Lubk, G. Van Tendeloo, *Comptes Rendus Phys.* **15**, 190 (2014)
- [3] A. Béché, R. Van Boxem, G. Van Tendeloo, J. Verbeeck, *Nat. Phys.* **10**, 26 (2014)
- [4] E. Karimi, V. Grillo, R.W. Boyd, E. Santamato, *Ultramicroscopy*. **138**, 22 (2014)
- [5] G. Möllenstedt and H. Düker, *Naturwissenschaften* **42**, 41 (1955)
- [6] G. Möllenstedt and H. Düker, *Z. Für Phys.* **145**, 377 (1956)
- [7] M. Duchamp, R.E. Dunin-Borkowski, O. Girard, D. Cooper, Patent 'Electrostatic Biprism', WO/2016/091314, 2016.
- [8] M. Duchamp, O. Girard, G. Pozzi, H. Soltner, F. Winkler, R. Speen, R.E. Dunin-Borkowski, D. Cooper, *Ultramicroscopy*. **185**, 81 (2018)

Acknowledgement

M.D. acknowledges the financial support from Nanyang Technological University start-up grant M4081924 and the Ministry of Education Academic Research Fund Tier 1 grants RG101/17.

The ultrafast and ultracold electron source

J.G.H. Franssen^{1,2}, T.C.H. de Raadt¹ and O.J. Luiten^{1,2}

(1) *Coherence and Quantum Technology, Department of Applied physics, Eindhoven University of Technology, The Netherlands*

(2) *Institute for Complex Molecular Systems, Eindhoven University of Technology, The Netherlands*

We are developing an ultrafast and ultracold electron source, based on near-threshold, femtosecond photoionization of laser-cooled and trapped Rubidium gas. Recently, we demonstrated electron crystallography of graphite for the first time using the ultracold source[2]. The ultimate goal is ultrafast, single-shot electron crystallography of macromolecules, which requires a high degree of control of the dense electron phase space distribution. The transverse phase space distribution has been extensively characterized in the past[2, 3, 4], resulting in electron temperatures as low as 10 K when using a femtosecond ionization scheme.

For characterizing the longitudinal phase space distribution we have developed a microwave cavity based diagnostic element to correlate electron bunch lengths to streak images. This allows us to measure the pulse length with sub-picosecond temporal resolution. We show that we can make *both* ultracold *and* ultrafast electron pulses which have an rms pulse duration of 20 picoseconds[5]. These bunches are sufficiently short to be compressed to 100 fs bunch lengths using established RF compression techniques.

Additionally we have used a dedicated Wien filter to measure the bunch energy spreads[6]. The simultaneous use of these diagnostic elements enables us to image the total longitudinal phase space distribution onto the detector, with both sub-ps time resolution and sub-eV energy resolution.

Finally we will present the status of our new compact ultracold electron experiment which is based on a grating magneto-optical-trap (GMOT), radio frequency acceleration and a TimePix electron detector.

Contact e-mail: j.g.h.franssen@tue.nl

- [1] Mourik *et al*, Struct. Dyn. **1** 034302 (2014)
- [2] Engelen *et al*, Ultramicroscopy **136**, 73-80 (2013)
- [3] Engelen *et al*, Nat. Commun **4**, 1693 (2013)
- [4] Engelen *et al*, Ultramicroscopy **147**, 61-69 (2014)
- [5] Franssen *et al*, Struct. Dyn. **4** 044010 (2017)
- [6] Franssen *et al*, J. Phys. B: At. Mol. Opt. Phys. **51**, 035007 (2018).

History-Dependent Radiative Interaction of Single Electron Quantum Wavepacket

Avraham Gover, Yiming Pan

Department of Electrical Engineering Physical Electronics,

Tel Aviv University, Ramat Aviv 69978, ISRAEL

E-mail: gover@eng.tau.ac.il

Introduction

The interpretation and the essence of the electron quantum wavepacket and its electromagnetic interactions have been a subject of debate since the early conception of quantum mechanics. In the following we analyzed the stimulated radiative interaction of a single-electron wavepacket of arbitrary size, establishing first the consistency of our analysis with previous theory and experimental measurements of PINEM, FEL and DLA. We then present the main result: derivation of a new “phase-dependent” stimulated radiative interaction regime of an electron wavepacket in which the physical significance of the wavepacket size and the history of its generation and transport to the interaction region are exhibited. We demonstrate then how the quantum wavepacket theory evolves to the classical point-particle limit in this regime.

Methods

Our one-dimensional interaction model is based on the first order perturbation solution of the relativistic “modified Schrödinger equation”, derived from Klein-Gordon equation:

$$i\hbar \frac{\partial \psi(z, t)}{\partial t} = (H_0 + H_I(t))\psi(z, t), \quad (1)$$

where $H_0 = \varepsilon_0 + v_0(-i\hbar\nabla - \mathbf{p}_0) + \frac{1}{2m^*}(-i\hbar\nabla - \mathbf{p}_0)^2$ is the free space Hamiltonian, $m^* = \gamma_0^3 m$,

and the interaction part is:

$$H_I(t) = - \frac{e(\mathbf{A} \cdot (-i\hbar\nabla) + (-i\hbar\nabla) \cdot \mathbf{A})}{2\gamma_0 m} \quad (2)$$

This model is fitting for discription of the variety of interaction schemes mentioned, some of them operating with a relativistic beam. In the present one-dimensional model of electron interaction in a "slow-wave" structure we use a longitudinal vector potential

$\mathbf{A} = -\frac{1}{2i\omega} \left(\mathbf{E}^{(0)}(z) e^{-i(\omega t + \phi_0)} - \mathbf{E}^{(0)*}(z) e^{i(\omega t + \phi_0)} \right)$, where $\mathbf{E}^{(0)}(z) = E_0 e^{iq_z z} \hat{\mathbf{e}}_z$ represents the dominant slow component of the radiation wave. We exemplify our modeling here for a case of Smith-Purcell radiation (see Fig. 1), for which satisfies synchronism condition with the electron. We now solve Eq.1 in the interaction region $0 < z < L_I$ using the first order perturbation theory in momentum space

$$\psi(z, t) = \psi^{(0)}(z, t) + \psi^{(1)}(z, t) = \int \frac{dp}{\sqrt{2\pi\hbar}} \left(c_p^{(0)} + c_p^{(1)} \right) e^{-i(E_p t - pz)/\hbar}. \quad (3)$$

And then calculate the electron momentum density distribution after interaction:

$$\begin{aligned} \rho(p') &= \rho^{(0)}(p') + \rho^{(1)}(p') + \rho^{(2)}(p') \\ &= \frac{\left| c^{(0)}(p') \right|^2 + 2 \operatorname{Re} \left\{ c^{(1)*}(p') c^{(0)}(p') \right\} + \left| c^{(1)}(p') \right|^2}{\int dp' \left(\left| c^{(0)}(p') \right|^2 + \left| c^{(1)}(p') \right|^2 \right)}, \end{aligned} \quad (4)$$

where $\rho^{(0)}(p')$ is the initial Gaussian momentum density distribution.

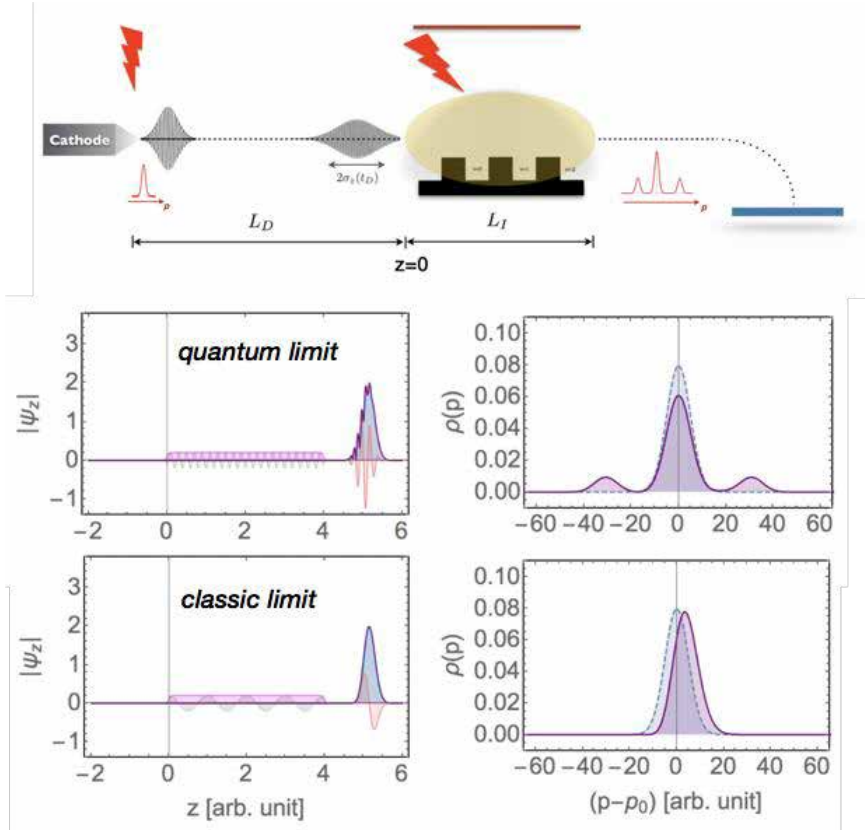


Fig. 1: The experiment setup. Single electron wavepackets are photo-emitted from a cathode driven by a femtosecond laser. After a free propagation length L_D , the expanded wavepacket passes next to the surface of a grating, and interacts with the near-field radiation, that is excited by an IR wavelength laser, phase locked to the photo-emitting laser. The momentum

distribution of the modulated wavepacket is measured with an electron energy spectrometer. The numerical simulation results of the wavepacket density and its momentum spectra after interaction are shown in the quantum (PINEM) limit and near classical point-particle limit.

Results

The near-classical acceleration of electron wavepacket was found in our analytical perturbation analysis to be attenuated relative to the classical “point-particle” momentum gain as:

$$\Delta p^{(1)} / \Delta p_{point} = e^{-\Gamma^2/2}, \quad \Gamma = \frac{\omega}{v_0} \sigma_z(t_D) = \frac{2\pi\sigma_z(t_D)}{\beta\lambda} \quad (5)$$

$$\Delta p_{point} = -\frac{eE_0 L_I}{v_0} \sin c\left(\frac{\bar{\theta}}{2}\right) \cos\left(\phi_0 + \frac{\bar{\theta}}{2}\right). \quad (6)$$

From inspection of the expression for the wavepacket expansion in free drift:

$$\sigma_z(t_D) = \sqrt{\sigma_{z_0}^2 + \left(\frac{\lambda_c^*}{4\pi} \frac{ct_D}{\sigma_{z_0}}\right)^2}, \quad (7)$$

wavepacket acceleration is only possible within a range of electron drift away from its emission source, $L_D \ll z_G$, so that $\Gamma = 2\pi\sigma_z(t_D)/\beta\lambda < 1$. Therefore, contrary to matter-wave interference approach, stimulated radiative interaction at different wavelengths and drift lengths enables measurement of the evolving electron wavepacket size $\sigma_z(t_D)$, and not the intrinsic “coherence length” σ_{z_0} .

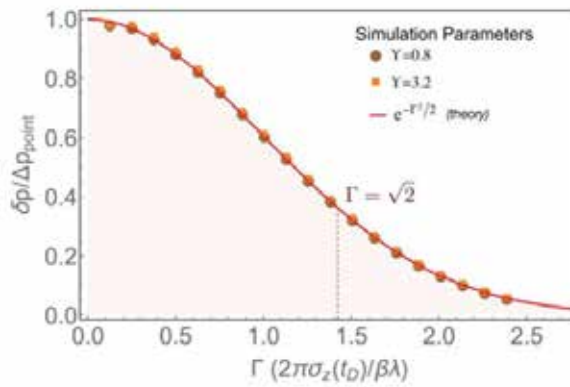


Fig 2: The reduction factor of wavepacket acceleration relative to the “point-particle” classical case, as calculated from numerical solution of Schrodinger equation (points), and compared to the first-order perturbation expression (red curve).

Discussion

Here we related to the fundamental questions of the physical significance of a single particle quantum wavepacket and the wave-to-particle transition to the classical electrodynamics limit. The presented semiclassical first order perturbation analysis and the numerical computations show that stimulated finite-length interaction of a single electron wavepacket with radiation can be dependent on the features of the wavepacket, its history and its spatial position relative to the phase of the accelerating radiation wave. Furthermore, the analysis can be extended to the case of FEL, Cherenkov and other interaction schemes.

References

- [1] A. Gover, Y. Pan, [arXiv:1702.06394v4](https://arxiv.org/abs/1702.06394v4).
- [2] Y. Pan, A. Gover, Quantum electrodynamics theory of electron wavepacket, to be submitted.

A design for combining multi-pass and OAM sorter for dose effective magnetic measurements

E. Karimi¹, R. Dunin Borkowski², V. Grillo³

¹ University of Ottawa, Ottawa, Canada

² Forschungszentrum, Jülich, 52425 Jülich, Germany.

³ CNR-NANO, Modena, Italy

E-mail: Vincenzo.grillo@cnr.it

Introduction

Electron microscopy has demonstrated to be one of the most powerful tool for the characterization of material properties ranging from atomic structure and strain to built-in fields. However new and interdisciplinary approaches to the use of the electron beam are adding new ideas to the way a measurement can be carried on in a microscope [1][2].

One of the most interesting revolutions in this sense has been the introduction of electron beam shaping [3][4] where the use of phase holograms [5] or fields distribution[6] is used to control the beam full wavefunction. This tool can be used to control the probe impinging to the sample but also to provide new analyzer.

In this sense it has been recently introduced the concept of Orbital Angular Momentum analyzer [7]. In fact it demonstrates that an appropriate change of basis permits to simplify the measurement of important quantities like the magnetic dipole moment.

One of the advantages here is that the unitary transformation permits to move from a phase measurement, normally difficult in direct imaging, to an amplitude measurement that is usually much easier and also more effective in terms of atomic information per electron. The concepts underlying this change of paradigm in microscopy are at the basis of the Q-SORT project.

A promised revolution is also expected to arise in the context of microscopy with multipass electron microscopy. In it an unprecedented set of electronic lenses permits to the electrons to transverse the sample region many times before it is analyzed [8]. This form of interaction is potentially useful in the analysis of weak phase objects such as biological materials.

The phase passing through this system p times receives a p -fold coherent increase. The phase measurement error therefore decreases as $1/p$ which beats any classical statistics scaling as $1/\sqrt{p}$. In a sense the multipass idea can be interpreted as a conditional form of beam shaping where the beam shape depends on the sample itself.

It is therefore natural to assume that there can be a natural bridge between these two idea.

The new method

The specific case we consider here is the measurement of a magnetic dipole. In many cases like time resolved magnetism or in the attempt of measuring molecular magnetism phenomena the dose control is a very important factor.

The multipass alone would produce a p-fold increase of the phase, but a phase-to-amplitude conversion mechanism would be necessary for the final measurement.

Defocusing of the wavefunction is in many cases little effective and qualitative leading to loss of resolution.

On the other hand OAM an sorter alone has already proved to be probably the most effective way to measure magnetic dipole with a reduced number of electrons but it only works with large dipole moments.

A combination of the two ideas is a measurement where, due to the multipass scheme the phase is enhanced and the analyzed through a OAM sorter.

Fig 1 shows the scheme of an electro-optical bench or column where the information of the electrons is cycled many times from the post sample to pre-sample condition.

In fact the Aharonov-Bohm phase due to a magnetic dipole with momentum m produces a characteristic OAM spectrum largely peaked at the a OAM value X_0 such that $X_0 = \frac{e\mu_0 m}{hr}$ where e is the electron charge μ_0 is magnetic permeability of vacuum, h is the plank constant r is the cutoff value of the beam. The use of a p-fold multipass just increases this value to $X = X_0 p$.

Assuming that to some extent this peak has a constant width σ_x the position of this peak can be calculated with a precision σ_x/\sqrt{N} where N is the number of electron acquired.

Fig 2 shows that typical OAM spectra for different magnetic dipole value(or number of pass). It is straightforward to see that the precision in the determination of the magnetic dipole then becomes

$$\sigma m = \frac{m}{X_0 p} \frac{\sigma_x(p)}{\sqrt{N}}$$

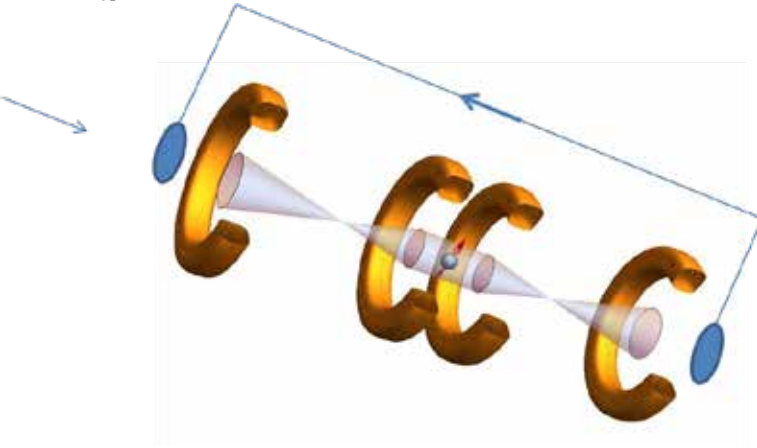


Fig. 1 Scheme of a multipass microscope where the wavefunction is passed many times through the magnetic sample.

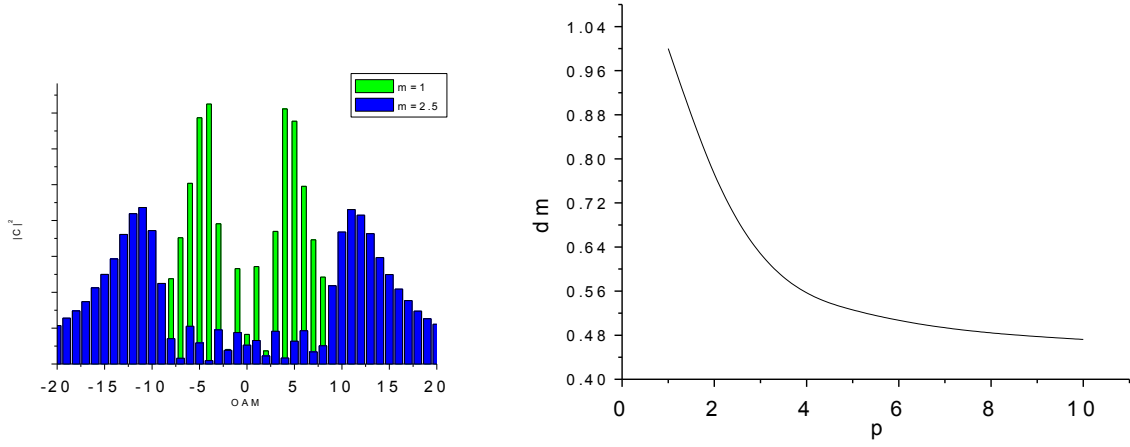


Fig. 2 (a) OAM spectrum for two different number of passes p or magnetic dipole moment m . The main peak shifts linearly with m or p (b) Error on the magnetic dipole determination as a function of passes.

This simple considerations bring us to predict that with p as large as 1000 the phase down to some hundred Bohr magneton could be reached.

Conclusion

The discussion above is just an example that should convince the reader that one possible future of quantum measurement lies in the synergy between quantum iteration and unitary transformation of the wave function through wave shaping.

References

- [1] C Ophus et al. Nature Communications **7**, 10719 (2016)
- [2] V. Grillo et al. Nature communications **8**, 689 (2017)
- [3] J Verbeeck et al, Nature **467**, 301 (2011)
- [4] V. Grillo Optics express **25**, 21851 (2017)
- [5] V. Grillo Applied Physics Letters **104**, 043109 (2014)
- [6] G. Pozzi Ultramicroscopy **181**, 191 (2017)
- [7] V. Grillo et al. Nature communications **8**, 15536 (2017)
- [8] T Juffmann et al., Scientific Reports **7**, 1699 (2017)

Acknowledgments

The work was supported by Q-SORT, a project funded by the European Union's Horizon 2020 Research and Innovation Programme under grant agreement No. 766970.

Generation of non-diffracting Bessel beams with amorphous carbon phase masks

L. Grünewald¹, D. Gerthsen¹ and S. Hettler¹

¹Laboratory for Electron Microscopy, KIT, Karlsruhe, Germany
E-mail: simon.hettler@kit.edu

Electron beam shaping is a promising tool for novel applications in electron microscopy [1]. One method to create beam shapes is to use a thin film with a specific thickness profile (phase mask (PM)). Silicon nitride (Si_3N_4) is commonly used as a PM material due to its mechanical stability, low scattering probability for electrons and commercial availability. However, Si_3N_4 is insulating and an additional conductive layer has to be deposited on the PM to avoid charging which increases scattering of electrons.

In this work we present methods to create quasi non-diffracting Bessel beams by using PMs made of amorphous carbon (aC). Bessel beams could be used as electron probes with high depth of focus in a scanning (transmission) electron microscope (S(T)EM) [2,3]. aC is conductive, mechanically stable and has a low scattering probability. Different fabrication steps involving optical lithography, physical vapor deposition (PVD) and focused ion beam (FIB) techniques are used to create a homogeneously flat aC-film surrounded by an obstructing Pt-aperture (Fig. 1a). Afterwards, the PM grating for the desired beam shape is milled in the aC-film with custom FIB-routines (Fig. 1b). By positioning an aC-PM in the condenser system of a TEM (CM 200) a Bessel beam is observed in the object plane (Fig. 1c) which can be controlled by adjustment of the condenser lenses.

We demonstrated that aC can be used as an alternative material to commonly used Si_3N_4 for the fabrication of beam-shaping PMs.

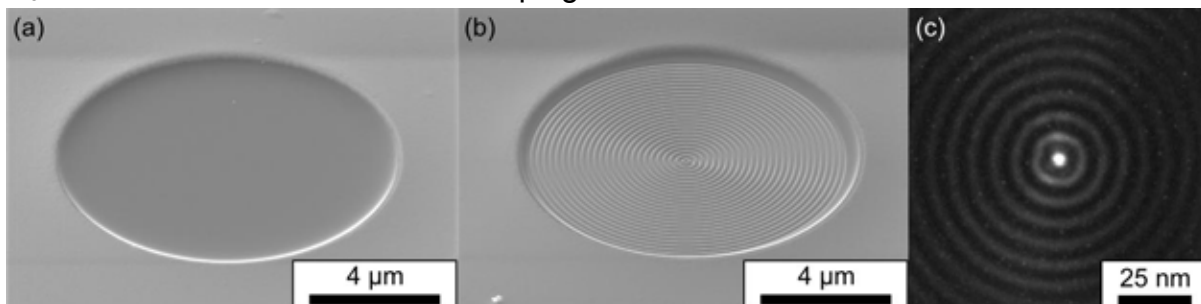


Figure 1: (a) Example of a flat aC-thin film surrounded by a Pt-aperture. Multiple fabrication steps (optical lithography, FIB, PVD) are involved. (b) FIB-milling is used to create the thickness profile in the aC-film for an on-axis Bessel beam. (a) and (b) are SEM secondary electron images at 5 keV. (c) The image shows a Bessel beam centered on the optical axis in the object plane of a TEM generated by a PM which was positioned in the condenser system.

References

- [1] Bliokh et al., *Physics Reports* **690**, 1 – 70 (2017)
- [2] Grillo et al., *Physical Review X* **4**, 011013 (2014)
- [3] Grillo et al., *Ultramicroscopy* **166**, 48 – 60 (2016)
- [4] Funding by the Carl-Zeiss-Stiftung is acknowledged.

Measuring the phase and transverse fields of plasmonic excitations

G. Guzzinati¹, A. Lubk², J. Krehl², J. Schultz², M. Kociak³, H. Lourenço-Martins³, J. Martin⁴, A. Béch  ¹, J. Verbeeck¹

¹EMAT, University of Antwerp, Antwerp, Belgium

²IFF, IFW Dresden, Dresden, Germany

³Laboratoire de Physique des Solides, Univ. Paris-Sud, Orsay, France

⁴Institut Charles Delaunay, Universit   de Technologie de Troyes, Troyes, France

E-mail: giulio.guzzinati@uantwerpen.be

Introduction

Electron energy loss spectroscopy has become one of the key techniques for the study of localized surface plasmon resonances, ever since the first demonstrations that it could be used to detect and image the dramatic spatial variations in the electrical field of the induced resonances of a single nanoparticle. Despite its great success, the standard experimental setup, based on measuring the angle-integrated, spatially- and spectrally-resolved energy loss cross section does have limits. While optical spectroscopies can make use of polarisation to directionally probe the response of a nanoparticle, an electronic beam can't discriminate between energy-degenerate eigenmodes and is also blind to optical activity and dichroism. Here we present two radically new approaches. The first one, is based on the idea of controlling, through phase manipulation techniques [1], the wave function of the electronic probe to fit the plasmonic modes under investigation, allowing to selectively detect plasmon modes on the basis of the symmetry of the time-dependent charge density. The second, based on an energy-filtered variant of conventional center-of-mass momentum measurement, allows to quantitatively probe the transverse fields of the induced resonances.

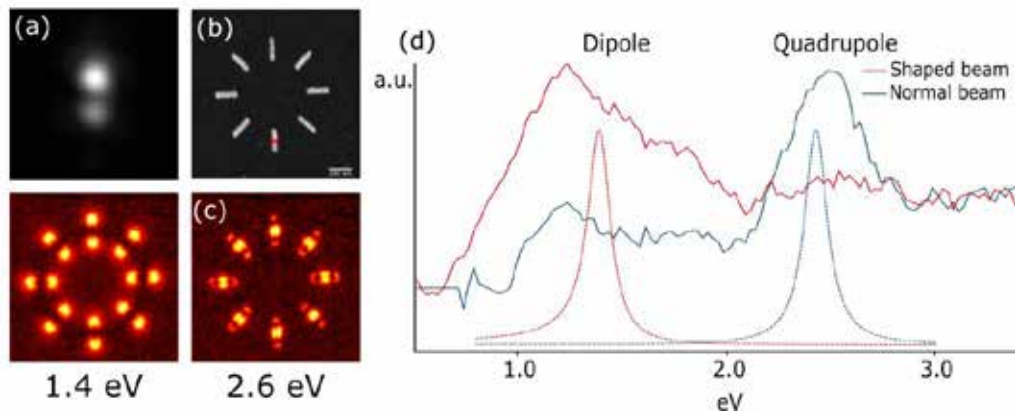


Figure 1 A modified electron beam with a 2-lobed profile (a) is used to selectively de-tect dipolar modes. Plasmonic nanorods (b) which show clear dipolar and quadru-polar modes (c) are probed with the modified beam (a) and a normal one, in the po-sition marked with a red cross (b). The modes are individually detected as shown in (d), also compared with simulations (dashed line).

Methods

Both methods are explored theoretically and experimentally. On the basis of the analytical calculations, numerical simulations are performed through custom codes built on top of the well-known MNPBEM toolbox, a Matlab toolbox for the simulation of the optical behavior of metallic nanoparticles[4]. Experimental tests of both approaches are performed in monochromated FEI Titan³ microscopes.

Results

We show that the phase in the electron beam's wave function couples to the electric potential of the plasmonic mode, allowing to selectively detect localized plasmonic excitations that possess the same symmetry as the electron probe [2]. We successfully demonstrate this by focusing on selectively detecting the dipolar and quadrupolar modes of a nanorod with a two-lobed probe, which we generate in a TEM by employing a Hilbert phase plate based on the Aharonov-Bohm effect.

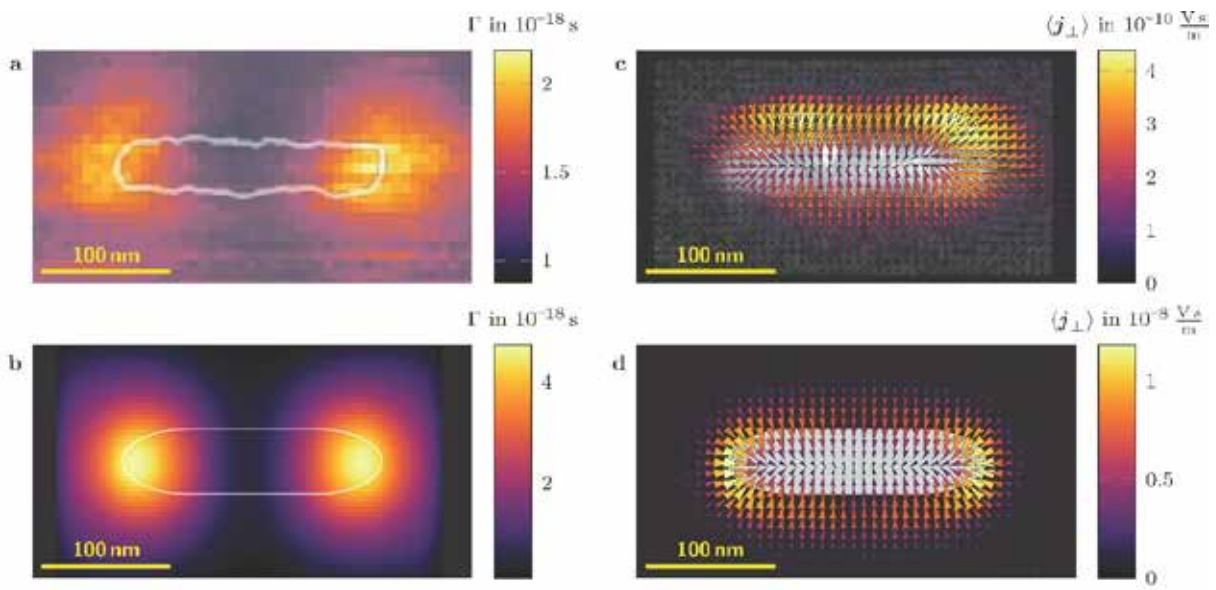


Figure 3 Experimentally measured loss probability (a) and transverse instantaneous fields (c) and comparison with numerical simulations (b,d).

Furthermore, we show how measuring the expectation value of the transverse momentum of electrons inelastically scattered at plasmonic energies allows to measure the deflection of the electron beam owing to the transverse induced fields of the plasmonic resonances. We present successful experimental implementation based on energy filtered nanodiffraction, making use of a post-column image filter. With the support of analytical calculations, we show that this gives quantitative access to these transverse fields, and allows to map previously inaccessible parts of the electromagnetic local density of states, and that the experimental results are in good agreement with numerical simulations.

Discussion

These experimental setups expand the wealth of information that can be obtained from plasmonic excitations in nanoparticles within a conventional transmission electron microscope, adding the charge symmetry and the transverse fields, possibly paving the way to a direct tomographic measurement of the plasmonic fields.

References

- [1] G. Guzzinati *et al.*, Ultramicroscopy **151**, 85 (2015)
- [2] G. Guzzinati *et al.*, Nature Communications, **8**, 14999 (2017)
- [3] J. Krehl *et al.* Nature Communications, In Review, arXiv:1803.04399
- [4] U. Hohenester, Comp. Phys. Commun. **185**, 1177 (2014).
- [5] G.G. acknowledges a Postdoctoral grant from Research Foundation Flanders (FWO).
A.B. and J.V. acknowledge funding from the Research Foundation Flanders (FWO) under project G093417N

Ultrafast Transmission Electron Microscopy with Highly Coherent Pulses

Tyler Harvey¹, Armin Feist¹, Marcel Möller¹, Nara Rubiano da Silva¹, Nora Bach¹, Till Domröse¹, Thomas Danz¹, John Gaida¹, Thomas Rittman¹, Katharina Priebe¹, Sascha Schäfer^{1,2}, Claus Ropers¹

¹ *4th Physical Institute, University of Göttingen, Göttingen, Germany*

² *Institute of Physics, University of Oldenburg, Oldenburg, Germany*

E-mail: tyler.harvey@uni-goettingen.de

Introduction

The spatial resolution provided by transmission electron microscopes is matched by only a few other techniques, but temporal resolution has historically been limited. Even with fast direct electron detectors, it is difficult to achieve better than microsecond temporal resolution to microseconds even with fast direct electron detectors. While one can infer much about the behavior of materials based on atomic-scale structural and chemical analysis, it's possible to learn more by directly imaging nanoscale dynamics. Both dynamic transmission electron microscopy (DTEM) and ultrafast transmission electron microscopy (UTEM) offer this capability through different approaches: DTEM employs a short series of pulses with a sufficient number of electrons to produce one image with each pulse; UTEM employs nearly-single-electron pulses and a stroboscopic pump-probe measurement scheme (see Fig. 1a). DTEM can image irreversible dynamics with nanosecond temporal resolution, but the spatial and spectral resolution are limited by the interaction of the many electrons in each pulse. UTEM can only image reversible processes, but does so with sub-picosecond temporal resolution. While the first UTEMs [1-2] could achieve better spatial and spectral resolution than a DTEM, the flat photocathode they used limited both. A UTEM with a needle-shaped photocathode, for which the emission is confined to nanometer-sized areas, produces highly coherent electron pulses that nearly match the spatial and spectral resolution of a standard TEM [3-6]. We employ this instrument to image lattice dynamics, probe resonances in magnetic nanostructures, and observe ultrafast demagnetization in real space.

Methods

The UTEM at the University of Göttingen employs single-photon photoemission to generate electron pulses from a laser-driven Schottky field-emitter. The emitter is based on a standard single-crystalline (100)-oriented tungsten needle with a zirconium oxide overlayer. Schottky emitters are usually operated at an elevated temperature of about 1800 K and an applied electric field in the range of 0.5-1 V/nm [7]. For a (100)-oriented apex facet, the ZrO overlayer results in a selective workfunction reduction, supporting tunneling-assisted thermal electron emission at moderate temperatures. For their use as photocathodes, the facet-specific reduction of the work function can be utilized to trigger localized linear photoemission from the tip apex. Specifically, we operate the photocathode at temperature low enough to extinguish continuous thermal emission. We then illuminate the apex with femtosecond laser

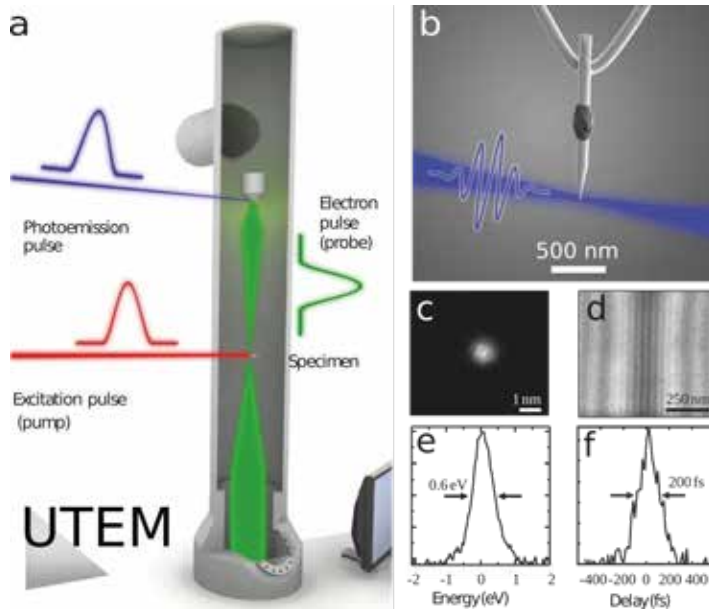


Fig. 1. (a) Schematic of Göttingen UTEM, with stroboscopic laser pump and electron probe. (b) Photoelectron pulses are produced by laser illumination of a heated tungsten tip. (c) Minimum electron spot size. (d) Photoelectron hologram measured with a biprism (adapted from [8]). (e,f) Measured optimal spectral and temporal width.

pulses at a central wavelength of 400 nm (see Fig. 1b). A linear scaling of the photoelectron current with the incident optical fluence is observed, allowing for a flexible tuning of the temporal electron pulse structure. The photoelectron pulses are accelerated to 120 keV in a JEOL 2100F. In the space-charge-free regime, the electron pulses show a narrow spectral width of 0.6 eV and a pulse duration of 200 fs (full-width-at-half-maximum, characterized by electron-light interferometry [8]) (see Fig. 1e,f). We have measured a minimum electron probe size of below 1 nm (Fig. 1c) and a beam emittance down to 1.8 nm-mrad, and a degree of transverse coherence exceeding 10%, calculated from the interference fringes generated by a Möllenstedt biprism provided by the Lichte group in Dresden (Fig. 1d) [8].

Results and Discussion

These exceptional beam properties allow for both coherent manipulation of the electron quantum state to produce electron pulse trains into attosecond bursts [9], as well as observation of structural, electronic and magnetic dynamics on the nm-fs scale. In first experiments (Fig. 2), we have demonstrated the broad applicability of ultrashort electron pulses in high-resolution imaging and diffraction, Lorentz microscopy [10], and scanning diffraction [11]. In one experiment (Fig. 2a), we attached electrodes to a Permalloy nanodisk and applied an alternating electrical bias. The resulting non-uniform spin current through the structure drives a gyrotropic motion of the magnetic vortex domain pattern. This prototypical experiment demonstrates that we can probe MHz and GHz resonant dynamics in magnetic structures. We can also probe demagnetization of magnetic structures. When we illuminated a similar Permalloy nanodisk with a fs optical pulse (Fig. 2b, 2c), we saw that the magnetic

contrast followed the established double-exponential model for demagnetization, with a sub-picosecond drop followed by a longer recovery. This tool can also be used to image structural dynamics. When we illuminated the edge of a graphite flake with a fs optical pulse, we observed a homogenous compression along the axis perpendicular to the plane of the flake (Fig. 2d, left) and a propagating shock wave of shearing motion of the top surface along the axis perpendicular to the edge of the flake (Fig. 2d, right). This collection of results demonstrates that a UTEM with a sharp-tip photoemitter is an excellent tool for high-spatial- and temporal-resolution studies of dynamics in materials.

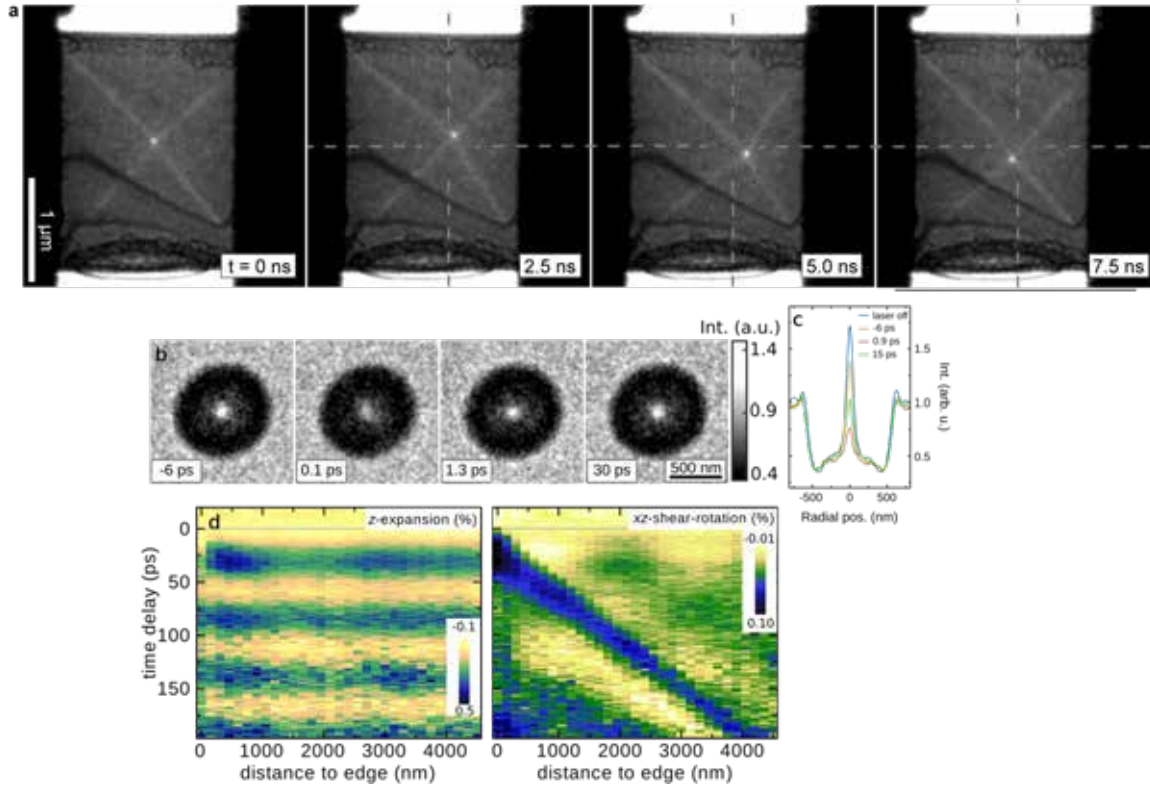


Fig. 2. (a) Gyrotropic motion of a magnetic vortex in a Permalloy nanodisk induced by an oscillating electrical bias. (b) Time series of demagnetization of a vortex domain induced by femtosecond laser pulse [10]. (c) Radial profiles of vortex images in (d) showing drop in contrast. (d) Optically excited strain dynamics near the edge of a graphite flake [11].

References

- [1] H. Dömer, and O. Bostanjoglo, Rev. Sci. Instrum. **74**, 4369 (2003).
- [2] A. H. Zewail, Science **328**, 187 (2010).
- [3] P. Hommelhoff, C. Kealhofer, and M. Kasevich, Phys. Rev. Lett. **97**, 24740 (2006).
- [4] C. Ropers *et al.*, Phys. Rev. Lett. **98**, 043907 (2007).
- [5] A. Paarmann *et al.*, J. Appl. Phys. **112**, 113109 (2012).
- [6] B. Cook, M. Bronsgeest, K. Hagen, and P. Kruit, Ultramicroscopy **109**, 403 (2009).
- [7] M. Fransen, M.H.F. Overwijk, and P. Kruit, Appl. Surf. Sci. **146**, 357 (1999).
- [8] A. Feist *et al.*, Ultramicroscopy **176**, 63 (2017).
- [9] K. E. Priebe *et al.*, Nature Photonics **11**, 793 (2017).
- [10] N. Rubiano da Silva *et al.*, arXiv:1710.03307.
- [11] A. Feist *et al.*, Struct. Dyn. **5**, 14302 (2018).

Analysis of non-diffractive electron Bessel beams for potential application in electron microscopy

S. Hettler¹, L. Grünewald¹ and M. Malac²

¹Laboratory for Electron Microscopy, KIT, Engesserstr. 7, Karlsruhe, Germany

²NRC-Nano and University of Alberta, Edmonton, Canada

E-mail: simon.hettler@kit.edu

The possibility to shape an electron beam, e.g. by (holographic) phase masks, can lead to novel imaging modes in electron microscopy (EM). Besides electron vortex beams [1], quasi non-diffractive Bessel beams (BBs) are promising for numerous applications [2]. We present a detailed analysis of single BBs with high intensity generated by direct phase masks (PMs). The PMs consist of nanostructured silicon nitride thin films surrounded by an obstructing Pt aperture. They are implemented above the first condenser lens C1 of a Hitachi HF-3300 equipped with a cold field-emission gun operated at 300 keV.

The non-diffractive behavior of the electron wave is observed up to a maximum propagation distance $z_{\max} = D/(2\lambda k_p)$ after transmission through the PM which depends on the diameter of the PM ($D = 50 \mu\text{m}$), the electron wavelength λ and the grating periodicity of the PM k_p . We installed several PMs with different k_p , Figure 1 shows a scanning EM image of a PM with $k_p = 0.4 \mu\text{m}^{-1}$. The condenser lens system of the transmission electron microscope can be used to adjust the effective propagation distance between the PM and the specimen plane and to demagnify the resulting BB. Figure 2a depicts a transmission EM image of a BB with a central beam diameter below 0.4 nm generated by the PM shown in Figure 1. The acquisition of an image series with varying excitation of the C1 lens allows to determine the intensity of the central maximum of the BB in dependence of the C1 lens current which is shown in Figure 2b. The curves acquired for PMs with different k_p exhibit the expected trend of increasing intensity with decreasing lens excitation up to the effective z_{\max} which is followed by a rapid drop of intensity. The peak to the left of the curves corresponds to the far field of the PM. The number of oscillations increases with the periodicity of the grating which also leads to a higher distance between the far field and z_{\max} . A higher k_p allows in principle the generation of BBs with a smaller central beam diameter that comes at the cost of a lower intensity of the central maximum.

The results from the detailed analysis of BBs generated by PMs agree well with theory and are the basis for an application in EM. Potential applications could be in scanning transmission EM tomography, ptychography, nano-beam diffraction or in scanning EM.

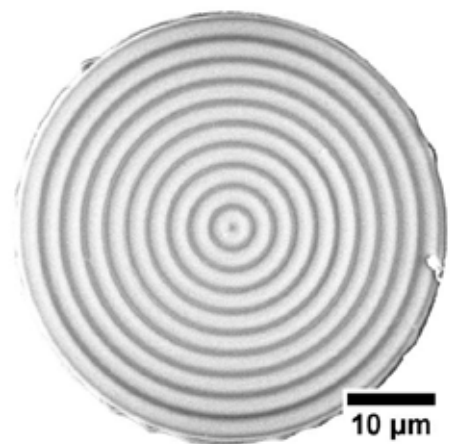


Figure 1: Scanning EM image of a PM with $k_p = 0.4 \mu\text{m}^{-1}$

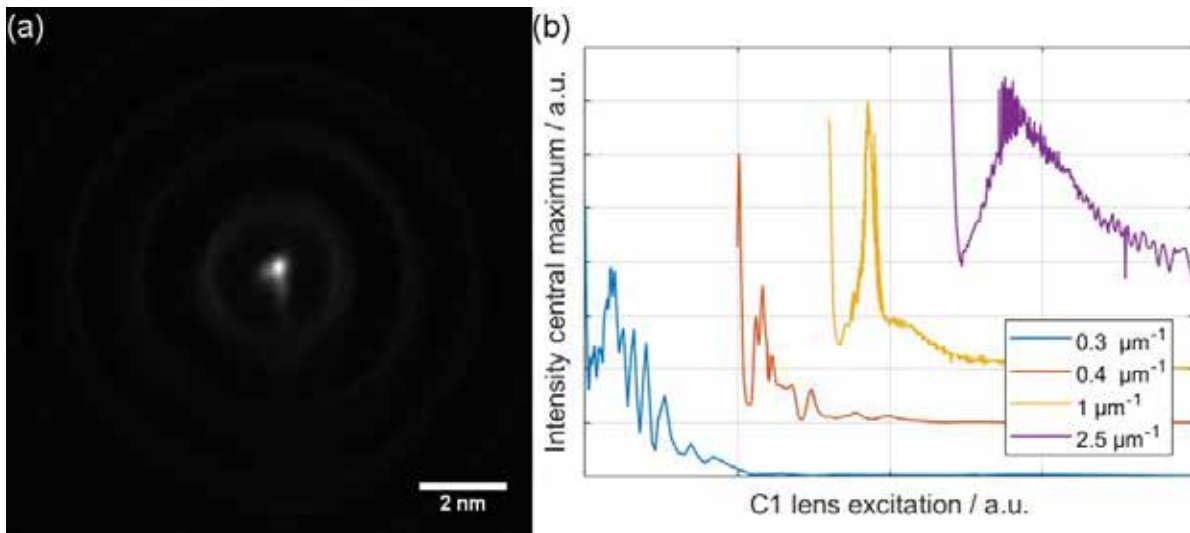


Fig. 2: (a) TEM image of a BB with a central beam diameter below 0.4 nm. (b) Analysis of the central maximum of the BBs reveals the effect of different grating periodicities.

References

- [1] Bliokh et al., Physics Reports **690**, 1 – 70 (2017).
- [2] Grillo et al., Ultramicroscopy **166**, 48 – 60 (2016).
- [3] Funding by the Carl-Zeiss-Stiftung is acknowledged.

Optical multi-pass microscopy

**T.Juffmann^{1,2}, B.B.Klopper², S.A.Koppell², S.Nimmrichter³ and
M.A.Kasevich²**

¹*Faculty of Physics, University of Vienna, Vienna, Austria*

²*Physics Department, Stanford University, Stanford, USA*

³*Centre for Quantum Technologies, National University of Singapore, Singapore*

E-mail: thomas.juffmann@univie.ac.at

Introduction

Multi-pass microscopy has recently been introduced as a method that is potentially capable of reducing sample damage in electron microscopy [1]. I will discuss optical proof-of-principle experiments [2] that show that multi-pass microscopy can enhance sensitivity in phase and in absorption measurements, as well as in scattering studies. Experimental challenges, and ways to mitigate them, will be discussed. I will further describe how a multi-passing setup can be used to iteratively apply orbital angular momentum to a beam of light [3], and how multi-pass measurements compare to ring-down and continuous wave cavity enhanced measurements [4].

- [1] T.Juffmann, S.A.Koppell, B.B.Klopper, C.Ophus, R.M.Glaeser & M.A.Kasevich, Scientific Reports 7, 1699 (2017)
- [2] T.Juffmann, B.B.Klopper, T.L.Frankort, P.Haslinger & M.A.Kasevich, Nature Communications 7, 12858 (2016)
- [3] B.B.Klopper, B. B., T.Juffmann, T. & M.A.Kasevich, Optics Letters 41, 5744 (2016)
- [4] S.Nimmrichter, CF.Chen, B.B.Klopper, M.A.Kasevich & T.Juffmann, arXiv:1704.05217 (2017)

Shaping electron wavepackets with light; Shaping light with electron wavepackets

I. Kaminer

*Faculty of Electrical Engineering, Technion, Haifa 32000, Israel
E-mail: kaminer@technion.ac.il*

Recent years have shown growing interest in shaping wavepackets of photons and electrons, e.g., imbuing them with orbital angular momentum or shaping them with other intriguing structures. My talk will discuss how such capabilities could enable new kinds of interactions between light and matter.

We will discuss how shaping electron wavepackets can alter fundamental processes of light emission: Using the exactly-periodic and highly stable nature of electron wave interference in electron microscope we can control the light emission frequency and angular spectrum.

Conversely, by shaping wavepackets of light we can alter the electron wavepacket and even reach ultrastrong interactions with electrons: Shaping the spatial/temporal profile of laser pulses we can imbue electrons with orbital angular momentum and control their acceleration.

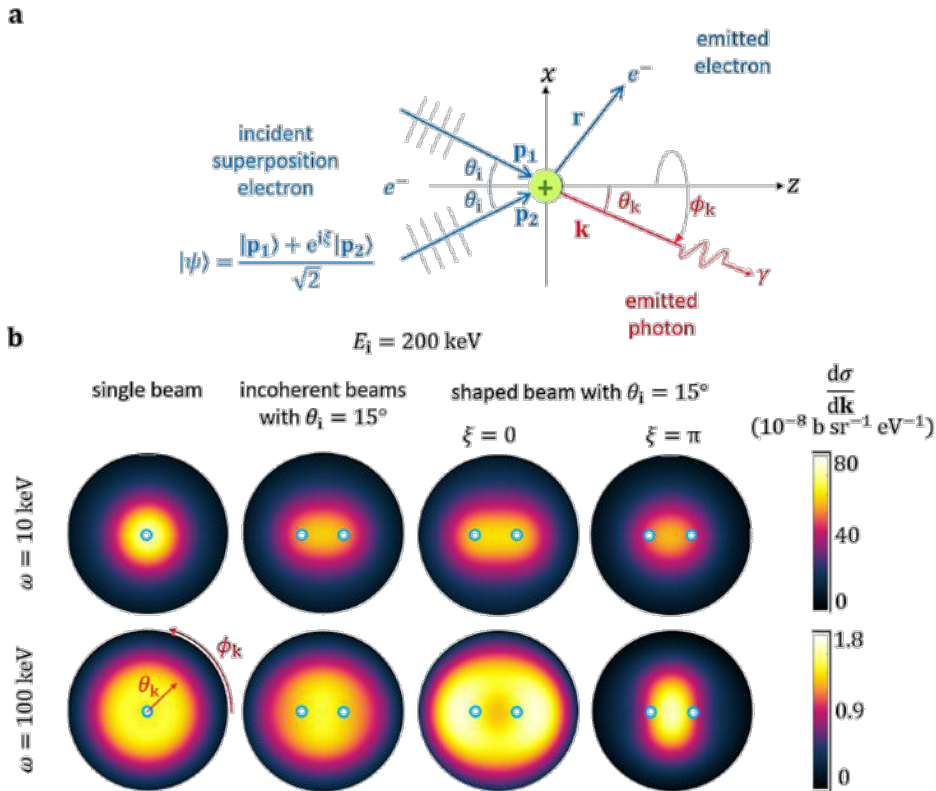


Fig. 1. Shaping radiation with electron interference. (a) A simple shaped electron (superposition of two momentum eigenstates) is scattered off a nucleus and emits a Bremsstrahlung photon in the process. (b) Comparison of angular differential cross section in the forward direction for an unshaped electron and a shaped electron. The blue circles indicate the direction of the incident electron momenta. We find that shaping has a clear effect on the photon emission pattern.

Electron-light interaction in Wigner phase space

P. Kling^{1,2}, M. Carmesin^{2,1}, and W. P. Schleich^{1,3},

¹ *Institut für Quantenphysik and Center for Integrated Quantum Science and Technology (IQST), Universität Ulm, D-89068 Ulm, Germany.*

² *Helmholtz-Zentrum Dresden-Rossendorf e.V., D-01328 Dresden, Germany.*

³ *Hagler Institute for Advanced Study, Institute for Quantum Science and Engineering (IQSE), and Texas A&M AgriLife Research, Texas A&M University, College Station, TX 77843-4242, USA.*

e-mail: peter.kling@uni-ulm.de

Introduction

The description of quantum mechanics in terms of Wigner functions [1] is as close as one can get to classical phase space. Since many schemes for the interaction of free electrons with light, like for example free-electron lasers (FELs) or Smith-Purcell radiation sources, operate in the classical limit, or at the borderline between classical and quantum physics, it is quite natural to study the dynamics of such processes in the framework of Wigner functions.

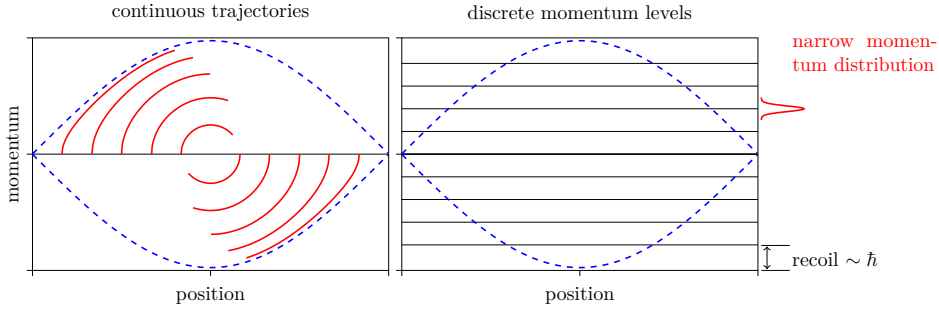


Figure 1: Electron motion in phase space: we contrast the continuous trajectories of the classical case (left) with the discrete momentum steps in the quantum regime (right). For the latter case we require, besides a high recoil, a narrow momentum distribution for quantum effects not being washed out.

The transition from classical to quantum, as it was shown for example in FEL theory [2, 3], occurs when the discrete recoil due to Compton scattering dominates the dynamics and the motion of an electron is characterized by discrete momentum steps instead of the continuous trajectories in the classical case (Fig. 1). In addition, we require a small momentum spread of the electrons, since for a large spread the discrete momentum steps would be smoothed out.

Recently, novel quantum effects for single-electron wave packets were predicted [4] which manifest themselves in the average momentum of the electrons. The Wigner function method enables us to observe such effects directly in the quantum state of the electron. With the help

of recently developed schemes for quantum state tomography of free electrons [5] we can even directly measure the Wigner function and thus gain all knowledge about the electron.

Methods & Results

We consider the time evolution of the Wigner function [1]

$$W(z, p; t) \equiv \frac{1}{2\pi\hbar} \int d\xi e^{-ip\xi/\hbar} \langle z + \xi/2 | \hat{\rho}(t) | z - \xi/2 \rangle$$

for an electron in an FEL configuration. To solve this dynamics we employ perturbation theory which results in an asymptotic expansion of the form $W \cong W^{(0)} + W^{(1)} \dots$ with $W^{(1)} \ll W^{(0)}$.

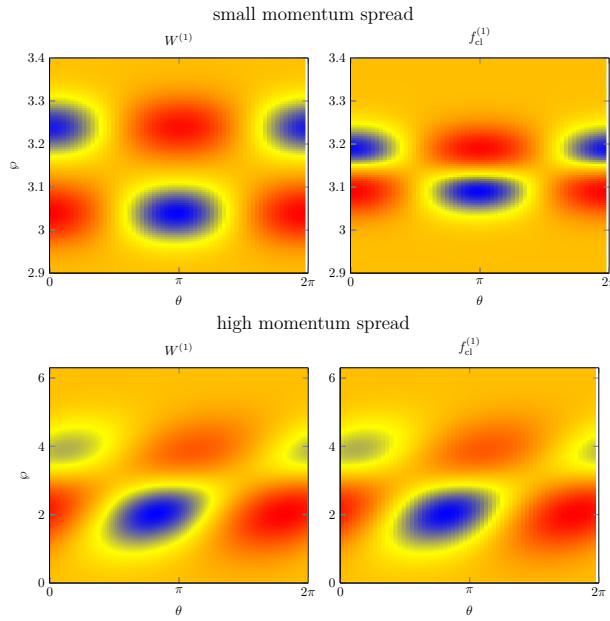


Figure 2: First-order contributions $W^{(1)}$ (left) and $f_{\text{cl}}^{(1)}$ (right) for the evolved Wigner function and classical distribution function, respectively, both subject to the dimensionless phase space (θ, φ) . In all cases the recoil is small. For a small initial momentum spread (above), however, the quantum mechanical and the classical description differ. Only for a broad momentum distribution (below) we obtain the ‘true classical limit’ of the electron state.

The equation of motion for the Wigner function W formally reduces to the one for a distribution function f_{cl} in classical phase space, if we neglect all terms including the quantum mechanical recoil. However, a small recoil is not the full story: for the time evolution of the Wigner function to resemble to its classical counterpart we require that the electrons are initially prepared in a ‘classical state’ [6]. In this case we deal with a statistical mixture of pure states, where the classical, statistical uncertainties are larger than the intrinsic quantum mechanical ones. Moreover, we require that the width of the initial momentum distribution is broad when

compared to the recoil. This transition to the ‘true classical limit’ for the Wigner function is illustrated in Fig. 2.

However, what happens if we employ instead pure states, that is single-electron wave packets? According to Ref. [4] we expect that the transition from a quantum plane wave to a classical point particle is governed by the ratio of the spatial size of the wave packet and of the wavelength of the radiation. Decreasing the width in position space, however, increases the width in momentum space. Thus, the behavior of the wave packet cannot necessarily be considered as ‘point-particle like’. In our phase space approach, we derive an additional condition for the point-particle limit which relates the momentum width of the wave packet to the interaction time.

Outlook

Our perturbative approach breaks down when we consider long interaction times. To go beyond the short-time limit we, therefore, propose two different methods: (i) In an analytic approach we approximate the effective potential, the electron experiences, as an anharmonic oscillator [7]. (ii) Moreover, we perform a numerical analysis which is based on the Mathieu equation [8].

References

- [1] W. P. Schleich, *Quantum Optics in Phase Space*, (Wiley, Weinheim, 2001).
- [2] A. Friedman, A. Gover, and G. Kurizki, Rev. Mod. Phys. **60**, 471 (1988).
- [3] P. Kling, E. Giese, R. Endrich, P. Preiss, R. Sauerbrey, and W. P. Schleich, New. J. Phys **17**, 123019 (2015).
P. Kling, R. Sauerbrey, P. Preiss, E. Giese, R. Endrich, and W. P. Schleich, Appl. Phys. B **123**, 9 (2017).
- [4] A. Gover, and Y. Pan, arXiv:1702.06394 (2017).
- [5] K. E. Priebe, C. Rathje, S. V. Yalunin, T. Hohage, A. Feist, S. Schäfer, and C. Ropers, Nature Photonics **11**, 793 (2017).
- [6] W. B. Case, Am. J. Phys. **76**, 937 (2008).
- [7] M. V. Fedorov, *Atomic and Free Electrons in a Strong Light Field* (Singapore, World Scientific, 1997).
- [8] W. Becker, Z. Phys. B **38**, 287 (1980).

A 10keV Multi-Pass Electron Microscope

S. Koppell¹, T. Juffmann², B. Klopfer¹, M. Mankos³, C. Ophus⁴, M.
Kasevich¹

¹*Stanford University, Stanford, USA*

²*University of Vienna, Vienna, Austria*

³*Electron Optica, Palo Alto, USA*

⁴*National Center for Electron Microscopy, Molecular Foundry, Lawrence Berkeley National
Laboratory, Berkeley, USA*

e-mail: skoppell@stanford.edu

Introduction

Imaging delicate samples with an electron microscope is a shot-noise limited process: resolution is generally limited by the critical dose of the sample rather than the quality of the electron optics. The current state-of-the-art technique, Cryo-Electron Microscopy (Cryo-EM), produces atomic-resolution reconstructions after averaging thousands of noisy images. This process is tedious and potentially erroneous, especially when multiple protein conformations are present. In addition, current techniques don't generate enough contrast to apply this averaging technique to small molecules (<800 kDa) [1].

Multi-Pass Transmission Electron Microscopy (MPTEM) has been proposed as a way to beat the shot noise limit. A MPTEM would use fewer electrons, but pass each one through the sample multiple times. For a thin-phase, low-loss sample the damage reduction at constant signal-to-noise is proportional to the number of passes. Simulations have shown that an order-of-magnitude damage reduction is possible with limiting factors like inelastic loss and phase-wrapping taken into account. [2].

We have designed a 10 keV MPTEM column, which is now being built by Delong Instruments. We will describe the critical elements of the design as well as our plans for validating the column.

Column Design

Our proof-of-concept column contains only electrostatic lenses to minimize its complexity and cost. Ultrafast electron pulses are generated from a laser-triggered tungsten tip [3] then coupled into a linear resonator containing the sample. The resonator is symmetric around the sample and consists of two objective lenses, two field lenses, and two gated mirrors. When a fast 100V pulse is applied to the gated mirrors, they temporarily become lenses - allowing electrons to leave or

enter the resonator. The mirrors are optimized to correct aberrations from the objective lenses to keep round-trip aberrations close to zero. When pulsed open, the gated mirrors are optimized to add minimal aberrations and to shield the beam from transient fields. We use Munro’s Electron Beam Software (MEBS) to characterize the electrostatic properties of our column and ANSYS High Frequency Simulation Suite (HFSS) to analyze the transient properties.

Using a numeric aperture of 3 mrad, the round-trip aberrations in our resonator (mainly spherical aberration) cause a 2nm blur on a 1 micron field of view. The out-coupling process also adds about 2nm blur. We have found that aberrations accrue sub-linearly with the number of passes. Taking diffraction into account, we expect 5-pass resolution to be better than 10nm and 10-pass resolution to be better than 20nm.

Column Validation

Graphene is an excellent candidate for a proof-of-concept measurement since it incurs little inelastic loss and generates so little contrast that it should be invisible for small doses. Figure 1 shows a model of a graphene sheet with a triangular hole. Figure 2 shows the expected results for various doses and numbers of passes.

Acknowledgements

This work is funded by the Moore Foundation as part of the Quantum Electron Microscope collaboration. The collaboration includes Stanford University (Kasevich group), Massachusetts Institute of Technology (Berggren group), Max Planck Institute of Quantum Optics (Hommelhoff group), and Technical University of Delft (Kruit group).

References

- [1] R. Glaeser & R. Hall, Biophysical Journal, **100** (2011)
- [2] T. Juffmann et al., Scientific Reports, **7** (2016)
- [3] Peter Hommelhoff et al., Phys. Rev. Lett., **97** (2006)

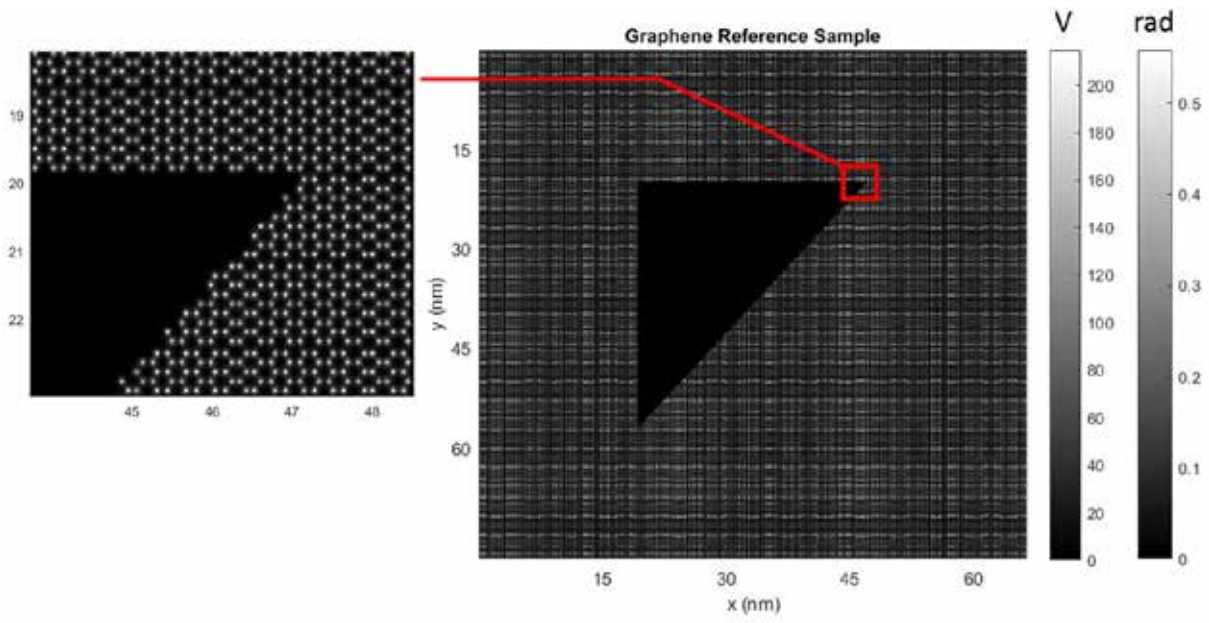


Figure 1: Model of a single graphene sheet. The color scale bars show the projected potential in Volts and the phase shift induced on a 10keV beam. The average phase thickness of the graphene is 0.1 rad.

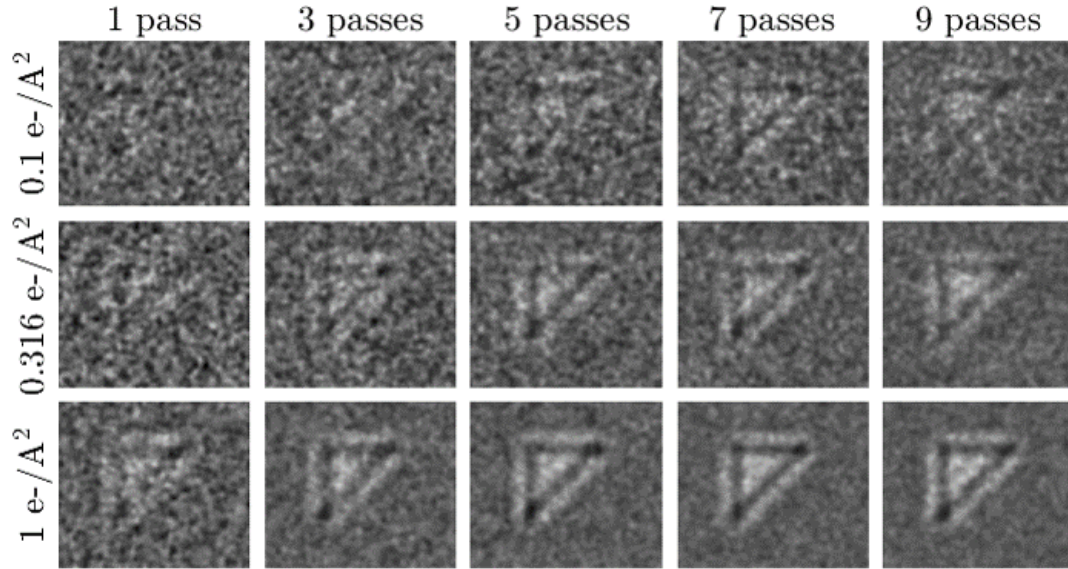


Figure 2: Simulated micrographs of the graphene sheet from figure 1. Phase contrast is generated with $5\mu\text{m}$ defocus. The simulation includes a 2.8% inelastic loss per pass and a spherical aberration coefficient of $C_s = 0.16\text{m}$. Along each row, the number of passes is varied while keeping the dose constant (the number of in-coupled electrons is roughly inversely proportional to the number of passes).

Electron Mode Conversion and Vortex Generation

C. Kramberger¹, S. Löffler¹, T. Schachinger¹, P. Hartel², M. Obermair³,
M. Dries³, D. Gerthsen³, P.-H. Lu⁴, A. H. Tavabi⁴, J. Barthel⁴,
R. E. Dunin-Borkowski,⁴ and P. Schattschneider¹,

¹*Technical University of Vienna, Vienna, Austria*

²*CEOS Corrected Electron Optical Systems GmbH, Heidelberg, Germany*

³*Karlsruher Institut für Technologie, Karlsruhe, Germany*

⁴*Forschungszentrum Jülich, Jülich, Germany*

e-mail: christian.kramberger-kaplan@tuwien.ac.at

Introduction

Since electrons and light can be described as propagating waves, there is potential for mutual inspiration and knowledge transfer between laser and electron beam physics. Laser beams can be mode converted between rectangular patterned Hermite profiles and radially symmetric Laguerre profiles by a pair of cylinder lenses, if the physical diameter of the beam, the distance between the lenses and the wavelength fulfill the conditions of mode matching [1]. The curvature of the phase front as well as the lateral extent have to be radially symmetric. See the illustrations in figure 1.

There are, however, fundamental challenges when such an optical mode converter is to be realized for electron beams. In particular the absence of cylinder lenses as well as true Gaussian sources for electron beams requires modifications of the setup. Spatially confined transient mode conversion of electrons has been demonstrated at a plane in between the two astigmatic line foci [2]. Here, we demonstrate a design for a close analogue to the optical mode converter which acts as a loss-less non-astigmatic vortex generator for electron beams.

The most appealing aspect of this approach to a vortex generator is the attainable maximal yield of fully converting the entire beam to a vortex state, without the need for astigmatism in the probe. Moreover, the electromagnetic quadrupoles can be freely rotated to prepare left and right handed vortices easily.

Methods

We propose to employ a Hilbert plate to prepare an incoming quasi Hermite(1,0) beam and to use the quadrupoles of a DCOR probe corrector from CEOS to realize a mode converter that

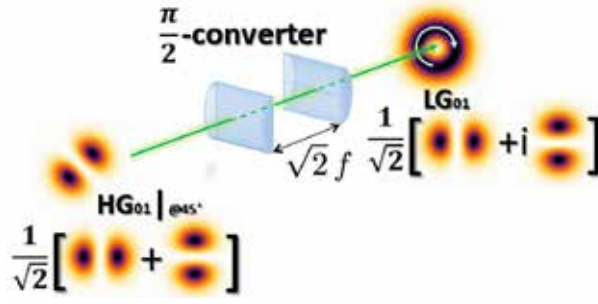


Figure 1: An optical mode converter transforms Hermite to Laguerre Gaussian profiles and vice versa.

<https://commons.wikimedia.org/wiki/File:Mode-converter.png>

avoids any astigmatism in the mode converted beam. The vortex is formed inside the corrector, and maintained thereafter.

We have developed a simulation software for wave propagation that can handle multiple optical elements and spacings in between them. Apertures, lenses and quadrupoles can be inserted, removed, shuffled around and modified. All optical elements in the simulation are represented by two dimensional complex absorbers and/or phase shifters. The propagation from one optical element to the next is calculated by Fresnel propagation in Fourier space. The latter is well justified for wavelengths of 2.5 pm (at 200 keV), beam diameters of μm and distances of cm.

Results

The optical setup was chosen to closely resemble the actual geometry of the PICO microscope at the ER-C in Jülich. In the simulated setup, we consider a round $10\mu\text{m}$ aperture at the second condenser lens (C2). The third condenser lens (C3) is turned off, and the C3 aperture holds a Hilbert plate. We would like to point out that the suggested setup is stable with respect to minor changes ($\leq 1\%$) in lens excitation and even the inclusion of a $1\mu\text{m}$ wide absorbing bar at the Hilbert plate can easily be compensated.

Figure 2 shows two equivalent electron beams for two different kind of Hilbert plates. For numerical reasons (pixel size 8 nm) the objective lens has a focal length of 30 mm. The simulated vortices are expected to be 10 to 15 times magnified compared to actual objective excitations. A notable characteristic is the flat phase after the adapter lens (ADL) at the entrance of the DCOR, which defies the expectations from simple Gaussian beam propagation and also geometric optics. In geometric optics, the ADL would have to be focused onto the 2^{nd} quadrupole, in order to mimic the optical mode converter. These strong deviations from classical behavior are only expected for $\leq 1\mu\text{m}$ wide electron beams, and become negligible around $3\mu\text{m}$ width.

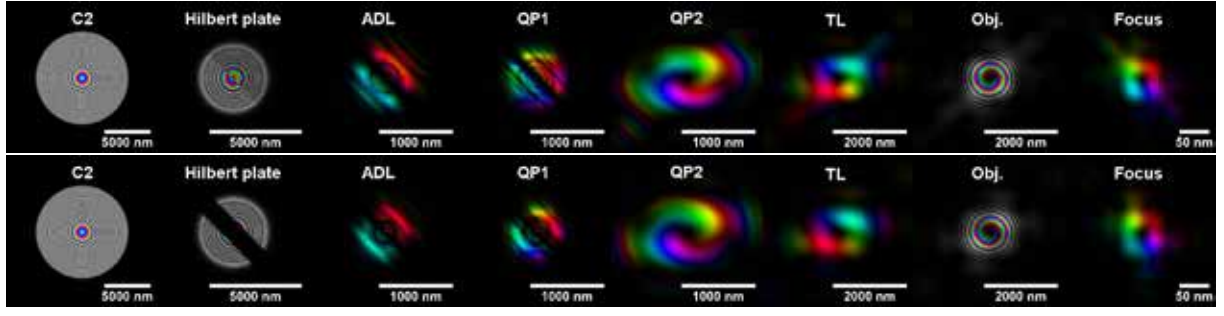


Figure 2: Phase colored beam profiles at 200 keV. With (bottom) and without (top) a central bar in the Hilbert plate. Cross sections in the rows are after the C2 aperture, Hilbert plate, adapter lens (ADL), 1st quadrupole (QP1), 2nd quadrupole (QP2), transfer lens (TL), objective lens (Obj.) and, lastly, in the focus.

Discussion

The required beam diameter of just under 1 μm or apertures below 1 mrad are definitely outside the realm of normal electron microscope operation. In normal operation, when the Fresnel number is $\geq 10^4$, electron beams are well described as Gaussian beams or even by geometric optics. The mode converter operates at the far end of the near field regime where geometric optics utterly fail and substantial deviations from Gaussian optics are observed. The intermediate range with Fresnel number ≥ 10 shows phenomena such as interference between aperture fringes and Airy fringes and defies in many places conventional intuition. We believe that the simulation of the intermediate near field wave propagation will greatly assist the experimental venture into the realm of coherent sub milliradian e-beam optics in search for an equivalent of the optical mode converter.

Acknowledgements

CK & PS acknowledge financial support of the Austrian Science Fund (FWF): P29687-N36
 TS acknowledges financial support of the Austrian Academy of Sciences: DOC-scholarship

References

- [1] Beijersbergen et al, Optics Comm., 96, 123-132, (1991)
- [2] Schattschneider et al, PRL, 109, 084801, (2012)

A setup for electron wave front manipulation using patterned electrostatic mirrors

M.A.R. Krielaart¹ and P. Kruit¹

¹*Delft University of Technology, Department of Imaging Physics, Lorentzweg 1
2826CJ, Delft , The Netherlands
E-mail: m.a.r.krielaart@tudelft.nl*

Introduction

Various methods for electron wave front manipulation have been demonstrated successfully in the field of electron optics. For example, transmission phase contrast enhancement is achieved using electrostatic (Boersch) phase plates [1] and electron vortex beams are generated by passing a beam through a fork-like structured phase plate [2,3]. In another application, phase manipulation may enable the coherent electron beam splitting that is necessary in quantum electron microscopy [4].

Most forms of phase manipulation are achieved by some form of transmission through a foil. The electron-matter interactions however result in undesired side effects such as inelastic scattering of the beam or charging of the phase plate. If instead a reflective mode of operation is used, these problems may be circumvented.

Here, we present a novel setup that can be placed in principle inside the column of an electron microscope. The setup consists of a primary optical axis and a secondary side-axis. A deflector couples the two parallel axis and two mirrors face each other on the secondary axis. In this manner, we expect to perform transmission-type alike phase manipulation, while no electron-matter interaction takes place.

Methods

A schematic of our setup is shown in figure 1. The setup consists of two parallel optical axis, which are separated by a small distance, of the order of 1 mm. The electrons that enter via the primary axis originate from an unmodified electron microscope column. This allows to use existing optics to provide an initial beam condition. The electron beam is focused towards an electrostatic or magnetic deflector on the primary axis. The purpose of this deflector is to couple the primary and secondary axis.

Next, an electromagnetic (Wien filter type) deflector is used to align the incident beam with the secondary axis. The beam is spread out over and reflected by mirror 1. Upon passing through the electromagnetic deflector, the Lorentz force now counteracts the electrostatic force and thus no net deflection occurs. The electron beam remains on the secondary axis and passes through another electromagnetic deflector. The latter is positioned such that only after reflection of the beam by mirror 2, the beam is deflected back towards the primary axis. Here, it passes the coupling deflector again and the beam resumes a trajectory parallel to the primary axis. The setup can be designed such that no net deflection dispersion errors remain after a full round trip of the electron.

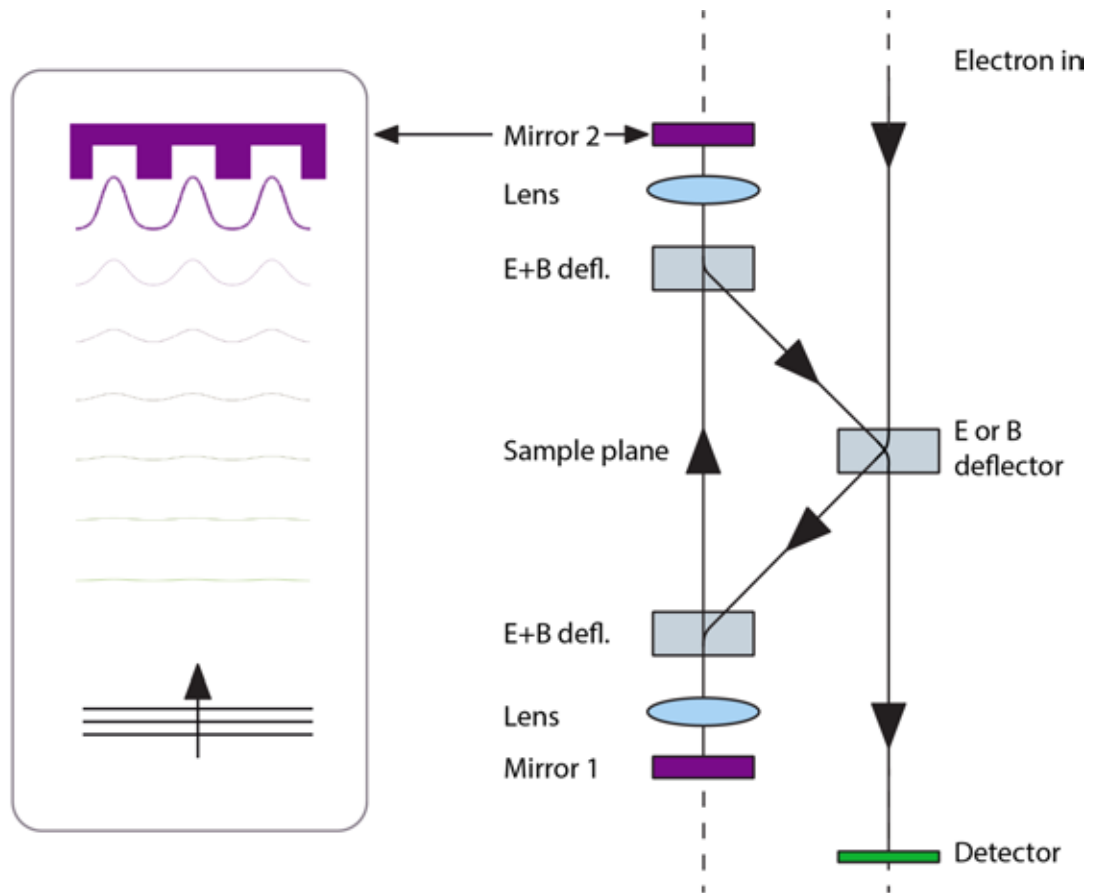


Fig. 1. Schematic of the setup. The incident electron is deflected from the primary axis towards a parallel secondary axis. Here, it is reflected two times before being deflected back towards the primary axis. Phase manipulation of the electron is achieved by shaping the electrostatic mirrors sufficiently.

In one possible mode of operation, mirror 1 consists of an aperture electrode. The resulting mirror potential allows for correction of spherical and/or chromatic aberration that is induced by the setup. Mirror 2 consists of a topological or electrostatic patterned mirror. For example, a grating-like structure will modulate the mirror potential periodically in space. Such electrostatic field is expected to result in phase lags within the wave front and thus diffraction in the far field.

Experimental set-up

We are preparing for initial tests of the principle by putting the double mirror unit in the sample chamber of a scanning electron microscope. The effect of the two opposing mirrors on the electron beam is then observed by placing a scintillator screen (detector) on the primary axis. By patterning mirror 2 with a grating like structure (see figure 1, left) we will attempt to demonstrate the action of such pattern by observing the diffracted beams.

The Wien-type deflectors (figure 2) consist of four electrodes that are fabricated from a magnetic susceptible (high- μ) metal. A coil is wound around each electrode to allow for bidirectional magnetic steering of the beam. The electrostatic deflection potentials are also

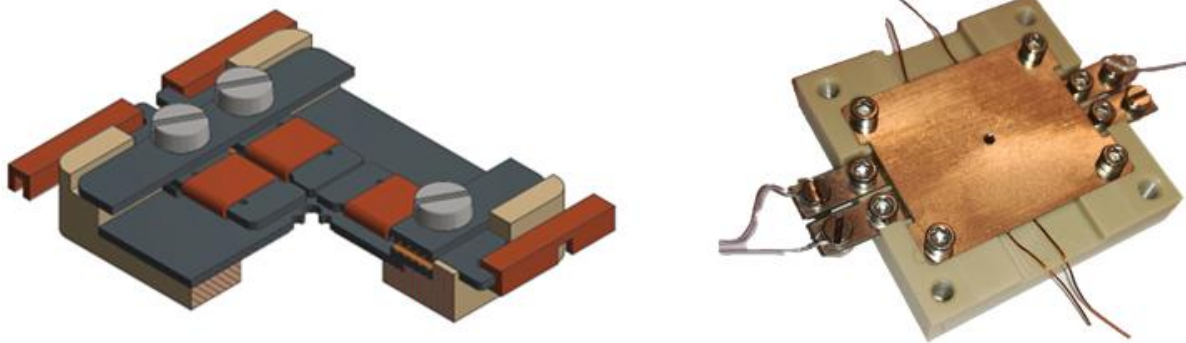


Fig. 2. Schematic (opened) of the electromagnetic deflector design. Three of the deflection electrodes with wound coil are shown. Electrostatic potential is applied via the brown contacts on the outside of the deflector housing. A photograph of the manufactured deflector is shown on the right.

applied to these electrodes. As a result, the magnetic and electrostatic potential fields should completely overlap.

Discussion

At this point, the setup is in development. We managed to reduce the size of the Wien-type deflectors such that the primary and secondary axis are separated by only 1 mm. This limits the deflection angle to 50 mrad thus suppressing any significant deflection aberration errors during the round trip of the electron through the setup. In addition we are investigating the field homogeneity of the deflectors.

The close proximity of the two optical axis is enabled by using MEMS fabricated lens elements. This allows for a compact design that may also fit within the column of a conventional electron microscope. However, MEMS elements yield high aberration coefficients as the electrons pass relatively close to the edge of the lens apertures. Thus, the design of mirror 1 is primarily determined by the total spherical aberration that results from a full round trip of the electron through the setup.

Acknowledgements

The authors like to acknowledge Ruud van Tol for his valuable mechanical support. This project is funded by the Gordon and Betty Moore Foundation and the Netherlands Organization for Scientific Research (NWO).

References

- [1] E. Majorovits et al, *Ultramicroscopy* **107**, pp 213 – 226 (2007)
- [2] M. Uchida and A. Tonomura, *Nature letters* **464**, pp 737 – 739 (2010)
- [3] J. Verbeeck, H. Tian and P. Schattschneider, *Nature letters* **467**, pp 301 – 304 (2010)
- [4] P. Kruit et. al, *Ultramicroscopy* **164**, pp 31 – 45 (2016).

Theoretical study of the interaction between phase-shaped electrons and surface plasmon modes

H. Lourenço-Martins¹, A. Lubk², G. Guzzinati³, J. Verbeeck³, M. Kociak¹

¹*Laboratoire de Physique des Solides, Orsay, France*

²*Leibniz Institute for Solid State and Materials Research, Dresden, Germany*

³*EMAT, University of Antwerp, Antwerp, Belgium*

e-mail: hugo.lourenco-martins@u-psud.fr

Introduction

Electron energy loss spectroscopy (EELS) in the low-loss region has attracted a large interest due to its efficiency in resolving plasmonic resonance at the nanometer scale [?]. However, standard low-loss EELS remained intrinsically unable to detect plasmonic phase and related properties. Nevertheless, phase shaped electron probes constitute a perfect candidate to overcome this limitation and measure the dichroic behavior of plasmons in an electron microscope - as recently pointed out through simulations by Asenjo-Garcia and García de Abajo [?]. Moreover, it has been recently demonstrated that such probes can be created in an electron microscope by tailoring the phase of the beam [?]. In a recent work [?], we performed the first EELS experiment with phase-shaped electron probes and demonstrate that indeed, under specific experimental conditions, information of electron phase can be deduced.

In this contribution, we present the formalism developed in order to model this experiment. Important experimental inputs, such as convergence and collection angles, are considered. Moreover, through a wide variety of numerical studies of interactions between different nano-structures (e.g. helix, rod) and phase shaped electron probes (e.g. vortex beams, Hermite-Gauss beams...), we will demonstrate the different information, unreachable with standard EELS, that phase-shaped probes give access to.

Methods

The simulation code was developed on top of the freely available package MNPBEM [?], a boundary element method simulation code. First, eigenmodes were numerically computed using MNPBEM. Once we obtained the eigenmodes and spectral functions, we integrated equation (??) using for ψ_{\perp} a numerically simulated probe profile.

Results

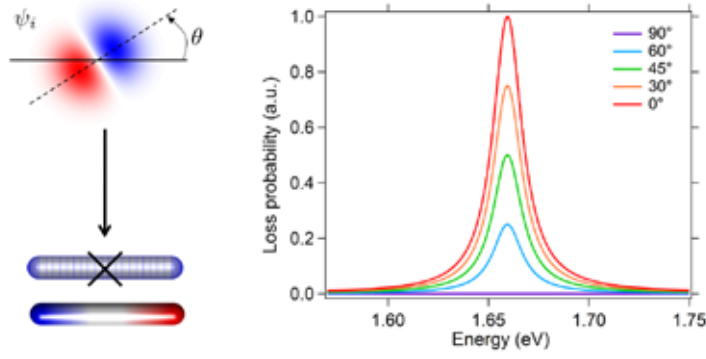


Figure 1: (a) Schematic representation of the simulation: a Hermite-Gauss beam is sent on the dipolar plasmon mode of a silver rod. (b) Corresponding EELS spectra for different orientations of the probe with respect to the rod showing a polarizer effect.

Using a semi-classical formalism for the electron-plasmon interaction [?] and a quasi-static modal decomposition for the surface plasmon [?], we demonstrate that the probability for an incident electron of wavefunction ψ_i with energy $\hbar\epsilon_i$ to lose a certain energy $\hbar\omega$ by interacting with a surface plasmons is:

$$\Gamma(\vec{r}_\perp, \omega) = \frac{2Le^2}{v\hbar} \sum_m \sum_f \Im \{-g_m(\omega)\} \left| \int d^3\vec{r} \psi_f(\vec{r}) \phi_m(\vec{r}) \psi_i^*(\vec{r}) \right|^2 \delta(\epsilon_f - \epsilon_i + \omega) \quad (1)$$

where we sum \sum_f over all the possible final states of energy $\hbar\epsilon_f$. In the latter equation, v and e are the velocity and the charge of the electron, L is the electron quantization length along the its direction of propagation, ϕ_m is the electrostatic potential associated to the m^{th} plasmon mode and g_m is the corresponding spectral function (basically a Lorentzian function peaked at the energy of the plasmon mode). Equation (??) shows that the loss probability takes the form of a transition matrix between an incident and a final electron states mediated by a plasmonic potential. Therefore it gives rise to selection rules which can be used to get information of the plasmon phase. Consequently EELS with phase-shaped electrons is formally analogue to atomic spectroscopy, as discussed in [?].

Therefore, by tailoring the phase of the beam to match the symmetry of a certain plasmon mode, one can selectively detect the desired mode. By playing with the phase of the incident electron, we are therefore able to deduce the symmetry of the plasmon. For example, on figure ??, we demonstrate that by using an Hermite-Gaussian beam with different orientations with respect to a silver nano-rod, one can selectively detect the dipole mode, which is the electronic

analogue of the polarizer effect.

In this work, we demonstrate that this method can be applied to measure several properties unreachable with standard EELS e.g. chirality, radial symmetry, spatial coherence to name a few.

Discussion

In a standard EELS experiments, electrons are integrated over few milliradians in the collection plane to increase the signal to noise ratio (SNR). On the contrary, with phase-shaped we only collect the electrons traveling on the optical axis. Indeed, if we integrate over few milliradians, we sum over several final states in (??) and therefore blur the dichroic effect. The philosophy of our experiment is therefore to study a specific electronic transition mediated by a plasmon mode. The corollary is that only a few number of electrons are collected and the majority of them disregarded, which consequently dramatically reduces the SNR. To overcome this limitation, we developed a relativistic form of the kinetic equation for the electron density matrix [?] and show that this experimental limitation can be overcome by sorting the electron before the detection [?].

References

- [1] J. Nelayah, Nature Physics 3, 348-353 (2007)
- [2] A. Asenjo-Garcia and J. García de Abajo, Phys. Rev. Lett. 113, 066102 (2014)
- [3] J. Verbeeck et al., Nature 467, 301-304 (2010)
- [4] G. Guzzinati et al., Nature Com. 8,14999 (2017)
- [5] U. Hohenester and A. Trügler, Comp. Phys. Com. 183,370-381 (2012)
- [6] J. García de Abajo, Review of Modern Physics 82, 209-275 (2010)
- [7] G. Boudarham and M. Kociak, Phys. Rev. B 85, 1-15 (2012)
- [8] P. Schattschneider et al., Phys. Rev. B 59, 10959-10969 (1999)
- [9] , V. Grillo et al., Nature Com. 8, 6-11 (2017)

Refractive wavefront shaping with a sculpted thin film enables aberration-corrected imaging on uncorrected electron microscopes

P.-H. Lu^{1*}, R. Shiloh^{2*}, R. Remez^{2*}, L. Jin¹, Y. Lereah², A. H. Tavabi¹,
R. E. Dunin-Borkowski¹, and A. Arie²

¹ Forschungszentrum Jülich, Jülich, Germany

² Tel Aviv University, Tel Aviv, Israel

* These authors contributed equally to this work.

E-mail: p.lu@fz-juelich.de

Introduction

The development of the transmission electron microscope (TEM) heralded a new age in the characterization of the atomic structure of matter. However, for a long time its spatial resolution was limited to approximately 100 times the electron wavelength, as a result of the unavoidable positive spherical aberration of electron lenses, as described by Otto Scherzer in a seminal paper in 1936 [1]. His theorem is based on a number of constraints, including the fact that electromagnetic fields generated by round lenses are axially symmetric and static and that the neighborhood of the optical axis is charge-free. He subsequently made several proposals for correcting spherical aberration by relaxing these constraints [2]. It was only two decades ago that Haider et al. [3] and Krivanek et al. [4] finally succeeded in experimentally correcting spherical aberration in the imaging and probe-forming lenses of electron microscopes, respectively, by using non-rotationally-symmetric multipole lenses. However, such correctors require major changes to an electron column, additional stable power supplies, water cooling, precise manufacture, accurate alignment and dedicated operation protocols. Thus, the only practical way to upgrade an uncorrected TEM is to replace it altogether, at considerable cost, by a new aberration-corrected microscope.

An alternative approach involves imparting a structured phase shift to the electron beam by means of changes in the mean inner potential and thickness of a material. The mean inner potential is related to the charge density distribution in a material [5], and can therefore be used to violate Scherzer's charge-free constraint [2]. Although extensive research has been carried out in this direction, attempts to fabricate phase-shifting thin films that act as spherical aberration correctors were never successfully translated into practice. Here, we describe how the primary spherical aberration of the probe-forming optics in a scanning transmission electron microscope (STEM) can now be compensated by using a refractive optical element consisting of a thickness-modulated thin film [6].

Methods

The thin film corrector was fabricated on a SiN membrane using focused ion beam milling with nanometer precision and installed in the Condenser 2 aperture plane on a 300 kV probe-

uncorrected FEI microscope with a known spherical aberration coefficient C_s of 2.7 mm (Figs. 1a-b). The thickness profile of the membrane is designed to compensate a given amount of phase distortion because of spherical aberration. As a result, the probe size could be effectively reduced by opening up the convergence semi-angle to the corresponding optimal value (marked as “x” in Fig. 1c) without probe broadening due to spherical aberration. A deviation of the C_s value or using the corrector at a different accelerating voltage would only result in a different optimal convergence semi-angle.

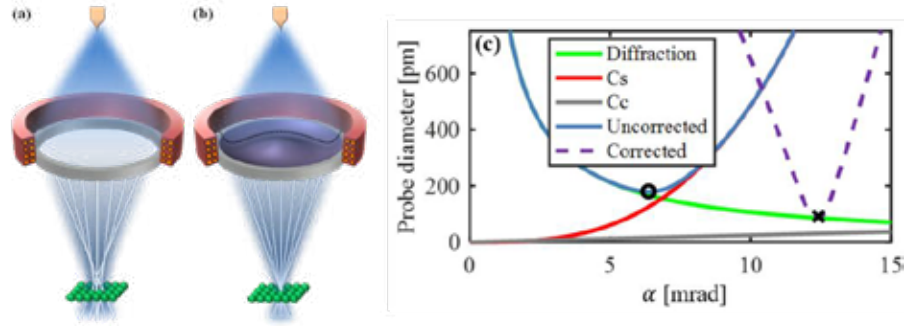


Fig. 1 (a-b) Schematic diagrams of the probe-forming optics without (a) and with (b) using the thin film aberration corrector. (c) The geometric diameter of the electron probe plotted as a function of the convergence semi-angle. It demonstrates the design guideline for opening up the convergence semi-angle without probe broadening due to spherical aberration.

Results

To test the performance of the thin film corrector, high-angle annular dark-field (HAADF) STEM images of crystalline Si $\langle 110 \rangle$ were recorded both without (Figs 2a,b,e,g) and with (Figs 2c,d,f,h) the thin film corrector. A clear improvement in spatial resolution was demonstrated using the corrector, allowing 136-pm-separated dumbbells to be resolved. Further analysis of a through-focus series of Ronchigrams will be presented to show a considerable enhancement of the aberration-free angle in accordance with the intended purpose of phase modulation and spherical aberration correction.

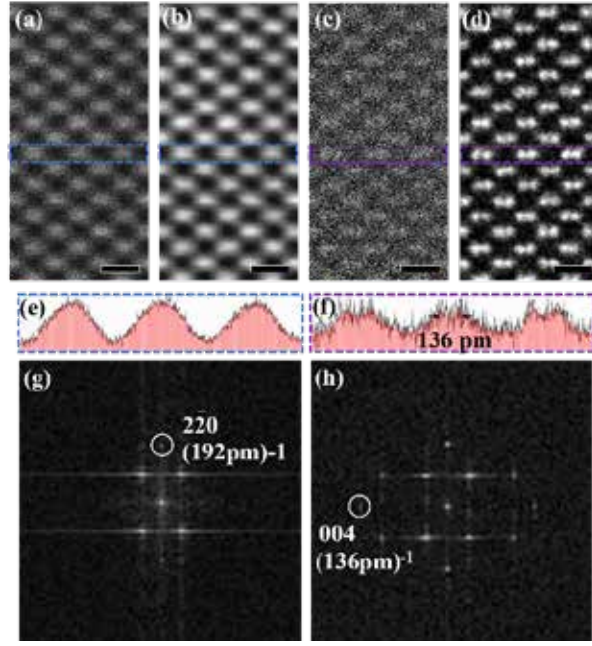


Fig. 2 HAADF STEM images of Si $\langle 110 \rangle$ were recorded without (a,b,e,g) and with (c,d,f,h) the thin film corrector. Images were denoised slightly (b,d) from the raw data (a,c). Intensity profiles of the marked region in (a,b) and (c,d) were plotted in (e) and (f), respectively, including the raw data in black lines and denoised data in pink histograms. (g) and (h) show the Fourier spectrum of the unprocessed images (a) and (c). Only after correction, the 136 pm-separated Si dumbbells become visible, both in the HAADF STEM image and in its Fourier spectrum. The scale bars in (a-d) are 500 pm.

Discussion

A prime challenge in the present concept is scattering by the matter-based thin film corrector. However, as most of the contrast degradation is due to the inelastic tail, it could be reduced by designing the probe-forming optics with an aperture near a crossover above the sample. In addition, using a fractured, thinner design or a different material [7] would also help.

Another frequent concern with the use of thin film phase plates is the issue of contamination. Distinct from phase plates for contrast enhancement located in the high intensity back focal plane of the objective lens, our thin film, which is placed in the condenser plane, is expected to experience a current density approximately 10 orders of magnitude smaller, thereby greatly diminishing charging and contamination. Repeated experiments spanning over 100 hours of irradiation showed no noticeable deterioration in performance.

A further advantage of the present design is that it corrects the electron probe on-axis, requiring practically no change in the standard measurement procedure. It therefore acts as a low cost, plug-and-play upgrade to uncorrected electron microscopes.

References

- [1] O. Scherzer, Zeitschrift Für Phys. **101**, 593 (1936)
- [2] O. Scherzer, J. Appl. Phys. **20**, 20 (1949)
- [3] M. Haider, H. Rose, S. Uhlemann, E. Schwan, B. Kabius, and K. Urban, Ultramicroscopy **75**, 53 (1998)
- [4] O. L. Krivanek, N. Dellby, and A. R. Lupini, Ultramicroscopy **78**, 1 (1999)
- [5] M. Beleggia, L. C. Gontard, and R. E. Dunin-Borkowski, J. Phys. D. Appl. Phys. **49**, 294003 (2016)
- [6] R. Shiloh*, R. Remez*, P.-H. Lu* *et al.*, arXiv:1705.05232 (2017)
- [7] M. Dries, S. Hettler, T. Schulze *et al.*, Microsc. Microanal. **22**, 955 (2016)
- [8] This work was supported by the German Research Foundation (German-Israeli Project cooperation Grant) and the Israel Science Foundation (Grant No. 1310/13). The authors are grateful to Les J. Allen and Juri Barthel for fruitful discussions.

Investigating the proximity of magnetic dichroic signal by atomic sized electron vortex and aberrated beam

Devendra Singh Negi¹, Juan Carlos Idrobo² and Ján Ruzs¹

¹*Uppsala University, Department of Physics and Astronomy, Uppsala, 75237, Sweden*

²*Oak Ridge National Laboratory, Center for Nanophase Materials Sciences, Oak Ridge, Tennessee, 37831, USA*

e-mail: devendra.negi@physics.uu.se

Introduction

Constant growth in nanotechnology and newly emerging nano magnetic structures and phenomena, demands for the tools and techniques, capable of nano and atomic scale magnetometry[1, 2]. In this context, electron magnetic circular dichroism (EMCD) technique in transmission electron microscope (TEM) is promising[3]. EMCD is analogous X-Ray based technique XMCD [4], but provides magnetic information with higher spatial resolution. Recently, atomic scale magnetic information was achieved in EMCD by astigmatic and electron vortex beams probe in TEM [5, 6]. In principle atomic scale magnetic information can be obtained by using atomic size probe in TEM. However, due to long range coulomb interaction, the atomic probe can cause the atomic excitation of distanced atomic columns. Therefore, in order to rationalize the spatial resolution of magnetic information, it is essential to study the proximity of delocalization in EMCD [7]. We study the proximity of magnetic dichroic signal in EMCD by atomic size electron vortex beam and aberrated beam [8].

Methods

Antiferromagnet, LaMnAsO was considered as a test bed material to study the atomic scale delocalization. Electron vortex beam ($\langle L_z \rangle = 1\hbar$) and four fold astigmatic beam ($C_{34b} = 17\mu m$) probes were used to probe the magnetic signal distribution on magnetic atomic columns. Inelastic scattering cross section of Mn- L_3 edge is computed with combined Multislice/Bloch waves approach, as implemented in with MATS.V2 software [9]. All calculation were carried out with z -locality approximation. Scattering angle range was set to ± 40 mrad in both $\theta_{x,y}$ directions respectively. The acceleration voltage of the probe was set to 100 KV.

Figure 1 shows general scheme of calculation. $[3 \times 3 \times 1]$ unit cell of LaMnAsO was considered

for the simulation. In order to attain maximum intensity from astigmatic probe, we introduced an aperture at the center of astigmatic probe.

Results

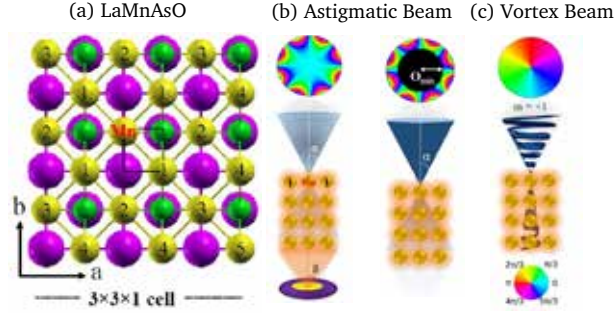


Figure 1: (a) LaMnAsO crystal structure. (b,c) Probes used to investigate the delocalization.

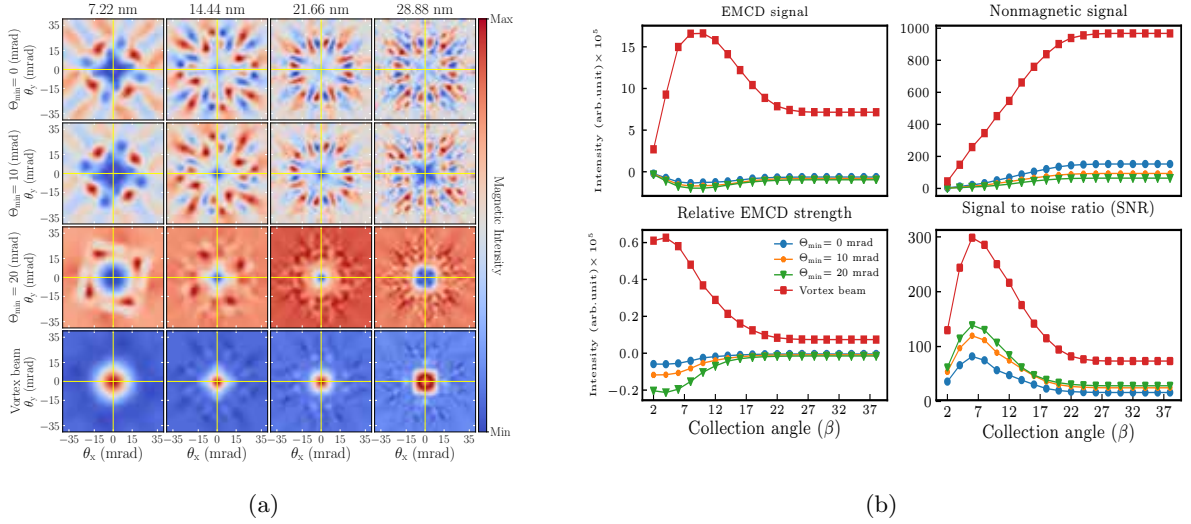


Figure 2: (a) EMCD signal from various probes at various thicknesses. (b) Radial profile of EMCD, nonmagnetic, relative EMCD, signal to noise ratio.

Figure 2 (a) shows the EMCD signal distribution in energy filtered diffraction pattern from various probes at different thicknesses. While probing with astigmatic probe, magnetic signal is distributed at higher scattering angle range, whereas with EVBs the magnetic signal strongly localizes within small scattering angle range. Figure 2 (b) indicates that EVBs dominates the astigmatic probes and excellent SNR can be obtained with EVBs within small collection angle range $\sim 6 - 8$ mrad. Figure 3 shows the EMCD and nonmagnetic signal distribution on nearest neighbored atomic column. With astigmatic probe, magnetic signal localizes on the nearest atomic column. With vortex beam the EMCD and magnetic signal strongly localize on the probed atomic column. Due to excellent localization and high SNR ratio as shown by EVBs,

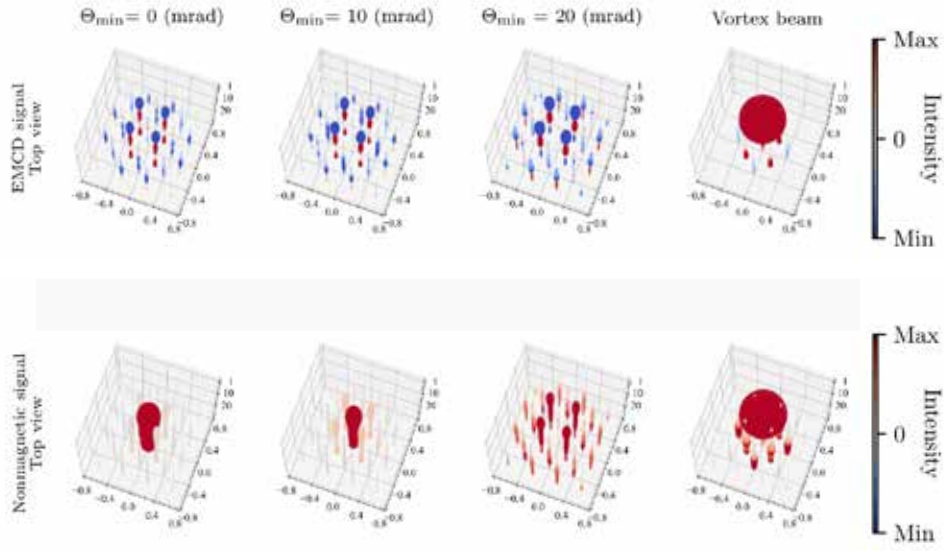


Figure 3: EMCD and nonmagnetic signal distribution on atomic columns.

we suggest that EVBs can be used to probe the crystal site-specific, interface, dopant magnetic properties etc. at atomic spatial resolution.

References

- [1] M. Fuechsle, et al. Nat. nanotechnology 7, 242 (2012).
- [2] R. Wiesendanger, et al. Science 255, 583 (1992).
- [3] P. Schattschneider, et al. Nature. 441, 486 (2006).
- [4] W. L. Chao et al. Nature 435, (2005) 1210.
- [5] J. Rusz, J. C. Idrobo and S. Bhowmick, Phys. Rev. Lett. 113, 145501 (2014).
- [6] J. Verbeeck , H.Tian, P.Schattschneider, Nature 467, 301 (2010).
- [7] J. Rusz et al. Phys. Rev. B 95, 174412 (2017).
- [8] D. S. Negi, J. C. Idrobo and Jan Rusz, Scientific Reports 8, 4019 (2018).
- [9] J. Rusz Ultramicroscopy 177, 20 (2017).

Acknowledgements

D. S. Negi, J. Rusz acknowledge funding from Swedish Research Council, Göran Gustafsson's foundation and Carl Tryggers foundation. J C I acknowledges support from the Center for Nanophase Materials Sciences, which is a DOE Office of Science User Facility. Calculations were performed using resources of the Swedish National Infrastructure for Computing at NSC Center.

Spontaneous and Stimulated Radiative emission of modulated free-electron quantum wavepackets - QED Analysis

Yiming Pan, Avraham Gover

*Department of Electrical Engineering Physical Electronics,
Tel Aviv University, Ramat Aviv 69978, ISRAEL*

Here we present a quantum electrodynamics (QED) analysis of spontaneous and stimulated radiative emission from optically-modulated electron quantum wavepackets. We show that the radiative emission/absorption and corresponding deceleration/acceleration of the wavepackets depend on the controllable quantum wavepacket size, and satisfy an electron-photon spectrum reciprocity of the photon emission into mode q with frequency ω and the particle energy transfer,

$$\Delta v_q + \Delta E/\hbar\omega = 0.$$

We then found for both unmodulated and modulated wavepacket cases that the photon emission rate

$$d v_q / dt = d v_q^{(1)} / dt + d v_q^{(2)} / dt$$

includes

two terms: a phase-dependent term

$$d v_q^{(1)} / dt$$

corresponding to the classical point-particle limit, and a phase-

independent term $d v_q^{(2)} / dt$ corresponding to the quantum plane-wave limit.

The characteristics of the radiative interaction of a wavepacket of length (duration) short relative to the radiation frequency, are close to the predictions of the classical point-particle interaction model [1]. In the long-sized wavepacket limit, the interaction is quantum, and it diminishes at high frequency, see the red line in Fig.1. Figure 1 shows the photon emission spectrum of an optically modulated quantum electron wavepacket as a function of the electron drift time and frequency in a Smith-Purcell radiation experiment [1-2]. Here we study

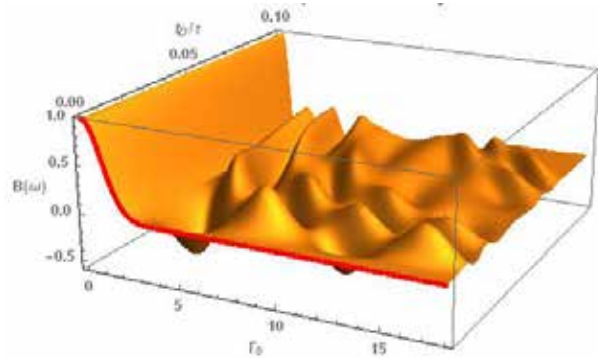


Fig.1: *The wavepacket-dependent stimulated radiance of modulated wavepacket and its dependence beyond the frequency cut-off.*

the harmonic frequency photon emission rate of the modulated electron wavepacket and its superradiance beyond the frequency cut-off [2]. This wavepacket-dependent emission transition from classical to quantum regime suggests a new direction to explore the light-matter interaction.

Reference:

- [1] A. Gover, Y. Pan, arXiv:1702.06394v4.
- [2] Y. Pan, A. Gover, Quantum Electrodynamics Theory of Electron Wavepacket, to be submitted.

Low-dose cryo electron ptychography via non-convex Bayesian optimization

Philipp M. Pelz^{1,2}, Robert Bückner¹, Günther Kassier¹, R. J. Dwayne Miller^{2,3}

¹*Max Planck Institute for the Structure and Dynamics of Matter, Center for Free Electron Laser Science, Luruper Chaussee 149, 22761 Hamburg, Germany*

²*Department of Physics, University of Hamburg, Hamburg 22761, Germany*

³*Departments of Chemistry and Physics, University of Toronto, 80 St. George Street, Toronto M5S 1H6, Canada*

E-mail: philipp.pelz@mpsd.mpg.de

Introduction

Electron ptychography has seen a recent surge of interest for phase sensitive imaging at atomic or near-atomic resolution. However, applications are so far mainly limited to radiation-hard samples, because the required doses are too high for imaging biological samples at high resolution.

We propose the use of non-convex Bayesian optimization to overcome this problem and show via numerical simulations that the dose required for successful reconstruction can be reduced by two orders of magnitude compared to previous experiments. As an important application we suggest using this method for imaging single biological macromolecules at cryogenic temperatures and demonstrate 2D single-particle reconstructions from simulated data with a resolution up to 5.4\AA at a dose of $20\text{ e}/\text{\AA}^2$. When averaging over only 30 low-dose datasets, a 2D resolution around 3.5\AA is possible for macromolecular complexes even below 100kDa. Experiments are currently ongoing and we might present first experimental results at the conference.

Results

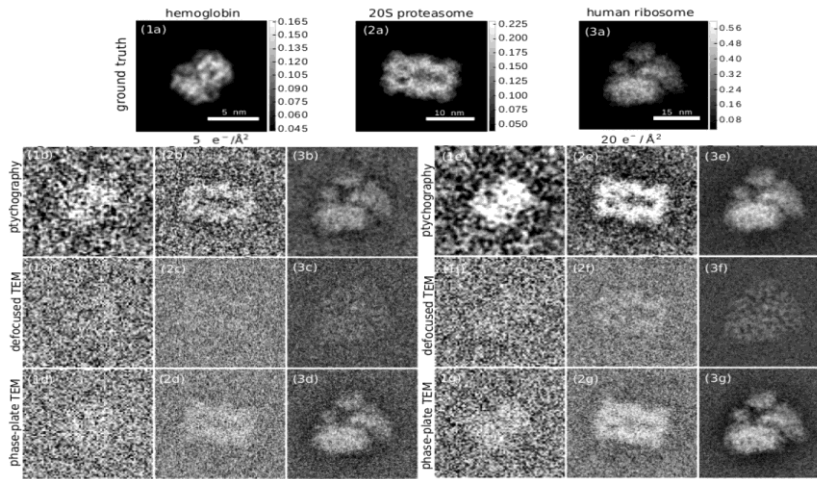


Fig. 2 Cryo-electron ptychography reconstructions from simulated data and simulated cryo-EM images for different doses and 3 macromolecules with growing molecular weights in columns 1-3. Row a): Phase of the transmission function, the ground truth for the ptychography reconstructions. The scale bar next to the figures is in rad. Rows b) and e): ptychography reconstruction at doses of $5 \text{ e}^-/\text{\AA}^2$ and $20 \text{ e}^-/\text{\AA}^2$. Rows c) and f): Simulated cryo-EM image with a defocus of $1.6 \mu\text{m}$ at a dose of $5 \text{ e}^-/\text{\AA}^2$ and $20 \text{ e}^-/\text{\AA}^2$. Rows d) and g): Simulated cryo-EM image with a Zernike phase plate and a defocus of 50 nm at doses of $5 \text{ e}^-/\text{\AA}^2$ and $20 \text{ e}^-/\text{\AA}^2$. Column (1) hemoglobin, column (2) 20S proteasome, column (3) human ribosome.

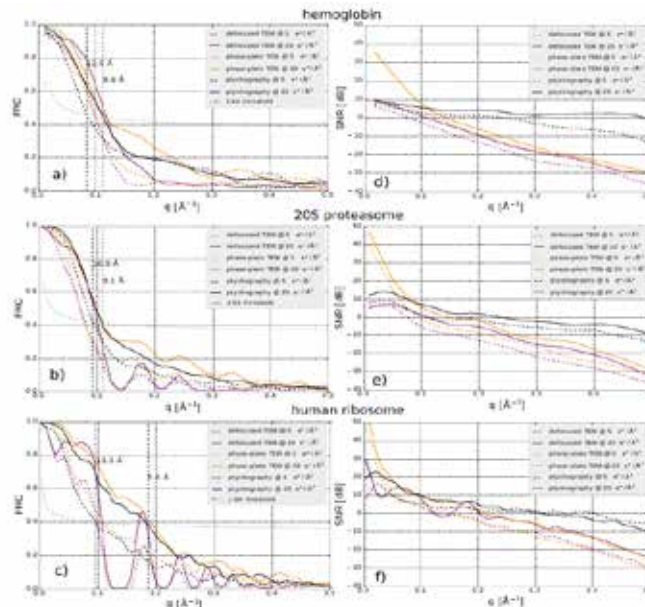


Fig. 2 FRC a) - c) and SNR d) - f) as a function of spatial frequency for the cryo-electron ptychography reconstructions and simulated cryo-EM images in Fig. 2

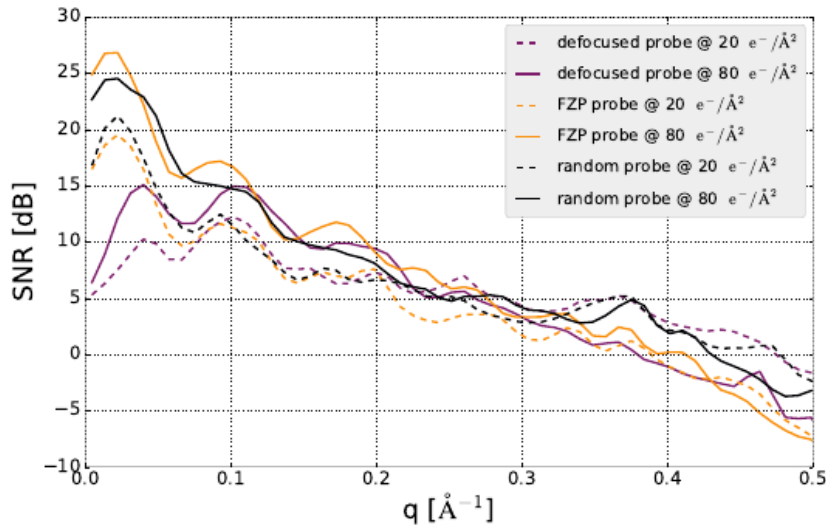


Fig. 3 SNR of reconstructions of the human ribosome at different radiation doses using the defocused probe, the Fresnel zone plate and the randomized probe.

Methods

We employ a recently developed on-convex Bayesian optimization algorithm with a strong denoising prior.

Discussion

We have, via numerical experiments, demonstrated the feasibility of retrieving high-resolution electron transmission phase information of biological macromolecules using ptychography and Bayesian optimization. With the methods presented in this paper, it should be possible to achieve a resolution better than 1nm for true single-particle imaging of molecular complexes with molecular weights ranging from below 100kDa to a few MDa, and a resolution around 3Å with simple averaging of 30 datasets. We have given an explanation of the optimization and initialization procedures used, and emphasize the importance of choosing an appropriate illumination function. The development of an optimized experimental scheme, including design of the illumination function and scanning scheme is a promising direction of research and may enable significant improvement to the results presented here.

References

- [1] Pelz, P. M., Qiu, W. X., Bückner, R., Kassier, G. & Miller, R. J. D. Low-dose cryo electron ptychography via non-convex Bayesian optimization. *Scientific Reports* **7**, 9883 (2017).

Digital imaging and detectors; the benefit of a trained neural network

Paul van Schayk, Peter J. Peters & Raimond Ravelli

*The Maastricht Multimodal Molecular Imaging institute
www.maastrichtuniversity.nl/m4i
Maastricht University, The Netherlands*

Digital imaging and detectors that count each electron individually provided a giant leap in resolution at which structural biologists can study macromolecules and complexes thereof. Ideally, the position, time and energy of each individual electron that arrives at the detector surface could be detected with sub-pixel accuracy. The ultimate direct-electron detector will have an ideal curve for both the detective quantum efficiency (DQE) and modulation transfer function (MTF), will have energy-resolving capacities, a large active area and are fast enough to record data at time scales during which sample drift is not an issue. The current range of commercially available direct electron detectors, while being an improvement over traditional film based or CCD solutions, do not reach ideal DQE and MTF figures. Moreover, their best DQE and MTF results have only been obtained at 300 keV. Hybrid pixel detectors (HPD) which have a separate sensor layer bump bonded to per-pixel electronics may have the properties to reach better DQE and MTF figures. Originally developed at CERN, the Timepix3 HPD is part of the Medipix detector family. The Timepix3 can read 120 MHit/s in a noise-less data-driven readout and has spectroscopic properties per pixel. In here, an initial characterisation of the Timepix3 HPD for application in electron microscopy is presented. The camera has been mounted under a 200kV FEI Tecnai Arctica microscope. The simulation package GEANT4Medipix, developed and validated by Kraphol et al. for X-rays, has been adapted to simulate the interactions of the incident electron track in the sensor layer, the drifting of hole pairs and the electronics responsible for digitising the electronic signal. Series of simulated digitised spectroscopic pixel output response has been used to train a convolution neural network to predict the incident position of the electron within a pixel cluster. The neural network is able to predict, on average, 0.41 pixel from the incident electron position and in 81% of the clusters the correct pixel containing the incident electron position. Global statistical characteristics of the simulated detector response is shown to be in good agreement with first experimental results. The trained neural network has been used to determine point of impact of individual electrons using real data and results are compared with traditional ways to determine point of impact such as centroid.

meV Resolution in Laser-Assisted Energy-Filtered Transmission Electron microscopy

E. Pomarico¹, I. Madan,¹ G. Berruto,¹ G. M. Vanacore,¹ K. Wang,² I. Kaminer,² F. J. García de Abajo,^{3,4} and F. Carbone¹

¹*Laboratory for Ultrafast Microscopy and Electron Scattering (LUMES), Institute of Physics, École Polytechnique Fédérale de Lausanne (EPFL), Lausanne, Switzerland*

²*Andrew and Erna Viterbi Department of Electrical Engineering, Technion-Israel Institute of Technology, Haifa, Israel*

³*ICFO - Institut de Ciències Fotoniques, The Barcelona Institute of Science and Technology, 08860 Castelldefels (Barcelona), Spain*

⁴*ICREA-Institució Catalana de Recerca i Estudis Avançats, Passeig Lluís Companys, 23, 08010 Barcelona, Spain*

E-mail: enrico.pomarico@epfl.ch

Introduction

The low-energy spectrum of quantum solids reflects the variety and the complexity of most of their topological, electronic, structural and magnetic properties [1]. To fully characterize and manipulate many-body excitations in the far-infrared energy range, combining simultaneously meV-spectral, nm-spatial and fs-temporal resolution is needed. Energy-filtered transmission electron microscopy (TEM) can provide imaging of phonons and plasmons in nanostructures with sub-nm [2] and 10s meV space/energy resolution [3,4], but only under static conditions. On the other hand, fs-resolved spectroscopy and microscopy techniques are very well established, but do not have sufficiently high resolution in space, because of the diffraction limit [5], or in energy, due to the spectral spread of the probe beam and the finite energy resolution of spectrometers [6].

We propose a laser-assisted ultrafast TEM method, where the energy resolution is not determined by the electron beam and spectrometer energy spreading, but solely by the laser pulse linewidth [7]. When electrons traverse a nanostructure, the transient electric field associated with them excites plasmonic resonances (PRs), manifesting themselves as features in an energy-loss spectrum (Fig. 1a). In ultrafast TEM, the intensity of the electron pulses is strongly attenuated to reduce space charge effects. Under these conditions, their energy bandwidth is broadened to the eV level, limiting the investigation of features at smaller energy scales. By illuminating the nanostructure with an optical pulse at a resonant energy, a specific PR can be excited and multiples of the PR energy can be exchanged with the imaging electron beam (Fig. 1b). This effect is at the basis of the photon-induced near-field electron microscopy (PINEM) [8-10]. By scanning the laser wavelength across the PRs and mapping their spatial profile after filtering all inelastically scattered electrons (Figure 1c), one can resolve the modes with an energy resolution only limited by the laser linewidth, and not by the electron-beam energy bandwidth.

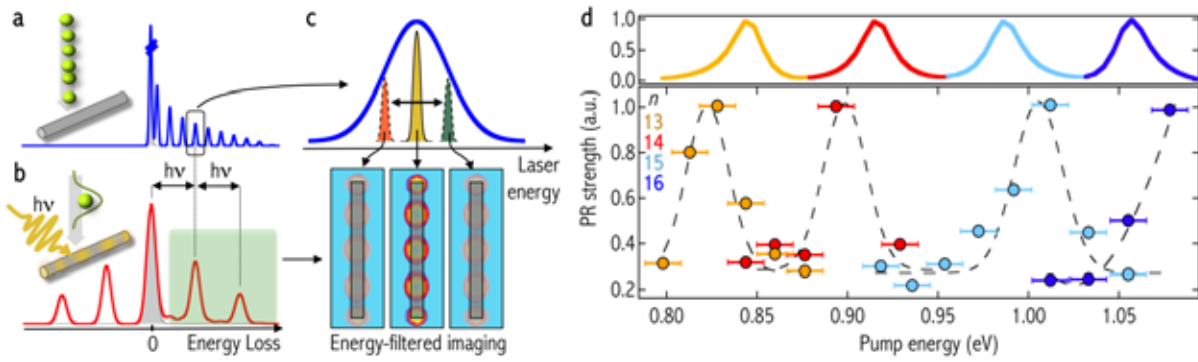


Fig. 1 **a.** Sketch of an EELS spectrum of PRs excited in a nanowire by passing electrons. **b** EELS spectrum under ultrafast TEM conditions. Upon photo-excitation of a specific PR with light pulses of energy $h\nu$, multiples of this energy are exchanged between the electrons and the plasmonic mode. **c.** The laser excitation wavelength is scanned and the PR profile is retrieved via a quantitative analysis of the energy-filtered images. **d.** Normalized PR strength for modes $n = 13-16$ obtained with an integrated spatial FT procedure upon scanning the laser energy. Simulations on top. The figure has been adapted from Ref. [7].

Methods and results

A 300 kHz train of linearly polarized, 800 nm, 80 fs, optical pulses is split to generate two beams. One beam is frequency tripled to deliver few-nJ ultraviolet pulses utilized to photoemit electrons from a LaB₆ cathode in a modified JEOL TEM operated at 200 kV [11]. The second beam is used to seed an optical parametric amplifier (OPA), producing infrared (IR) signal beams between 1150 nm (1080 meV) and 1550 nm (800 meV), with energy per pulse in the 1–2 μ J range, depending on the wavelength. The near-IR pulses are focused inside the TEM on the sample, which is based on silver nanowires of 100 nm diameter lying on a 50 nm thick Si₃N₄ support film. Electrons probe the excited specimen, are then energy-filtered by a Gatan electron energy-loss spectrometer and detected by a CCD camera.

Spectral profiles of PRs optically excited in a 8 μ m long Ag nanowire have been retrieved by PINEM via the IR tuneable optical pulses from the OPA combined with a quantitative analysis of the energy-filtered images. In resonance with a certain PR, a clear spatial profile, revealing the order of the mode n , is obtained. By performing the spatial Fourier transform (FT) of the images and plotting the area under the FT curves associated with a particular PR as a function of the driving laser wavelength, the plasmonic spectral profile is obtained with an energy resolution of 20 meV, which corresponds to the bandwidth of the near-IR pulses. Fig. 1d shows the measured spectra for $n = 13-16$ modes, which are in rather good agreement with simulations based on boundary-element-method calculations of the optical field [12].

Discussion

This method represents a valuable tool to provide a full dynamic characterization and control of low energy excitations without relying on the energy broadening of the incident

electron beam. In fact, the central frequency and the resolution used to image a specific mode are solely determined by the light excitation properties. Optical sources of high monochromaticity and controlled temporal profile are readily available at energies covering a wide spectral range and can provide a broader parameter space compared with state-of-the-art electron optics. If one partially sacrifices time-resolution, ultra-high resolution experiments (even below 1 meV) can be even conceived, by using the intrinsic small linewidth of laser sources or spectral shaping techniques.

A number of fields could benefit from the combination of high resolution in energy, space and time provided by this laser-assisted TEM technique. New fundamental aspects about the coupling between different collective excitations, such as phonons and plasmons in a nanostructure, could emerge. For instance, by exciting the IR active phonons in carbon nanotubes at around 200 meV [13], one could investigate the spatial changes and the spectral shift of PRs as a function of the wire elongation. Other perspectives in chemistry and sensing, like tailoring the chemical sensitivity of nanosensors could be opened with this technique [14]. As an example, the effect of plasmonic enhancement that can be induced by nanostructures on the surface plasmon polaritons (SPPs) excited on a grating [15,16] could be tracked spatially and spectrally in a complete way.

References

- [1] W. Witczak-Krempa et al, *Annual Review of Condensed Matter Physics* **5**, 57 (2014).
- [2] P. D. Nellist et al, *Physical Review Letters* **81**, 4156 (1998).
- [3] O. L. Krivanek et al, *Nature* **514**, 209 (2014).
- [4] M. J. Lagos et al, *Nature* **543**, 529 (2017).
- [5] M. Burrelli et al, *Physical Review Letters* **105**, 123901 (2010).
- [6] D. T. Valley et al, *Nano letters* **16**, 7302- 8 (2016).
- [7] E. Pomarico et al, *ACS Photonics*, doi:10.1021/acsp Photonics.7b01393 (2017).
- [8] B. Barwick et al, *Nature* **462**, 902 (2009).
- [9] S. T. Park et al, *New Journal of Physics* **12**, 123028 (2010).
- [10] L. Piazza et al, *Nature Communications* **6**, 6407 (2015).
- [11] L. Piazza et al, *Chemical Physics* **423**, 79 (2013).
- [12] F. J. García de Abajo et al, *Physical Review B* **94**, 041404 (2016).
- [13] U. J. Kim et al, *Physical Review Letters* **95**, 157402 (2005).
- [14] J. N. Anker et al, *Nature Materials* **7**, 442 (2008).
- [15] A. W. Wark et al, *Analytical Chemistry* **79**, 6697 - 701 (2007).
- [16] J. Lv et al, *Journal of Nanomaterials* **2015**, 1 (2015).

Tailoring the Spectral and Angular Response of Smith-Purcell Radiation

Roei Remez^{1*}, Niv Shapira¹, Charles Roques-Carmes², Romain Tirole^{2,3}, Yi Yang², Yossi Lereah¹, Marin Soljačić², Ido Kaminer^{2,4} and Ady Arie¹

¹*School of Electrical Engineering, Fleischman Faculty of Engineering, Tel Aviv University, Tel Aviv, Israel.*

²*Research Lab of Electronics, MIT, Cambridge, MA 02139, USA*

³*Department of Physics, Faculty of Natural Sciences, Imperial College London, London SW7 2AZ, UK*

⁴*Department of Electrical Engineering, Technion – Israel Institute of Technology, Haifa 32000, Israel*

*Correspondence to: roei.remez@gmail.com.

The Smith Purcell effect was first observed in 1953 [1] and has been studied extensively ever since, as it holds the promise to generate radiation in otherwise unreachable spectral ranges. However, this effect, which is observed when an electron passes next to a metallic grating, was mainly studied up until now using periodic gratings, and the radiation direction and wavelength λ_0 are therefore always associated by the dispersion equation:

$$\lambda_0 = \frac{\Lambda}{n} \left(\sin \phi \sin \theta_n - \frac{c}{v_0} \right) \quad (1)$$

where n , the diffraction order, is a negative integer, v_0 is the velocity of the electron, c is the speed of light, Λ is the grating period and θ_n, ϕ are the direction angles of the emission, defined in Fig. 1(b). When coupling the radiation emitted towards direction (θ_n, ϕ) to a spectrometer in ordinary Smith-Purcell experiments, the resulting spectrum for the first diffraction order ($n = -1$) is a single peak around λ_0 .

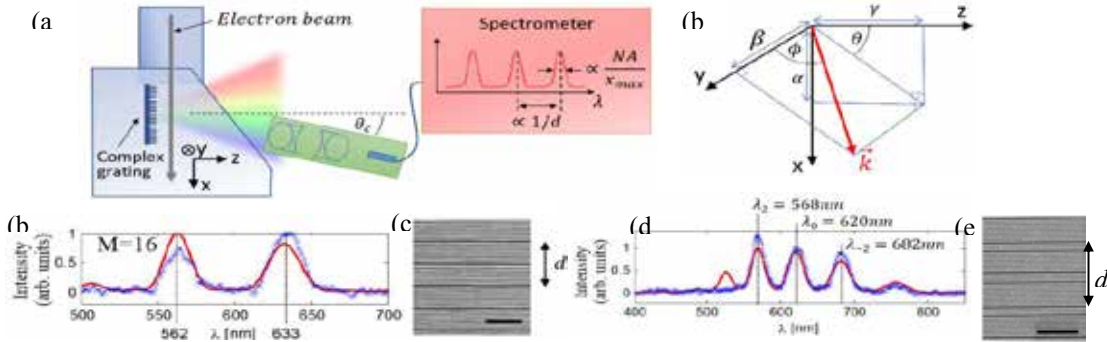


Fig. 1. (a) The experimental setup. Inset to (a) – the spectral response of the first diffraction order of the radiation exhibit multiple peaks with spacing and width inversely proportional to d and the interaction length $2x_{\max}$. (b) – Definition of angles and momentum components of the emitted light. (b,d) - Spectrum and (c,e) grating images of twin-peak and triple-peak Smith Purcell experiments. The solid red curves are the theoretical predictions of the

spectrum, and blue x is the experimental results. Peaks locations are calculated according to eq. (2).

In our work [2], we show that the spectrum of the radiation can be tailored to a desired shape by using non-periodic gratings. First, we show that half-period jumps in the grating can be used to create twin- and triple-peak spectral responses (Fig. 2(b-e)). The same multi-peak behaviour is obtained when one examines the radiation at a constant wavelength, varying the observation angle θ . The special gratings produce spectral peaks which are centered according to a new dispersion equation (for $\phi = \pi/2$):

$$\lambda_{mn} = \frac{\sin\theta_c - \frac{c}{v_0}}{\frac{n}{\Lambda} + \frac{m}{d}} \quad (2)$$

Where θ_c is the angle of observation, d is the period of the supercell of the modified grating, and m is an integer (positive or negative). A more detailed study on the design steps and the effect of interaction length can be found in Ref. [2].

Second, we suggest theoretically that the same concept can be used to create a converging radiation in y-z axis, effectively producing the effect of a cylindrical lens (Fig. 2). This is done by continuously changing the grating's period Λ , effectively resulting in a chirped grating. The expression for the grating period as a function of x , for a lens with focal length $f_{len}(\lambda_c)$ is given by:

$$\Lambda(x) = \frac{n\lambda_c}{\frac{x}{\sqrt{f_{len}^2 - x^2}} - \frac{c}{v_0}} \approx \frac{n\lambda_c}{\frac{x}{f_{len}} - \frac{c}{v_0}} \quad (3)$$

These manipulations of Smith-Purcell radiation are especially interesting for deep-UV and X-Ray applications, where lenses and filters are inefficient or inexistent.

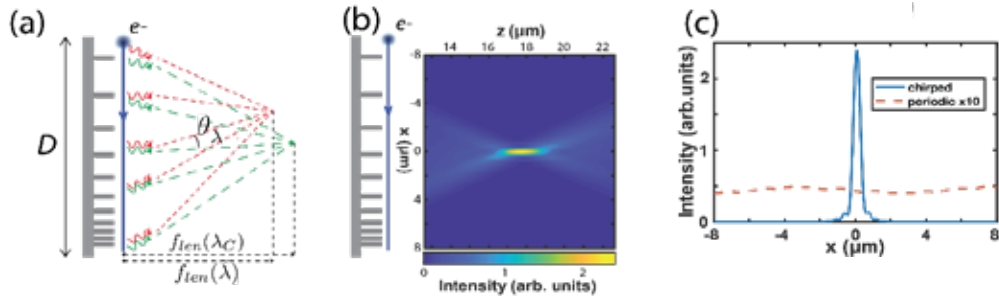


Fig. 2 Design of a Smith-Purcell cylindrical lens. (a) Concept drawing, showing focus for a design wavelength λ_c at focal length $f_{len}(\lambda_c)$. Large chromatic aberrations will cause a different tilt $\theta(\lambda)$ and focal length $f(\lambda)$ for other wavelengths. (b) Full-wave simulation of radiation propagation, showing the expected focusing effect, for $D=40\mu\text{m}$, acceleration voltage 20keV and $\lambda_c = 600\text{nm}$. (c) Comparison chirped-grating far-field radiation in the focal plane, with a grating of constant period $\Lambda=163\text{nm}$ (the intensity being multiplied by 10 to appear on the same scale).

References

- [1] S. J. Smith and E. M. Purcell, Phys. Rev. **92**, 1069 (1953).
- [2] R. Remez, N. Shapira, C. Roques-Carmes, R. Tirole, Y. Yang, Y. Lereah, M. Soljačić, I. Kaminer, and A. Arie, Phys. Rev. A **96**, 61801 (2017).

Controlling the propagation along atomic columns by intelligent electron beam shaping

E. Rotunno¹ and V. Grillo¹

¹ S3, CNR-NANO, Via Campi 213/A, 41100 Modena, Italy

E-mail: enzo.rotunno86@gmail.com

Most of the beams used so far in electron microscopy are normally shaped by an hard aperture whose radius is selected in order to limit the aberrations effect [1] leading to a beam shape close to an Airy disc.

The introduction of holographic electron beam shaping has completely changed this paradigm allowing for the engineering of probes with different kinds of complex wave fronts. [2][3][4]

In this work we report on a detailed analysis of the propagation of electron beams having different shapes in a model system, namely a [100] oriented cubic GaN crystal. The analyses are based on the comparison between multislice simulations and a reformulated Bloch wave based on the concept of Transverse Energy as the only quantum number. This model allows for a quantitative description of the propagation on the bases of the free space properties of each beam.

We first consider the special case of the 0-th order Bessel beam (Figures 1c-d) compared to the ordinary STEM probe (Figures 1a-b) in order to understand in details the “pendellösung” oscillation: the discrete momentum spectrum of the Bessel beams produces, as a result, a very strong selection on the excited Bloch states that can be exploited to characterize the beam propagation.

Finally, we will introduce the actual diffraction-free solution of the propagation of beams in a crystal to highlight the difference with the Bessel beam. In fact, shaping the beam as an approximate 1s state, which can be considered as a Gaussian beam, allows for the minimization of the diffraction/pendellösung effects observed in both aperture limited and Bessel probes (Figures 1e-f).

We then foresee the possibility to engineer the pendellösung oscillation of the probe in STEM experiments.

References

- [1] O. Scherzer, J. Appl. Phys. **20**, 20 (1949).
- [2] J. Verbeeck, H. Tian, P. Schattschneider Nature **467**, 301 (2010).
- [3] V. Grillo, E. Karimi, G. C. Gazzadi, S. Frabboni, M. R. Dennis and R. W. Boyd, Physical Review X **4**, 011013 (2014).
- [4] V. Grillo, E. Rotunno, B. McMorrán, S. Frabboni, Microsc. Microanal. 1889-1890 (2015)

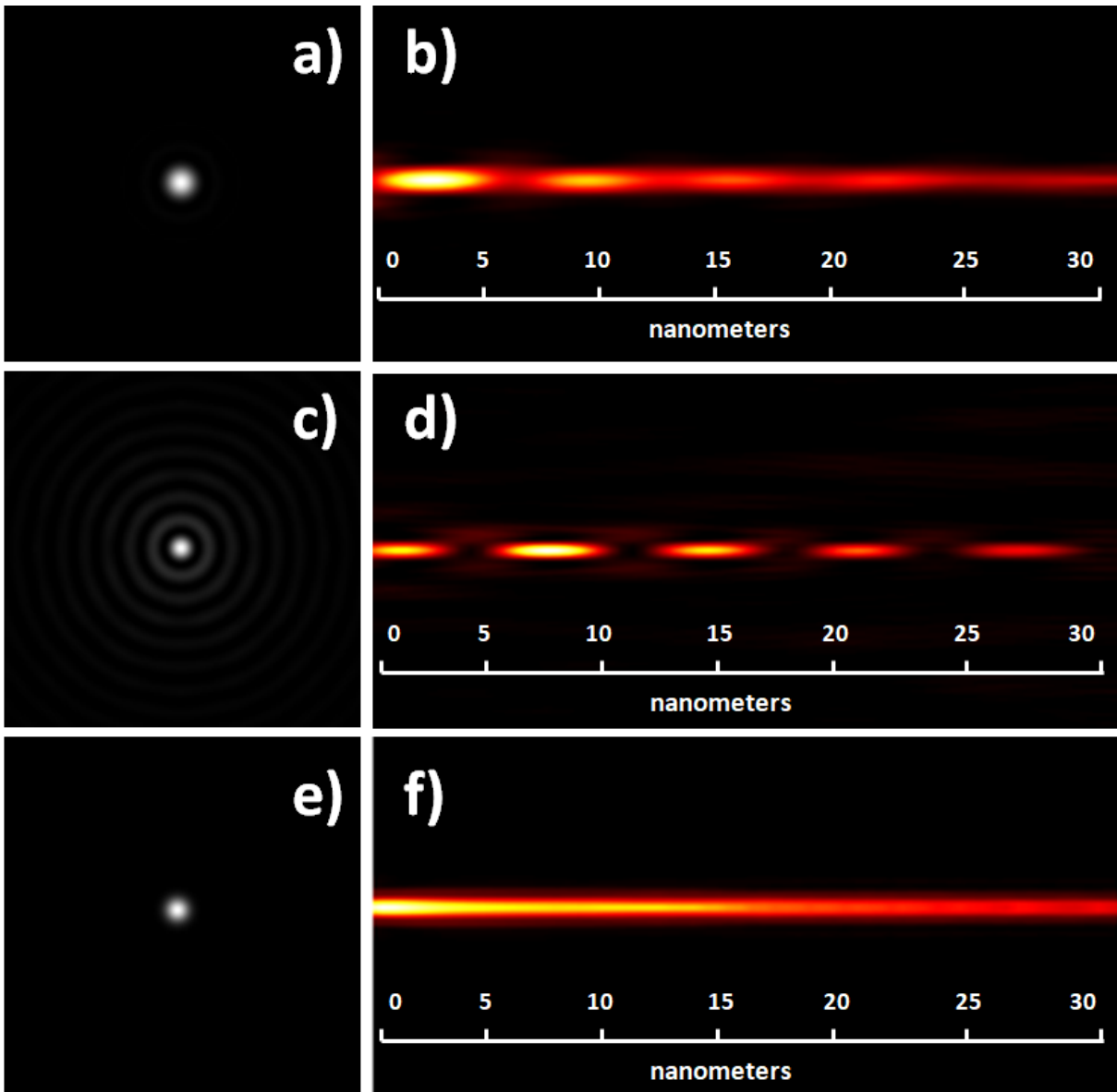


Fig. 6: a) simulated image of a probe formed by a 22 mrad aperture at 300KeV and its evolution (b) along a [100] GaN column. c) simulated image of a Bessel probe formed by a 20-22 mrad ring aperture at 300KeV and its evolution (d). e) simulated image of a Gaussian probe at 300KeV and its evolution (f).

The Cubic Phases of Wave packets in Linear Potential

Gary G. Rozenman^{1*}, Lev Shemer², Matthias Zimmermann³, Maxim Efremov³,
Wolfgang P. Schleich^{3,4} and Ady Arie¹

¹Dept. of Physical Electronics, Faculty of Engineering, Tel-Aviv University, Tel-Aviv 69978, Israel

²School of Mechanical Engineering, Faculty of Engineering, Tel-Aviv University, Tel-Aviv 69978, Israel

³Institut für Quantenphysik and Center for Integrated Quantum Science and Technology (IQST),
Universität Ulm, 89081 Ulm, Germany

⁴Hagler Institute for Advanced Study at Texas A&M University, Texas A&M AgriLife Research,
Institute for Quantum Science and Engineering (IQSE), and Department of Physics and
Astronomy, Texas A&M University, College Station, TX 77843-4242, USA

Since the early work on quantum mechanics, phases have always played an important role in understanding the properties of quantum mechanical systems. As such, the quantum mechanical propagator of a massive particle in a linear gravitational potential was derived already in 1927 by Kennard [1,2] and contains a phase that scales with the third power of the time T^3 during which the particle experiences the corresponding force. However, in conventional interferometers the T^3 -phase cancels out since both the signal and reference arms are usually exposed to the same acceleration. One of the alternative ways to overcome this issue is by utilizing a hydrodynamic system which satisfies the nonlinear Schrödinger equation. Since the work of Dysthe on the 4th order modification of the nonlinear Schrödinger equation for water waves [3], it has been shown that wave propagation dynamics in surface gravity water-waves in many aspects is analogous to that of wave functions of quantum mechanical particles [4]. Therefore, by utilizing surface gravity water waves the full waveform can be recorded and the phases can be directly extracted.

In this project, we extend the study of this analogy to a case of free particles in linear potential, both theoretically and experimentally. This extension allows us to measure the phases of both Gaussian and Airy wave packets in linear potential and reveal the different cubic phase terms. More specifically, we address the cases of cubic phases which appear in de-accelerating Gaussian wave packets and self-accelerating Airy wave packets. We also measure the additional cubic phase terms which appear in Airy wave packets under linear potential. Our precise measurements allow us to extract each cubic term separately and compare it with the known theoretical cubic phases of both Airy and Gaussian wave packets.

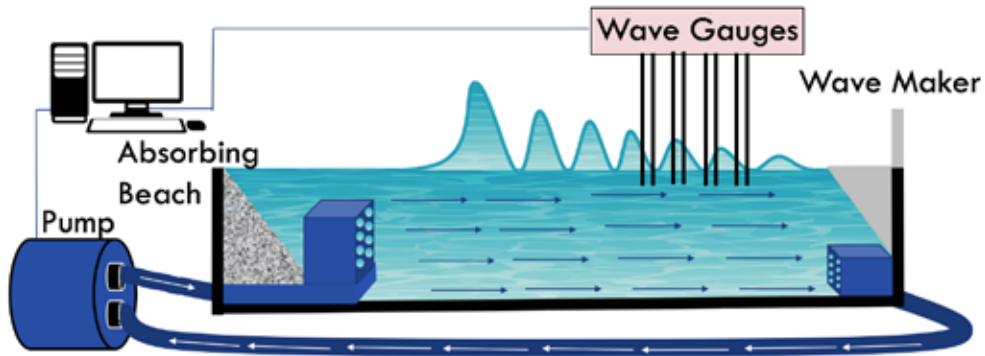


Fig1: A schematic illustration of the experimental set-up

The linear potential we apply in our experiments is obtained by operating a water pump that creates a quadratic time-dependent flow $\phi \sim t^2$. The different wave packets are generated at origin by a programmable wave maker, and the water wave itself is measured at different points along the 5-meter tank using wave gauges. At the end of the water tank an Absorbing beach is placed which absorbs the incoming waves and eliminates cases of reflections.

The goal of this talk is to explain how surface gravity water-waves are analogous to quantum mechanics, to present our experimental set-up and experimental observations of different terms of the T³-phase accumulated by a wave packet having initially a Gaussian or Airy function envelope. In addition, we also take an advantage of having an Airy wave packet in linear potential which is in the opposite direction of the self-acceleration and show for the first time, for water wave pulses, that this property can be canceled out.

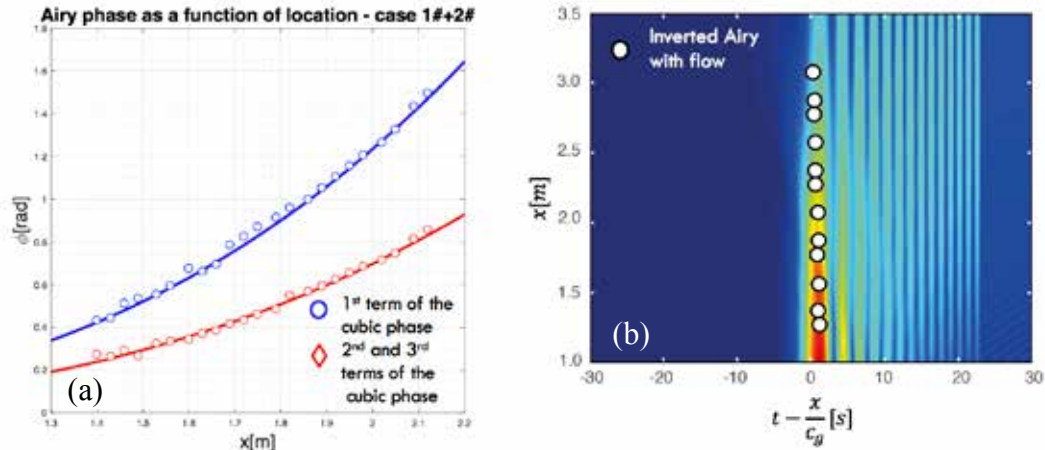


Fig2: a) Extracted cubic phase offset $\phi \sim x^3$ from inverted Airy wave packets in a case of self-acceleration only and self-acceleration with linear potential
b) location of the main lobe of inverted Airy wave packets in the moving frame of reference under linear potential. As it can be seen, the self-acceleration in the moving frame is canceled out.

-
- [1] E. H. Kennard, Zur Quantenmechanik einfacher Bewegungstypen Zeitschrift für Physik, Volume 44, Issue 4-5, pp. 326-352, 1927.
 - [2] M. Zimmermann *et al*, T³ -Interferometer for atoms, Appl. Phys. B, 123:102, 2017.
 - [3] K. B. Dysthe, Note on a modification to the nonlinear Schrödinger equation for application to deep water waves, Proc. R. Soc. Lond. A, 369 105-114, 1979.
 - [4] Shenhe. Fu *et al*, Propagation Dynamics of Airy Water-Wave Pulses, PRL, 115, 034501, 2015.

Temporal manipulation of sub-relativistic electron beams using light and matter

**Roy Shiloh, Martin Kozák, Joshua McNeur, Peyman Yousefi,
Norbert Schönenberger, Johannes Illmer, Ang Li, Timo Eckstein,
Anna Mittelbach, and Peter Hommelhoff**

*Department of Physics, Friedrich-Alexander-Universität Erlangen-Nürnberg (FAU),
Staudtstrasse 1, 91058 Erlangen, Germany
E-mail: roy.shiloh@fau.de*

Since the advent of the laser, experimental studies of interaction of electrons with photons gained momentum. The large fields routinely attained today, spanning the GV/m range, provide an unprecedented tool in manipulating free electrons whether temporally or spatially. Prominent examples include the on-going Accelerator On a Chip (ACHIP) international collaboration, where dielectric laser acceleration schemes are investigated [1,2]. Such acceleration schemes rely on the synchronization of evanescent fields generated by the interaction of a femtosecond laser and nanostructures, with an electron pulse. Aside from acceleration, different auxiliary dielectric elements can be envisioned such as a bunching structure and a focusing structure [3].

A different approach of temporal manipulation involves the second-order ponderomotive field, in which two crossed laser beams generate an optical wave, either standing or co-propagating with the electrons pulses. Free electrons impinging on such a transverse intensity grating will predominantly diffract as in the Kapitza-Dirac effect, or strongly disperse in a longitudinal grating [4]. In the latter case, a relatively long (~ 100 fs) electron pulse may be structured into a train of attosecond bunches with lengths below 300 as [5]. Such highly-bunched electron trains are interesting for the fine probing and imaging of structural and chemical changes in atoms, molecules, and solids.

In this contribution, I will present the latest developments in our group and in the field, including examples of fabricated devices, on-going experiments, and future goals.

References

- [1] R. J. England, R. J. Noble, K. Bane, D. H. Dowell, C.-K. Ng, J. E. Spencer, S. Tantawi, Z. Wu, R. L. Byer, E. Peralta, K. Soong, C.-M. Chang, B. Montazeri, S. J. Wolf, B. Cowan, J. Dawson, W. Gai, P. Hommelhoff, Y.-C. Huang, C. Jing, C. McGuinness, R. B. Palmer, B. Naranjo, J. Rosenzweig, G. Travish, A. Mizrahi, L. Schachter, C. Sears, G. R. Werner, and R. B. Yoder, *Rev. Mod. Phys.* **86**, 1337 (2014).
- [2] K. P. Wootton, J. McNeur, and K. J. Leedle, in *Rev. Accel. Sci. Technol.* (2017), pp. 105–126.
- [3] J. McNeur, M. Kozák, N. Schönenberger, K. J. Leedle, H. Deng, A. Ceballos, H. Hoogland, A. Ruehl, I. Hartl, R. Holzwarth, O. Solgaard, J. S. Harris, R. L. Byer, and P. Hommelhoff, arXiv:1604.07684.
- [4] M. Kozák, T. Eckstein, N. Schönenberger, and P. Hommelhoff, *Nat. Phys.* **14**, 121 (2017).
- [5] M. Kozák, N. Schönenberger, and P. Hommelhoff, *Phys. Rev. Lett.* **accepted**, (2018).

Imaging through a multimode fibre using modal correction and time of flight to give 3D images

Daan Stellinga¹, David B. Phillips², Matthew Edgar¹, Sergey Turtaev³, Tomáš Čížmár³, Miles J. Padgett¹

1) School of Physics and Astronomy, University of Glasgow, G12 8QQ, UK

2) University of Exeter, Physics building, Stocker Road, Exeter, EX4 4QL, UK

3) School of Science and Engineering, University of Dundee, Nethergate, Dundee, DD1 4HN, UK

Abstract: Imaging through a multimode fibre can be achieved using a DMD to unscramble the modal cross-talk. Using Q-switched laser we extend these 2D images to include the time of flight as a first step towards 3D imaging through a fibre.

Introduction

Optical multimode fibres (MMFs) carry a high number of modes through a flexible, small diameter and low loss medium. This makes their information capacity high enough to allow the retrieval of spatially encoded information or even conventional images through minimally invasive entry points. However, due to the different propagation velocities of these modes MMFs scramble light in a manner similar to scattering media, leading to coherent light forming speckle patterns on the output [1,2]. Using a digital micromirror device (DMD) we can measure the transmission matrix for a MMF, and subsequently use this matrix to accurately unscramble the modal information or even control the light at the output end of the fibre. This lets us retrieve images through the MMF using single-pixel techniques, by effectively scanning an object with a specific set of illumination patterns [2,3].

A pulsed source has previously been used in single pixel imaging to extract time of flight information alongside the spatial image, thereby providing an accurate depth map of the scene, and by extension delivering 3D images [4]. With our work, using a pulsed laser source rather than continuous wave, we endeavor to add 3D imaging of macroscopic objects to MMF imaging.

Experimental setup and results

A green 532 nm Q-switched laser with a repetition rate of approximately 7.5 kHz and a pulse width of 670 ps was mode filtered by a single mode fibre, then expanded and collimated onto a DMD. The DMD was placed in the Fourier plane of the input facet of the MMF, such that a set of grating periods and orientations on the DMD corresponds to a set of spots on the fibre input facet. A transmission matrix for the system was then measured by simultaneously illuminating with a reference spot and a scanning spot whilst recording the speckle pattern on a scattering surface approximately 10cm beyond the fibre output [1-3]. This setup is shown schematically in figure 1a.

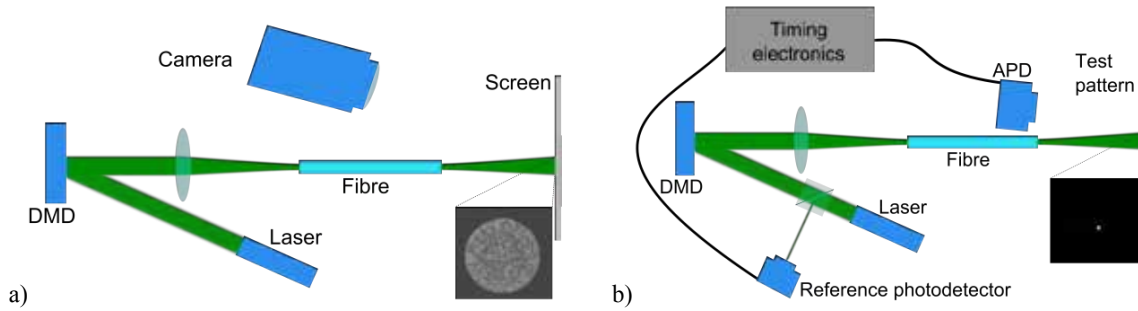


Fig. 1. Experimental setup. a) Characterisation stage: a set of spots scanned across the input facet of a multimode fibre produces a series of speckle patterns at the output, which is recorded by a camera to determine the transmission matrix of the system. b) Imaging stage: the measured transmission matrix is used to scan spots across a test pattern while an APD records the reflected light in a time resolved manner.

With this transmission matrix we then determine the required combination of gratings to display on the DMD to achieve a spot in the far field beyond the MMF, figure 1b. By scanning spots in such a manner and recording, for a given pulse, the total number of photons reflected by the scene using an avalanche photodiode (APD) a 2D image can be generated. In our experiment a chess board was used as the test pattern see figure 2a.

That same APD when triggered by a reference pulse is fast enough to allow the recording of a histogram of the time of flight of the measured photons, thereby also providing a measure of depth resolution to the image [4], see figure 2b. In our current measurement we are able to determine the distance to a flat object, with an increased signal to noise the distance to individual pixels in the acquired 2D image could be determined.

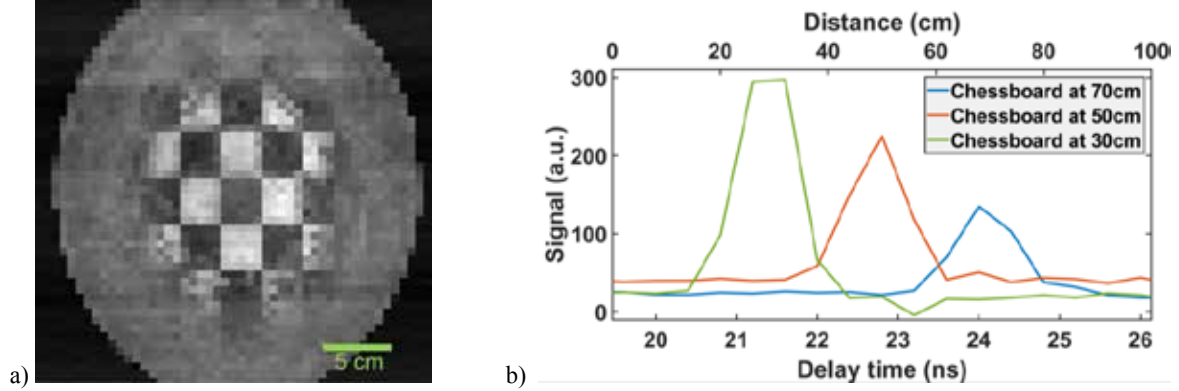


Fig. 2. Results of imaging through a multimode fibre as described in the text. a) 2D image of a chessboard positioned at 50cm beyond the fibre. b) Time of flight histograms of delay time between a reference pulse and the measured signal from the image in a, with the chessboard placed at 70cm, 50cm and 30cm beyond the fibre.

Conclusion

We have extended existing work on MMF imaging to scenes in the far field of the MMF output fibre. Moreover, we have accomplished this with a sub-nanosecond pulsed source, providing access to not only 2D image data from our measurements but also associated time of flight data. This shows a first step towards 3D imaging beyond multimode fibres.

[1] T. Čižmár and K. Dholakia, “Exploiting multimode waveguides for pure fibre-based imaging,” *Nat. Comm.* **3**, 1027 (2012).

[2] M. Plöschner, T. Tyc, and T. Čižmár, “Seeing through chaos in multimode fibres,” *Nat. Phot.* **9**, 529-535 (2015).

[3] S. Turtaev, I. T. Leite, K. J. Mitchell, M. J. Padgett, D. B. Phillips, and T. Čižmár, “Comparison of nematic liquid-crystal and DMD based spatial light modulation in complex photonics,” *Opt. Exp.* **25**, 29874-29884 (2017).

[4] M-J. Sun, M. P. Edgar, G. M. Gibson, B. Sun, N. Radwell, R. Lamb, and M. J. Padgett, “Single-pixel three-dimensional imaging with time-based depth resolution,” *Nat. Comm.* **7**, 1201 (2016).

Aberration-Corrected Quantum Electron Microscopy

M. Turchetti^{1*}, C-S. Kim¹, R. G. Hobbs¹, N. Abedzadeh¹, K. K. Berggren¹, P. Kruit²

¹*Research Laboratory of Electronics, Massachusetts Institute of Technology, Cambridge, MA 02139, United States.*

²*Department of Imaging Physics, Delft University of Technology, Lorentzweg 1, 2628CJ Delft, Netherlands.*

**E-Mail: turchett@mit.edu*

Quantum electron microscopy (QEM) is one of the most promising approaches that could overcome the resolution limit imposed by the radiation damage due to the minimum electron dose necessary to surpass shot noise. This is recognized as the main resolution limit when imaging biological specimens [1]. A QEM scheme exploits the concept of interaction-free measurement in a resonant electron optical cavity, whose purpose is to generate and sustain two coupled states of the electron wavefunction, the reference and the sample states [2].

Here we propose a possible design for this resonant electron cavity, which can be located in conventional scanning electron microscopes. This design is comprised of an electron gate and a tetrode diffractive electron mirror. The first controls the access of the electron in the cavity, while the second acts as a two-state coupler for the reference and the sample states. We initially confirmed electron trajectories using field and axial rays, which are effectively reference and sample beams, respectively, in the electron cavity (Fig 1a). However, this base scheme suffers the presence of strong aberration generated by the tetrode electron mirror. Specifically, aberrations build up with each electron roundtrip, disrupting the electron wavefunction and limiting the achievable resolution.

In this work, we focused on spherical aberration as it has a larger influence on our system. We propose two possible modifications to the initial scheme in order to address this issue. One involves substitution of the electron gate mirror with a hyperbolic triode mirror which generates aberrations of the opposite sign (Fig. 1b) [3]. The second one, instead, employs an active correction and involves insertion of a quadrupole-octupole corrector inside the cavity (Fig. 1c). The corrector consists of four multipole elements, on which a superposition of quadrupole and octupole fields is applied to correct the aberrations. We designed and simulated both systems and demonstrated a considerable decreasing in spherical aberration, leading to a better stability of the resonator, which in turn would allow a larger number of roundtrips. Fig. 1d and e show the electron trajectory simulations of the electron beam marginal and paraxial rays (field ray) in the two systems demonstrating a trace stability during resonance below 10 nm in both cases. This could significantly improve the resolution of the QEM system.

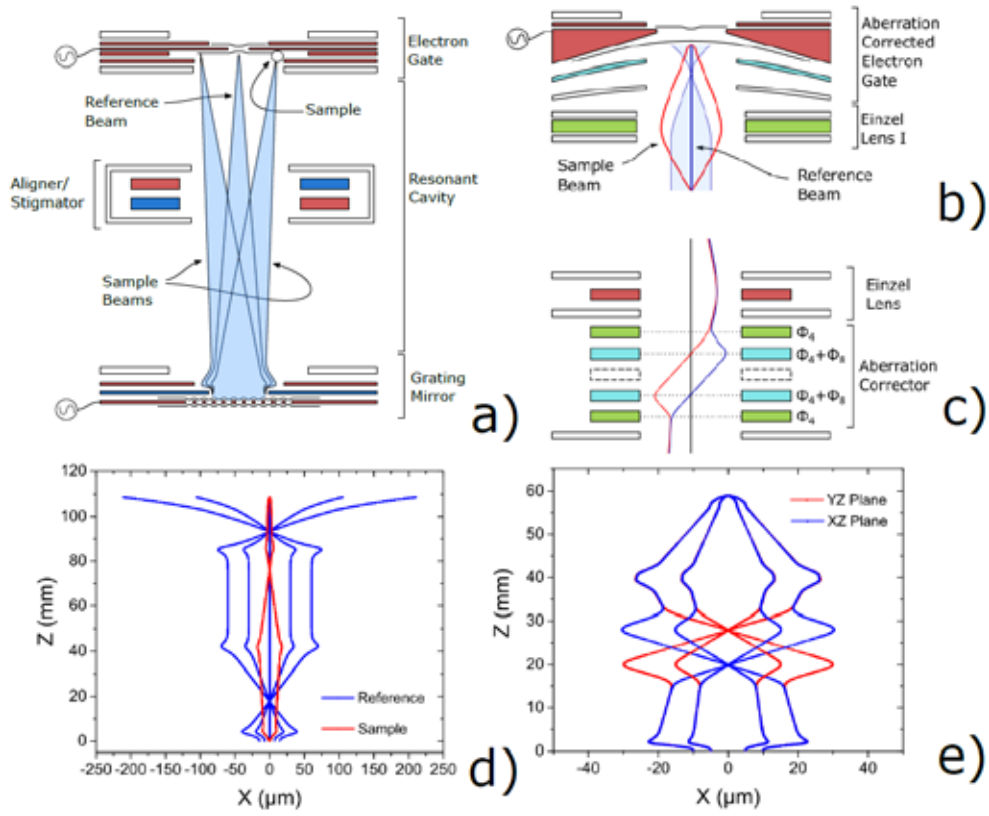


Fig. 1: (a) Schematics of the base electron resonant cavity, comprised of an electron gate and a tetrode grating mirror. (b) Sketch of the hyperbolic electron mirror used to substitute the electron gate in order to correct spherical aberration. (c) The same cavity equipped with a quadrupole-octupole spherical aberration corrector. (d) Electron trajectory simulation of both the axial ray of the sample beam and the marginal ray and a paraxial ray composing the reference beam in the resonant cavity where the electron gate has been substituted by a hyperbolic electron mirror. In these simulations, Z is the direction of the optical axis while X and Y are the azimuthal directions. (e) Electron trajectories simulation of the marginal ray and a paraxial ray of the reference beam. The simulation is performed both in XZ and YZ planes as the system, in this case, is not symmetrical.

References

- [1] R. Henderson, The potential and limitations of neutrons, electrons and X-rays for atomic resolution microscopy of unstained biological molecules, *Q. Rev. Biophys.* 28, 171 (1995).
- [2] P. Kruit, et al., Designs for a quantum electron microscope, *Ultramicroscopy* 164, 31 (2016).
- [3] J.P.S. Fitzgerald et al., Adaptive aberration correction using a triode hyperbolic electron mirror, *Ultramicroscopy* 111, 1495 (2011).

Production of arbitrary phase apertures for electron ptychography beams

W. Van den Broek,¹ P.M. Pelz,² P.-H. Lu,³ M. Kruth,³ V. Grillo,⁴ R.E. Dunin-Borkowski,³
C.T. Koch,¹ R.J. Dwayne Miller ²

¹ *Institut für Physik & IRIS Adlershof, Humboldt-Universität zu Berlin, Newtonstr. 15, 12489 Berlin,
Germany*

² *Max Planck Institute for the Structure and Dynamics of Matter, Center for Free Electron Laser
Science, Luruper Chaussee 149, 22761 Hamburg, Germany*

³ *Ernst Ruska-Centre (ER-C) for Microscopy and Spectroscopy with Electrons, Forschungszentrum
Jülich, 52425 Jülich, Germany*

⁴ *CNR-Istituto Nanoscienze, Centro S3, 41125 Modena, Italy*
e-mail: vandenbroek@physik.hu-berlin.de

Introduction

In ptychography a condensed beam is scanned over the specimen and diffraction patterns are recorded for each beam position. Under sufficient overlap of the beams the specimen's exit wave, and even projected potential [1, 2], can be retrieved.

Conventionally [3] an out-of-focus condensed beam is used resulting in a broad electron beam of a few nanometers diameter that is stepped with nm-sized increments. With such beams the angles of incidence are not homogeneous but vary with the azimuth and the distance from the center. Good results were obtained in [4] where a in-focus condensed beam and a fast detector were used to record convergent beam electron diffraction patterns at 0.095 nm intervals. The authors of this abstract posit that these unexpectedly good results are in part because an in-focus convergent beam probes the specimen with all available angles of incidence at once.

In this abstract a phase aperture – also known as a diffuser – is proposed that seeks to combine the advantages of these two approaches: a wide beam where in each location all incident angles are represented.

Aperture design and production

The phase apertures were designed to be used in the FEI Titan HOLO microscope in ER-C, Jülich. The acceleration voltage is 300 kV, and the spherical aberration is 2.7 mm corresponding to a Scherzer angle of 7.4 mrad.

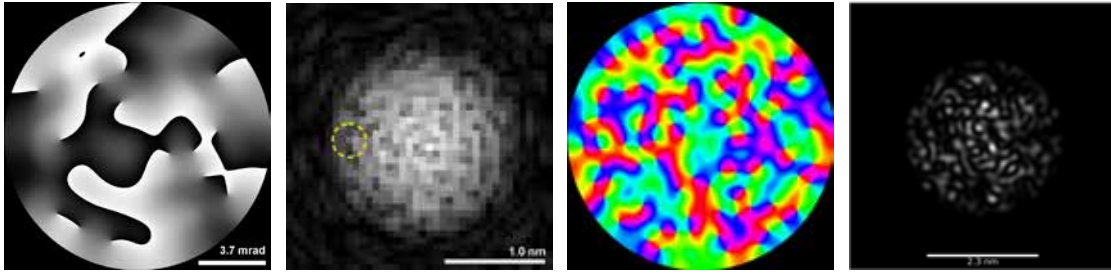


Figure 1: The first and third images are computed phase apertures with image values ranging from 0 to 2π . The second and fourth images are the amplitudes of the in-focus beams corresponding to the apertures to their left.

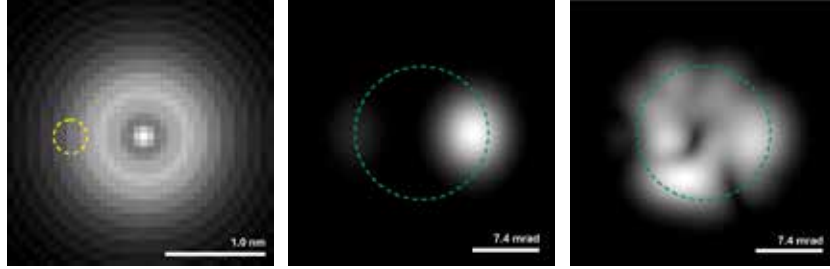


Figure 2: *Left*: Amplitude of condensed beam defocused by 110 nm. *Middle*: Magnitude of the frequency content within the yellow ring to the left. *Right*: Magnitude of the frequency content within the yellow ring in Figure 1; green rings indicate aperture outline.

A Gerchberg-Saxton algorithm was developed that iterates back and forth between real space and reciprocal space; each time enforcing the respective constraints: in real space the intensity profile of the beam is forced to a cosine of width 2 nm and in reciprocal space the intensity is set to 1 for angles below the Scherzer angle and to 0 above. While for the aperture in [5], a binary radial mask was used as the real space constraint.

When an initialization of the phase aperture with random values between 0 rad and 2π rad is used, the algorithm yields results like in Figure 1. The resulting beam was tested for robustness against random and systematic errors in the phase, and absorption effects in the aperture material.

In Figure 2 it is illustrated how each location in these beams has all angles of incidence, which is not the case for a simple out-of-focus condensed beam.

The phase modulation of the diffuser was realized as a result of the mean inner potential of a thin film with spatial thickness variation. The diffusers were fabricated on a 200-nm-thick silicon nitride (SiN) membrane over a 200- μm -thick Si substrate using FEI Helios NanoLab 460F1 focused ion beam (FIB) milling. A 150-nm-thick Au layer was coated on the membrane except the region of diffusers to strongly scatter incident electrons as a diaphragm as well as to reduce charging due to enhanced conductivity. The as-fabricated diffusers were inserted to the probe-forming optics, specifically, the Condenser 2 aperture plane, of the FEI Titan HOLO microscope for the characterization and further experiments on electron ptychography.

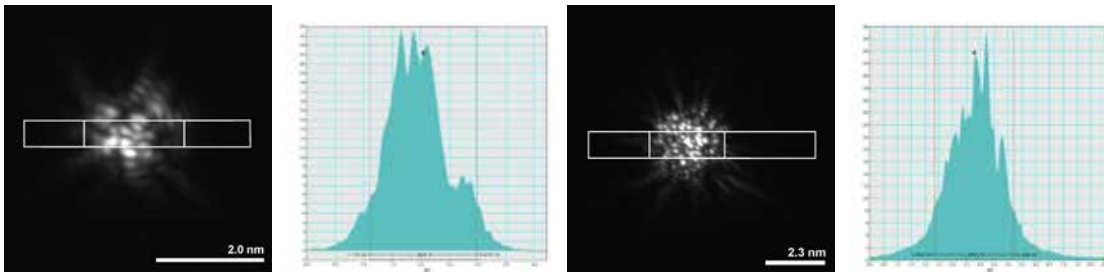


Figure 3: Experimentally recorded beam amplitudes from the phase apertures in Figure 1, and to their left the respective profiles.

Results

As can be observed in Figure 3, the widths of the experimental beams are reasonably close to the designed values: 1.9 nm and 2.8 nm while 2.0 nm and 3.2 nm were aimed for, respectively. Next these beams will be used in broad beam ptychography experiments.

Acknowledgments

W.V.d.B. acknowledges funding from the DFG project BR 5095/2-1 (“Compressed sensing in ptychography and transmission electron microscopy”). P.-H. Lu and R.E. Dunin-Borkowski acknowledge the German-Israeli Project cooperation grant from the German Research Foundation.

References

- [1] W. Van den Broek and C.T. Koch, Phys. Rev. Lett. 109, 245502 (2012).
- [2] W. Van den Broek and C.T. Koch, Phys. Rev. B 87, 184108 (2013)
- [3] A.M. Maiden and J.M. Rodenburg, Ultramicroscopy 109, 1256–1262 (2009)
- [4] H. Yang, et al., Nature Communications 7, 12532 (2016)
- [5] P.M. Pelz, et al., Scientific Reports 7, 9883 (2017)

Simulated Quantum Electron Microscope Images

Y.J. van Staaden, M.A.R. Krielaart and P. Kruit

*Delft University of Technology, Department of Imaging Physics,
Delft, The Netherlands
E-mail: p.kruit@tudelft.nl*

Introduction

Biological specimen often face significant damage if bombarded by charged particles. The amount of charged particles one can use in electron microscopy techniques are therefore often limited when imaging such samples. Limiting the dose sets a limit on the achievable resolution as well: the dose limited resolution. Quantum electron microscopy is potentially a method that can shift the boundary of the dose-limited resolution. It extends the concept of the interaction free measurement¹ to electrons^{2,3} to gain more information about the specimen without increasing the dose when compared to using a single-pass TEM.

Simulations of the imaging capability of the Quantum Electron Microscope (QEM) and conventional TEM are made to compare the two microscopy techniques in terms of beam induced specimen damage. Initially the model of the QEM will be kept very simple. It will resemble optical imaging with a spatially dependent transmission. In addition, only a specimen of a single transmittance will be examined. In practice all kinds of interactions can take place, amongst which delocalized interactions. In the near future the effect of a phase-shift induced by the sample on the passing particle will be taken into account as well.

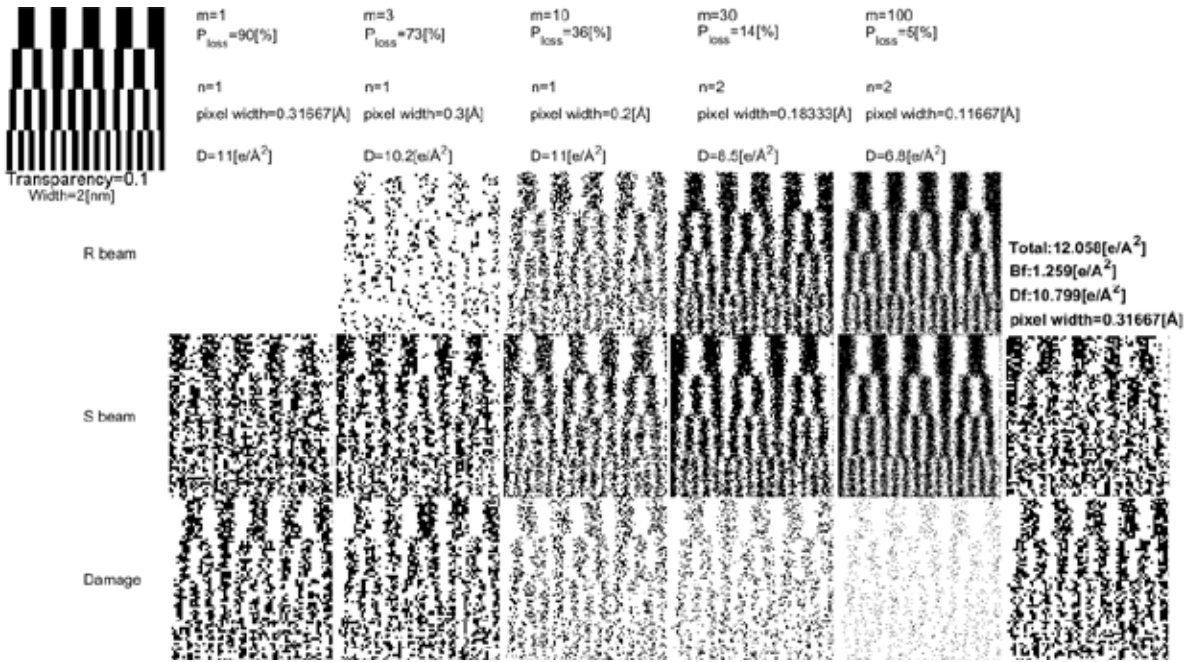
Methods

The simulation emulates an electron gun with a Poisson distribution and a finite spot size with which an electron is fired at a pixel. In the TEM the full electron will attempt to pass the sample whereas in the QEM this is done with a fraction of the wave function, effectively permitting multiple cycles without increasing the dose. After m cycles the wave function is measured and the electron collapses in either the reference, the sample or the damage beam with respective probabilities as given by Thomas et al.⁴. The latter is of course only possible if the electron scatters sufficiently or is measured through an electron energy loss spectrometer.

The process is repeated n times, after which the electron gun will take aim at the next pixel. After all of the pixels have been assessed the results of the electron distributions for each detector, and the pixels for which damage occurred, is presented. To compare imaging capability effectively, the pixel size and n is chosen such to minimize the difference of damage afflicted between the QEM and the TEM simulations.

Results

In Fig. 1 the top left image is the specimen to be imaged. In this case a typical resolution sample consisting of varying spaced vertical lines is used. The black lines are characterized by a transmission α of 0.1, whereas the white lines represent fully transparent regions. The probability of an entire electron scattering and thus damaging the sample is $1-\alpha$.



From top to bottom the rows depicts the obtained electron distributions in the *R(eference)-*, *S(ample)-*

Fig. 1 First column: Specimen to be imaged (black is a transparency of 0.1). Second to sixth column: Simulated images for approximately constant dose and increasing number of cycles in a QEM. Last column: a single-pass TEM (dark field and bright field). Black pixels indicate detected electrons in the respective simulation results.

and *Damage beam*. The columns depict the results for a chosen amount of cycles, m , increased from left to right. The right most column depicts the single pass TEM bright field and dark field result. In the first row for each column the damage probability per electron and the damage per area is denoted by P_{loss} and D respectively. The 5th and 6th column have an n raised from 1 to 2. The pixel size decreases from the second column to the 6th column.

Discussion

The presented result (Fig. 1) clearly shows an increase in image quality compared to that of the single-pass TEM for approximately equal damage. Merely the first one or two rows of lines can be distinguished in the single-pass TEM case. After $m = 30$ cycles the QEM can distinguish the first three sets of lines in a convincing manner. The increase in quality is due to the decrease in damage probability per electron as one increases the amount of cycles, m , in the QEM. This allows for a smaller pixel size and a larger number of electrons per pixel, n , to be used.

References

- [1] A.C. Elitzur and L. Vaidman. Found. Phys, **23**, pp. 987 – 997 (1993).
- [2] W. P. Putnam and M.F. Yanik. Physical Review A, **80** (4), 040902 (2009).
- [3] P. Kruit et al, Ultramicroscopy **164**, pp. 31 – 45 (2016).
- [4] S. Thomas, C. Kohstall, P. Kruit and P. Hommelhoff. Physical Review A, **90** (5), 053840 (2014).

Attosecond coherent control of a free-electron wave-function via semi-infinite light fields and plasmon polaritons

G. M. Vanacore¹, I. Madan¹, G. Berruto¹, E. Pomarico¹, K. Wang², R. J. Lamb³, D. McGrouther³, I. Kaminer², B. Barwick⁴, F. Javier Garcia de Abajo^{5,6}, F. Carbone¹

¹*Institute, Town, Country*

¹*Institute of Physics, Laboratory for Ultrafast Microscopy and Electron Scattering (LUMES), Ecole Polytechnique Fédérale de Lausanne, Station 6, CH-1015 Lausanne, Switzerland*

²*Technion Department of Physics*

³*SUPA, School of Physics and Astronomy, University of Glasgow, Glasgow G12 8QQ, UK*

⁴*Ripon College, 300 W. Seward St., Ripon, WI 54971, United States*

⁵*ICFO-Institut de Ciències Fotoniques, The Barcelona Institute of Science and Technology, 08860 Castelldefels (Barcelona), Spain*

⁶*ICREA-Institució Catalana de Recerca i Estudis Avançats, Passeig Lluís Companys 23, 08010 Barcelona, Spain*

E-mail: giovanni.vanacore@epfl.ch

Introduction

The interaction between light and charged particles can be exploited for generating radiation, such as in synchrotrons and free electron lasers, or for controlling electron beams in applications such as time-resolved electron microscopy for the dynamical investigation of materials and molecules [1-3]. By using electromagnetic fields the coherent control of a free-electron wavefunction can be pushed to unexplored timescales, even below the attosecond regime, which would enable new applications in light-assisted quantum devices and diagnostics at extremely small timescales, such as those governing intramolecular electronic motions and nuclear processes. In this contribution, we report on a generalized method for the coherent manipulation of free electrons with attosecond precision [4], and show that it can be pushed down to the zeptosecond regime with existing technology.

Results and Discussion

A relativistic pulsed electron beam was made to interact with an appropriately synthesized electromagnetic field. The field was generated either by a sequence of two fs laser pulses reflected at the surface of a mirror (semi-infinite field), or by the coherent superposition of the surface plasmon polaritons (SPPs) optically-generated from nanofabricated structures (near field). The energy-momentum exchange resulting from the electron-field interaction was directly mapped via momentum-resolved ultrafast electron energy-loss spectroscopy (see Fig. 1a-c). When the two phase-locked light pulses were delayed by fractions of the optical cycle, we observed coherent oscillations in the electrons energy-momentum states (see Fig. 1d-e). This effect is the result of coherently constructive and destructive phase modulation of the

electron wave-function while varying the relative phase between the two driving optical pulses (see schematics in Fig. 1f).

Besides the longitudinal phase space modulation, our method offers the possibility to manipulate the electron wave-function also in the transverse space. This was performed by the phase-controlled combination of the electron interaction with both a semi-infinite light field and a plasmon polariton propagating on a plasmonic waveguide. The non-local interference between the traveling plasmon wave and the light field, as mediated by the electrons, creates a standing wave distribution which can transversely perturb the electron wave-function in a controlled manner. Here, we describe the case of SPPs generated at the edge of a circular nanocavity carved in a Ag layer deposited on a Si_3N_4 thin film, and demonstrate that the resulting near-field distribution transiently creates a vortex plasmon carrying a defined orbital angular momentum (OAM), which can be efficiently transferred to the interacting electrons as a result of the coherent interaction.

The potential of our approach to reach the attosecond timescale and below should pave the way to achieve unprecedented insights into non-equilibrium phenomena in advanced materials, and should play a decisive role in the rational design and engineering of future applications.

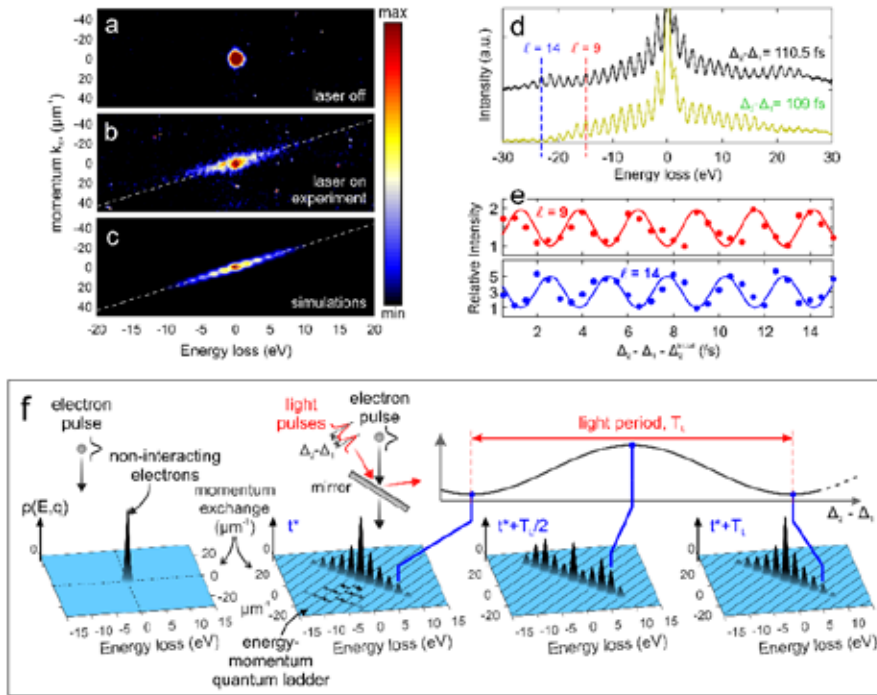


Fig. 1. Attosecond coherent control of an electron wavefunction. (a) Electron beam measured in the momentum-energy plane k_x -E in the absence of optical illumination. (b)-(c) Measured (b) and simulated (c) momentum-energy maps for illumination with a properly synthesized semi-infinite field distribution composed of two light pulses delayed by fraction of the optical cycle. (d) Measured EELS spectra as a function of relative delay between the two optical pulses. (e) Relative intensity of the $l = 9$ and $l = 14$ sidebands plotted as a function of time

delay between the two optical pulses, exhibiting a periodic modulation of period ≈ 2.6 fs (equal to the optical cycle $2\pi/\omega$) and a relative π phase shift. (f) Schematic representation of electron-wave-function modulation, showing snapshots of the strong energy-momentum electron density redistribution for different values of the phase shift between the two optical pulses.

References

- [1] G. M. Vanacore, A. W. P. Fitzpatrick, A. H. Zewail, *Nano Today* **11**, 228-249 (2015).
- [2] L. Piazza, T.T.A. Lummen, E. Quiñonez, Y. Murooka, B.W. Reed, B. Barwick, F. Carbone, *Nat. Commun.* **6**, 6407 (2015).
- [3] T. T. A. Lummen, R. J. Lamb, G. Berruto, T. LaGrange, L. Dal Negro, F. Javier García de Abajo, D. McGrouther, B. Barwick, F. Carbone, *Nat. Commun.* **7**, 13156 (2016).
- [4] G. M. Vanacore, I. Madan, G. Berruto, K. Wang, E. Pomarico, R. J. Lamb, D. McGrouther, I. Kaminer, B. Barwick, F. Javier Garcia de Abajo, F. Carbone, arXiv1712.08441v1.

Design and demonstration of a programmable phase plate for electrons

J. Verbeeck¹, A. Béché¹, G. Guzzinati¹, D. Jannis¹, Knut Müller-Caspary¹

¹EMAT, University of Antwerp, Groenenborgerlaan 171 Antwerp, Belgium

E-mail: jo.verbeeck@uantwerp.be

Abstract

In light optics, spatial light modulators currently allow full control over the wavefront of optical waves which has led to a rapidly expanding field of applications ranging from astrophysics to advanced light microscopy, laser cutting, endoscopy, free space communication, data encryption, quantum information and many more. These modulators rely on different working principles including deformable mirror surfaces and liquid crystals locally altering the refractive index, but all have in common that a computer can now control the optical transfer function in a programmable way akin to pixels on a computer screen.

In electron optics, one could say that such control over the optical transfer function is common to all electron optical devices as the optical properties naturally depend on potentials on electrodes and currents through solenoids. Especially in modern aberration correctors, a high degree of flexibility in tuning the phase transfer is available and used to cancel aberrations up to a certain order by means of a complicated setup of multipolar lenses requiring a large number of computer controlled current sources. These correctors approach the flexibility of a spatial light modulator in light optics, yet still pose constraints on the kind of phase plate that can be realized. Indeed, Maxwell equations put rather severe restrictions on realizable fields in free space and the resulting phase transfer tends to be a smooth function that is ideal for aberration correction, but less so for other applications requiring rapid changes of phase in central regions of the device.

A good example of a phase plate with a rapid phase jump is the so-called Zernike phase plate that can be used to increase the contrast in weak phase object imaging. Many different realizations and variants of such phase plates were made with some making use of a miniaturized electrostatic einzel lens allowing to control the phase shift in a small region in the center of the phase plate by applying a voltage to the central electrode of the lens.

The downside of such designs is that they are typically placed in the objective aperture to provide a phase filter on the exit wave in the back focal plane where the material of the lens system will inevitably block some part of this exit wave creating loss of information and leading to image artefacts.

In this talk we extend this idea to an array of einzel lenses which we use as a probe forming aperture. We demonstrate a proof of concept realization with a 2x2 array of einzel lenses leading to a phase controlled 4 slit interference experiment in an existing transmission electron microscope. We discuss the design and behaviour of the proof of concept including its effect on coherence and the role of delocalized inelastic scattering.

We further will discuss the upscaling of the current device, which is the goal of a recently started ERC proof of concept grant (ADAPTEM) aiming for at least a 5x5 demonstrator. We discuss the possible uses of such a device as a tool for the study of exotic electron waves, including electron vortex beams, Bessel beams, Airy beams, snake Beams, helicon beams and many more. We demonstrate that even with relatively few phase elements, a highly desirable device can be produced for studying such waves.

Alternatively, the device could also show promise as a low-cost aberration corrector for TEM and SEM and we demonstrate that even with a relatively low amount of well-chosen phase elements such correctors could find their use for specific applications.

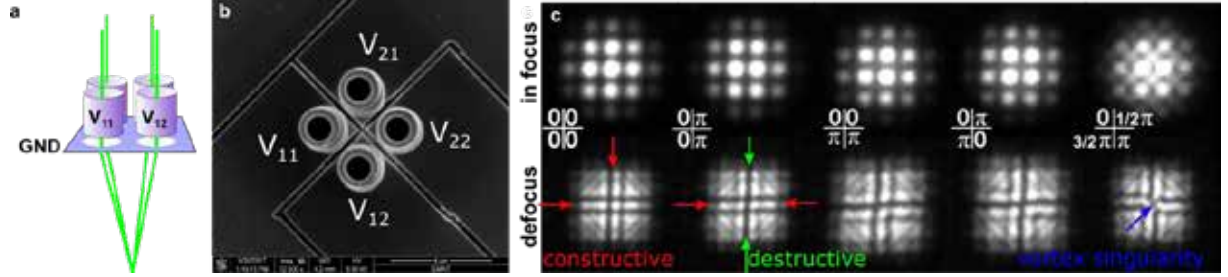


Fig. 1 a) schematic set up of the 2x2 phase programmable array. b) SEM image of the device showing 4 cylindrical electrodes that can be put on separate electrostatic potentials V_{ij} . c) Resulting interference pattern when mounted in the TEM showing the complete control of the phase of the 4 interfering beams resulting in different patterns.

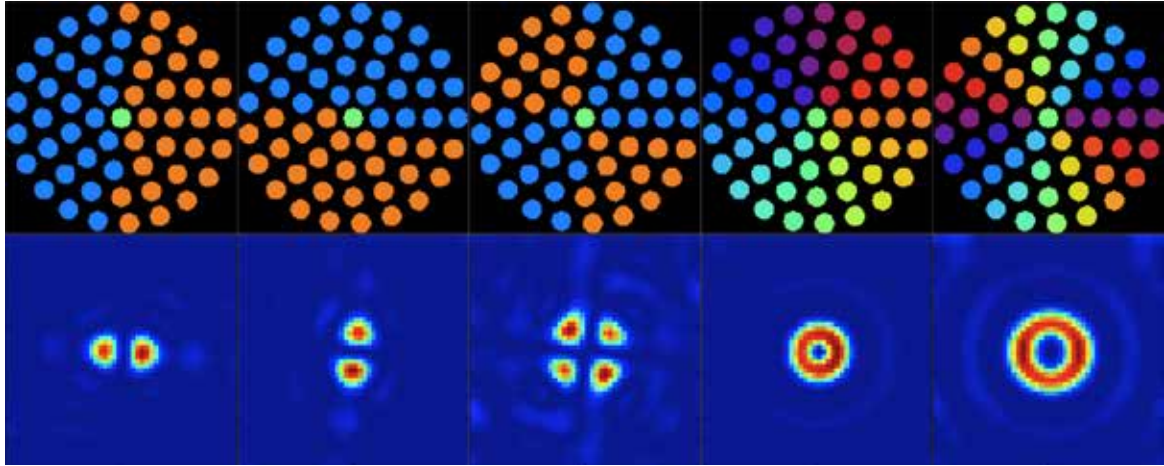


Fig. 2 A simulated upscaled version of this device could serve as an attractive tool to study exciting electron beams. From left to right HG_{10} , HG_{01} , HG_{11} , LG_{01} , LG_{02} beams.

Acknowledgements

J.V. and A.B. acknowledge funding from the Fund for Scientific Research Flanders FWO project G093417N and the European Research Council, ERC Starting Grant 278510 VORTEX and ERC proof of concept project DLV- 789598 ADAPTEM. The Qu-Ant-EM microscope was partly funded by the Hercules fund from the Flemish Government.

References

- [1] J. Verbeeck, A. B  ch  , K. M  ller-Caspary, G. Guzzinati, M. Anh Luong, M. Den Hertog, Ultramicroscopy **190**, 58–65 (2018) and <https://arxiv.org/abs/1711.11373>

Experimental realization of a cylindrical quantum basis set for bandwidth-limited two dimensional electron wavefronts

G. Thirunavukkarasu, M. Mousley, M. Babiker and Jun Yuan

Department of Physics, University of York, Heslington, York YO10 5DD, UK

To minimize the effect of lens aberration, beam-stopping apertures have to be used in conventional electron microscopy, but they are known to limit the spatial resolution. The aberration correction techniques are forms of wavefront engineering, aimed at increasing the usable angular size of the aberration-free wavefront, allowing larger apertures to be used. Such techniques have been very successful in pushing electron microscope resolution beyond the angstrom level, leading to dramatic advances in the characterization of advanced materials at the atomic scale. However, further advances have been stalled due to the technical complexity involved.

In this presentation, I aim to show that conventional electron microscopy has explored a very small subset of the electron optical landscape because only the lowest order electron-optical modes possible in a cylindrical electron-optical system have been utilized. We have recently generated higher order electron beams which are characterized not only by their azimuthal index l , the so called the electron vortex beams with topological defects [1], but which are also characterized additionally by radial index p . The electron beams with different angular and radial orders which we put forward form a natural quantum basis set (normal modes) for the two dimensional quantum wavefronts of any aperture (bandwidth) limited beams. We present the experimental realization of such electron beams using computer-generated holograms. We demonstrate not only the faithful reproduction of this new quantum basis set through first order diffraction [2], but we also present new results on the higher order diffraction. While the phase amplification associated with the higher order diffracted beams resulted in the amplification of the azimuthal quantum numbers, it produces strong even-odd effect on the radial quantum number. This demonstrates dramatically different the natures of the two quantum numbers l and p .

As these orthonormal quantum modes offer an alternative description of any aperture (bandwidth) limited electron waves to that normally provided by the standard plane wave basis set, opportunities for new avenues towards conducting electron microscopy will be explored.

References

[1] S. M. Lloyd, M. Babiker, G. Thirunavukkarasu and J Yuan, “Electron vortices: Beams with orbital angular momentum”, *Rev. Mod. Phys.* **89**, 035004 (2017)

[2] G. Thirunavukkarasu, M. Mousley, M. Babiker, and J. Yuan, ‘Normal modes and mode transformation of pure electron vortex beams, *Phil Trans R Soc* **A375**:20150438 (2017)

Atomic scale imaging of magnetic circular dichroism by achromatic spatially-resolved electron energy-loss magnetic chiral dichroism

Xiaoyan Zhong¹, Zechao Wang¹, Lei Jin², Ján Rusz³, Hanbo Jiang¹,

Yutaka Moritomo⁴, Joachim Mayer^{2,5}, Rafal E Dunin-Borkowski²,

Rong Yu¹, Jing Zhu¹

¹National Center for Electron Microscopy in Beijing, Key Laboratory of Advanced Materials (MOE), The State Key Laboratory of New Ceramics and Fine Processing, School of Materials Science and Engineering, Tsinghua University, Beijing 100084, P.R. China

²Ernst Ruska-Centre for Microscopy and Spectroscopy with Electrons and Peter Grünberg Institute, Forschungszentrum Jülich GmbH, 52425 Jülich, Germany

³Department of Physics and Astronomy, Uppsala University, P.O. Box 516, 75120 Uppsala, Sweden

⁴Graduate School of Pure & Applied Science and Faculty of Pure & Applied Science, University of Tsukuba, Tennodai 1-1-1, Tsukuba, Ibaraki 305-7571, Japan

⁵Central Facility for Electron Microscopy, RWTH Aachen University, 52074 Aachen, Germany

The atomic-level knowledge of local spin configuration of the magnetic materials is of great importance to predict and control their physical properties, in order to meet the challenges of ever-increasing demands on performance of functional materials. However, it is highly challenging to experimentally characterize magnetic properties of such materials with atomic scale spatial resolution.

The leading techniques in spatially resolved magnetic imaging are magnetic exchange force microscopy and spin polarized scanning tunneling microscopy. However, as they are surface sensitive, very little information can be obtained regarding bulk or buried materials. The X-ray magnetic circular dichroism (XMCD) combined with photoelectron emission microscopy (PEEM) technique is a very attractive alternative because it has the spatial resolution as high as the polarized x-ray beam size besides element specific feature, as it is less surface sensitive and can be used to look at the interior of the thin films. However, the length scale of magnetic contrast using highly brilliant left and right circularly polarized X-ray beams is around 15nm [1].

The best option to push the spatial resolution of the spectromicroscopies lies in the electron beam equivalent technique electron energy-loss magnetic chiral dichroism (EMCD) [2], which is also called electron magnetic circular dichroism. Physically, XMCD and EMCD

shares the same underlying physics in which the angular momentum transferred during X-ray absorption or inelastic electron scattering can selectively excite magnetic sublevels in atoms. The structured electron beams generated through interference of suitably phased plane waves can produce beams with orbital angular momentum, which is in kind Q-sort technique. Electron beams can be easily focused compared with X-rays, allowing for atomic scale magnetism to be probed. Previously, we have found a strong EMCD signal in transition metal oxides allowing them to use standing wave methods to identify the different spin states of Fe atoms with site specificity [3].

In principle EMCD can offer higher spatial resolution and greater depth sensitivity due to the short de Broglie wavelength and penetration of high-energy electrons compared to XMCD. Recently by using EMCD and achromatic electron microscopy, we are able to access the magnetic circular dichroism with unit-cell resolution and even with atomic resolution [4,5]. Combining with advanced capability of structural and chemical imaging by using aberration-corrected transmission electron microscopy, all the information including magnetic polarization, atomic configurations, chemical states can be simultaneously accessed from the very same sample region. In the examples of complex oxides including $\text{Sr}_2\text{FeMoO}_6$, NiFe_2O_4 and $\text{La}_{0.7}\text{Sr}_{0.3}\text{MnO}_3$ [3-6], we would like to show how to achieve local atomic-scale magnetic, chemical and structural information and understand the structure-property relationship of these magnetic materials at the atomic level.

References

- [1] W. L. Chao, B. D. Harteneck, J. A. Liddle, E. H. Anderson, and D. T. Attwood, Soft X-ray microscopy at a spatial resolution better than 15nm, *Nature* **435** (2005), 1210-1213.
- [2] Schattschneider, P. et al. Detection of magnetic circular dichroism using a transmission electron microscope. *Nature* **441**, 486–488 (2006).
- [3] Z. Q. Wang, X. Y. Zhong*, R. Yu, Z. Y. Cheng, J. Zhu*, Quantitative experimental determination of site-specific magnetic structures by transmitted electrons. *Nature Communications*, **4** (2013), 1395.
- [4] Z. C. Wang, A. H. Tavabi, L. Jin, J. Rusz, D. Tyutyunnikov, H. B. Jiang, Y. Moritomo, J. Mayer, R. E. Dunin-Borkowski, R. Yu, J. Zhu and X. Y. Zhong*. Atomic scale imaging of magnetic circular dichroism by achromatic electron microscopy. *Nature Materials*, **17**, (2018), 332.
- [5] L. Jin, C. L. Jia, I. Lindfors-Vrejoiu, X. Y. Zhong, H. C. Du, R. E. Dunin-Borkowski, Direct Demonstration of a Magnetic Dead Layer Resulting from A-Site Cation Inhomogeneity in a (La,Sr)MnO₃ Epitaxial Film System, *Advanced Materials Interfaces*, **3** (2016), 1600414.
- [6] Z. C. Wang, X. Y. Zhong*, L. Jin, X. F. Chen, Y. Moritomo, and J. Mayer. Effects of dynamic diffraction conditions on magnetic parameter determination in a double perovskite $\text{Sr}_2\text{FeMoO}_6$ using electron energy-loss magnetic chiral dichroism. *Ultramicroscopy* **176**, (2017) 212.

The cubic phase in quantum mechanics and hydrodynamics

**M. Zimmermann¹, M.A. Efremov¹, W.P. Schleich^{1,2},
G. Rozenman³, L. Shemer⁴, and A. Arie³**

¹*Institut für Quantenphysik and Center for Integrated Quantum Science and Technology (IQST),
Ulm University, Ulm, Germany*

²*Hagler Institute for Advanced Study at Texas A&M University, Texas A&M AgriLife Research,
Institute for Quantum Science and Engineering (IQSE), and Department of Physics and Astronomy,
Texas A&M University, College Station, USA*

³*Department of Physical Electronics, Faculty of Engineering, Tel-Aviv University, Tel Aviv, Israel*

⁴*School of Mechanical Engineering, Faculty of Engineering, Tel-Aviv University, Tel-Aviv, Israel*

e-mail: matthias.zimmermann@uni-ulm.de

The quantum mechanical propagator of a massive particle in a linear potential is well-known to contain a phase φ_a scaling with the third power of propagation time T and the square of the acceleration a [1].

In quantum mechanics such phases can be measured by using interferometer techniques, where two different accelerations are applied along two interferometer branches. In particular, an atom interferometer with a phase scaling as T^3 is presented in [2]. In this proposed scheme, Fig. 1, the atom experiences two different accelerations a_1 or a_2 depending on its internal state $|g_1\rangle$ or $|g_2\rangle$, respectively. As a result, the atom accumulates two different phases $\varphi_a^{(1,2)}$ and the total interferometer phase scales as T^3 .

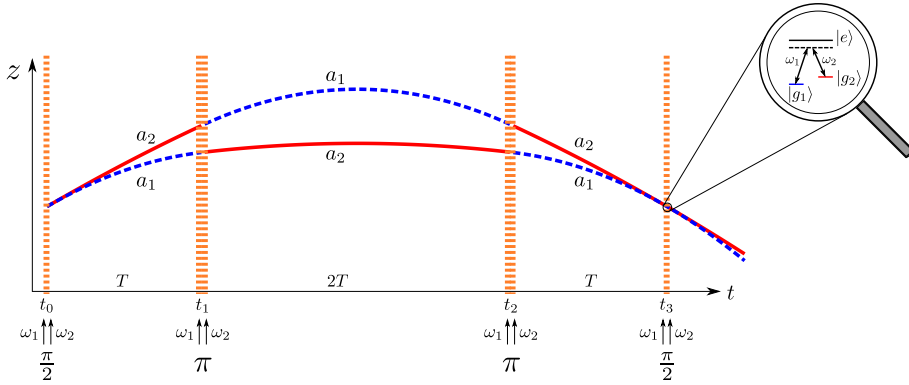


Figure 1: Space-time diagram of the T^3 -interferometer. Four short Raman pulses effectively drive transitions between the two internal states $|g_1\rangle$ and $|g_2\rangle$ of a three-level atom.

Moreover, the propagation of surface gravity water-waves is described by the Dysthe equation [3] which reduces in the linear regime to the same form as the Schrödinger equation. Therefore it is intriguing to study the similarities of surface gravity water-waves and quantum mechanical systems [4]. In this talk we compare and contrast the cubic phase of the atom interferometer

to the one which can be observed in an experiment using surface gravity water-waves. We display two main differences between these two systems: (i) in quantum mechanics it is crucial to use two different accelerations, whereas in hydrodynamics a single one is sufficient and, (ii) the cubic phase of the atom interferometer is independent of the initial state, while the cubic phase accumulated during the propagation of water-waves does show a strong dependence on the initial wave pulse.

References

- [1] E.H. KENNARD, *Zeitschrift für Physik* **44**:326 (1927)
- [2] M. ZIMMERMANN et al., *Appl. Phys. B* **123**:102 (2017)
- [3] K. B. DYSTHE, *Proc. R. Soc. Lond. A* **369**:105-114 (1979)
- [4] S. FU et al., *Phys. Rev. Lett.* **115**:034501 (2015)

Q-SORT Science Bash

Schönheit und Nutzen
der Nanobiologie

Beauty and benefits
of nanobiology

R.B.G. Ravelli, F. Nijpels,
G. Weissenberger, R. Henderikx,
A. Gijsbers, P. Huysmans, B. Beulen,
C. Berger, C. Lopez-Iglesias,
and P.J. Peters

The Maastricht Multimodal Molecular
Imaging institute

Maastricht University,
The Netherlands

www.maastrichtuniversity.nl/m4i

Im Bereich der Lebenswissenschaften ermöglicht die Elektronenmikroskopie (EM) ein tiefgehendes Verständnis des Grundbegriffs des Lebens. EM ist unverzichtbar, um biologische Strukturen sowohl auf zellulärer als auch auf molekularer Ebene anzugehen. Es hat gezeigt, wie jede Zelle des menschlichen Körpers in Membrankompartimente mit spezialisierten Funktionen unterteilt ist, die zusammen eine Vielzahl von Prozessen organisieren, wie zum Beispiel Proteinsynthese, Energieproduktion und Verteilung von genetischem Material. Jüngste Entwicklungen in EM bei extrem niedrigen Temperaturen erlauben es Wissenschaftlern sogar, auf atomare Auflösung zu zoomen und einzelne Proteine oder Proteinkomplexe in der nativen Umgebung der Zelle zu sehen. Dies liefert kritische Einblicke in die molekularen Prozesse von Krankheiten (z. B. Transformation von Krebszellen, krankheitsverursachende Mechanismen im alternden Gehirn) und menschliche Entwicklung (z. B. Differenzierung und Erneuerung von Stammzellen).

Tatsächlich liegen den meisten Krankheiten molekulare und zelluläre Defekte zugrunde, und EM bietet in einzigartiger Weise die Auflösung, um die Lokalisierung und Struktur von Molekülen wie Proteinen zusammen mit der entscheidenden Strukturinformation zu untersuchen. EM-Anwendungen finden sich in der grundlegenden biologischen Forschung, einschließlich Infektiologie (zB EM-Studien, um zu verstehen, wie HIV eine lebende Säugetierzelle infiziert), Neurobiologie (Identifizierung von spezifischen Regionen im Gehirn, gefolgt von nanoskopischen Untersuchungen mit EM) und Pathologie (Untersuchung subtiler pathologischer Prozesse) Phänotypen, die für die Lichtmikroskopie zu klein sind). Neueste Innovationen in der automatisierten Bildgebung in 2D (x, y-Achsen; großskalige EM) und 3D (x, y, z-Achsen; Volumen-EM) eröffnen neue Möglichkeiten, die Architektur von Zellen im Kontext ihrer komplexen Umgebung aufzudecken. wie Tumore und sogar ganze Gehirne.

Auf molekularer Ebene waren bis vor kurzem nur Röntgenkristallographie und NMR-Spektroskopie in der Lage, die für die Beschreibung der Struktur notwendige Auflösung zu liefern und die biologische Funktion von Makromolekülen auf atomarer Ebene zu verstehen. Die Einschränkung der Kristallographie besteht jedoch darin, dass nur Systeme, die in hohen Ausbeuten erhalten und kristallisiert werden können, für diese Technik zugänglich sind. Das Aufkommen einer neuen Generation von EMs, bei denen Proben bei kryogenen Temperaturen untersucht werden (Kryo-EM), hat dieses Gebiet revolutioniert. Cryo-EM, von Nature Methods als „Methode des Jahres 2015“ ausgewählt, ermöglicht strukturelle Untersuchungen biologischer Systeme ohne Kristallisation. Nicht nur die akademische Forschung wurde dadurch revolutioniert, auch die Pharma- und Biotech-Industrie hat diese aufkommende Technologie angenommen. Zum Beispiel haben Genentech, Novartis, Pfizer und andere Unternehmen in ihre eigenen Kryo-EM-Einrichtungen investiert. Cryo-EM eröffnet eine neue Art der biologischen Forschung. Darüber hinaus umfasst es eine Schlüsselaufklärung und ein räumliches Bereichsfenster, das (bio) chemiegetriebene Forschung zu molekularstruktur- und biologiegetriebener Forschung zur zellulären Struktur ermöglicht. Zum Beispiel offenbart ein atomares Modell von HIV-1-Capsid-SP1, das durch Kryo-EM aufgeklärt wurde, Strukturen, die den Zusammenbau und die Reifung regulieren. Diese Revolutionen im EM-Bereich haben zu einer weltweiten Begeisterung für EM geführt, was sich in den zahlreichen hochwirksamen Studien widerspiegelt, die in renommierten Fachzeitschriften veröffentlicht wurden (z. B. über 200 Artikel in Nature, Cell und Science in den letzten 3 Jahren).

<https://www.youtube.com/watch?v=Y5wvMPtYhSg>

In the area of the **life sciences**, Electron Microscopy (EM) enables the in-depth understanding of the basic concept of life. EM is indispensable to address biological structures both at cellular and molecular scales. It has revealed how each cell of the human body is divided into membrane compartments with specialized functions that together organize a diversity of processes, such as protein synthesis, energy production, and distribution of genetic material. Recent developments in EM at extremely low temperatures even allow scientists to zoom in to atomic resolution and see individual proteins or protein complexes within the native environment of the cell. This provides critical insights in the molecular processes of diseases (e.g. transformation of cancer cells, disease-causing mechanisms in the ageing brain) and human development (e.g. differentiation and renewal of stem cells).

Indeed, molecular and cellular defects underlie most diseases, and EM uniquely provides the resolution to study localization and structure of molecules such as proteins, together with the crucial structural information. EM applications are found in fundamental biological research, including infectiology (e.g., EM studies to understand how HIV infects a living mammalian cell), neurobiology (identification of specific regions within the brain, followed by nanoscopic investigation with EM) and pathology (studying subtle pathologic phenotypes that are too small for light microscopy). Recent innovations in automated imaging in 2D (x,y axes; large-scale EM) and 3D (x,y,z axes; volume-EM) are creating unprecedented possibilities to reveal the architecture of cells within the context of their complex environment, such as tumors and even entire brains.

On the molecular level, until recently, only X-ray crystallography and NMR spectroscopy were able to deliver the resolution necessary to describe the structure and understand the biological function of macromolecules at an atomic level. The limitation of crystallography, however, is that only systems that can be obtained at high yields and crystallized are accessible for this technique. The advent of a new generation of EMs, where samples are studied at cryogenic temperatures (**cryo-EM**), has revolutionized this field. *Cryo-EM, selected the 'method of the year 2015' by Nature Methods, allows structural studies of biological systems without the need for crystallization.* Not only has academic research been revolutionized by this, pharmaceutical and biotech industry have also embraced this emerging technology. For example, Genentech, Novartis, Pfizer and other companies have invested in their own top-end cryo-EM facilities. Cryo-EM opens a whole new avenue of biological research. Moreover, it covers a key resolution and spatial range window, that allows (bio)chemistry-driven research on molecular structure and biology-driven research on cellular structure to be bridged. For example, an atomic model of HIV-1 capsid-SP1 elucidated by cryo-EM reveals structures regulating assembly and maturation. These revolutions in the EM field have created worldwide excitement for EM, which is reflected in the numerous high-impact studies published in prestigious journals (e.g., over 200 papers in *Nature*, *Cell* and *Science* in the past 3 years).

From:
<http://www.e-microscopy.nl/#mission>

<https://www.youtube.com/watch?v=Y5wvMPtYhSg>

List of poster abstracts (by presenting author)

A Numerical Analysis of Interaction-Free Measurement for Low-Dose Imaging Using Conditional Sample Re-illumination

Akshay Agarwal^{1,*}, Vivek Goyal² and Karl K. Berggren¹

¹ *Research Laboratory of Electronics, Department of Electrical Engineering and Computer Science, MIT*

² *Department of Electrical and Computer Engineering, Boston University*
**E-mail: akshayag@mit.edu*

Introduction

Interaction-free measurement (IFM) was first proposed by Elitzur and Vaidman [1] as a thought experiment, for detecting the presence of an object without damaging it (in some cases). Following this, Kwiat and co-workers utilized the Quantum Zeno effect to propose an alternative IFM scheme which could potentially reach a success probability of 1 [2]. Over the next decade, theoretical work focused on analyzing the limits of IFM for imaging semitransparent objects, objects with non-uniform transparency distribution, and also incorporating non-ideal detectors and system losses [3-5].

With recent progress in nanofabrication, it has become possible to perform amplitude division interferometry, and therefore incorporate a Mach-Zehnder interferometer, in a standard transmission electron microscope (TEM) [6,7]. In this work, we numerically investigated the limits of performance of a Mach-Zehnder interferometer-based IFM scheme with a Poisson source. We combined IFM with a re-illumination scheme in which the sample is illuminated multiple times, based on the statistics of previous rounds of illumination. This conditional re-illumination scheme reduced the probability of imaging errors at low illumination doses [3].

Methods

In this work, we first considered the imaging of a black-and-white object using both classical and IFM schemes. “Black” here refers to an object pixel that scatters electrons, while “white” refers to a pixel that transmits electrons without scattering. Since electrons in a TEM are scattered (and not absorbed) by objects, we can, in principle, count each electron that is incident on the sample using Direct Electron Detectors. As shown in figure 1, we accounted for the counting of all incident electrons by including two (three) detectors in a classical (IFM) imaging scheme: detectors D_1 (D_1 and D_2) for transmitted electrons, and detector D_3 for scattered electrons. At the start of our calculations, we assumed a prior probability q of a given pixel being black. Then, we found expressions to update q based on the electron detection statistics, assuming a Poisson beam with mean λt . If the value of q was within a pre-defined minimum acceptable error threshold ϵ , we made an inference on whether the pixel was black or white. If this condition was not met, we re-updated q using a second round of detection statistics. Sample damage was quantified by \bar{n}_{damage} , defined as the expected number of electrons scattered off a black pixel. This process was repeated a maximum of

N_{\max} times. The total illumination dose, $\lambda t_{\text{tot}} = \lambda t \times N_{\max}$ was kept constant by reducing λt for increasing N_{\max} . We performed Monte-Carlo simulations to calculate the error probability P_{err} and \bar{n}_{damage} , for various values of λt_{tot} and N_{\max} , using the single-stage update expressions described earlier. The calculated values of P_{err} and \bar{n}_{damage} traced out a curve for each value of N_{\max} .

Results

Figure 2(a) shows the results of these simulations for IFM without D_3 ; we see that \bar{n}_{damage} reduced for constant P_{err} and increasing N_{\max} . This shows the utility of conditional re-illumination in reducing sample damage. Figure 2(b) shows the results of imaging utilizing conditional re-illumination, for both classical and IFM imaging with D_3 . These results were calculated for $\epsilon = 0.05$, with $N_{\max} = 1$ (circles with dotted line) and $N_{\max} = 50$ (crosses with dashed lines) illuminations. For both schemes, conditional re-illumination offered a reduction in \bar{n}_{damage} at 50 illuminations as compared to single-stage illumination. For classical imaging with D_3 , \bar{n}_{damage} was reduced to 1 at $N_{\max} = 50$. At high N_{\max} , the probability of the beam having more than one electrons was very low. Most pixels received at most one electron, which was sufficient to infer their transparency. For IFM with D_3 , \bar{n}_{damage} saturated to 0.67 for $N_{\max} = 50$. This is equal to the probability of a D_3 event, given that either a D_2 or D_3 event occurred, which was when illumination in our simulation was stopped.

Discussion

Our results show that conditional re-illumination can be used to reduce sample damage to the level of single electrons. The choice of imaging scheme depends on the tolerable error and damage rates. If a very low error rate is desired, classical imaging with D_3 produces the lowest sample damage. On the other hand, if an error rate of a few percent is tolerable, IFM with D_3 can reduce the expected sample damage to below 1 electron per pixel. The calculations presented here are limited by the requirement of black-and-white samples and perfect detectors. We are currently expanding our calculations to include greyscale samples and detector losses, and to incorporate multiple interferometer stages, as envisaged by Putman and Yanik [8], and Kruit et al. [9].

References

- [1] A. C. Elitzur and L. Vaidman, Found. Phys. **23**, 7, 987–997, 1993
- [2] P. Kruit et al., Ultramicroscopy **164**, 31–45, 2016
- [3] G. Mitchison et al., Phys. Rev. A. **65**, 2, 1–6, 2002
- [4] G. Krenn et al., Phys. Rev. A **61**, 5, 52102, 2000
- [5] S. Thomas et. al, Phys. Rev. **90**, 5, 1–10, 2014
- [6] A. Agarwal et al., Sci. Rep. **7**, 1, 1–10, 2017
- [7] A. H. Tavabi et al., Eur. Phys. J. Appl. Phys. **78**, 1, 10701, 2017
- [8] P. Kwiat et al., Phys. Rev. Lett. **74**, 24, 4763–4766, 1995
- [9] W. P. Putnam and M. F. Yanik, Phys. Rev. A **80**, 4, 1–4, 2009

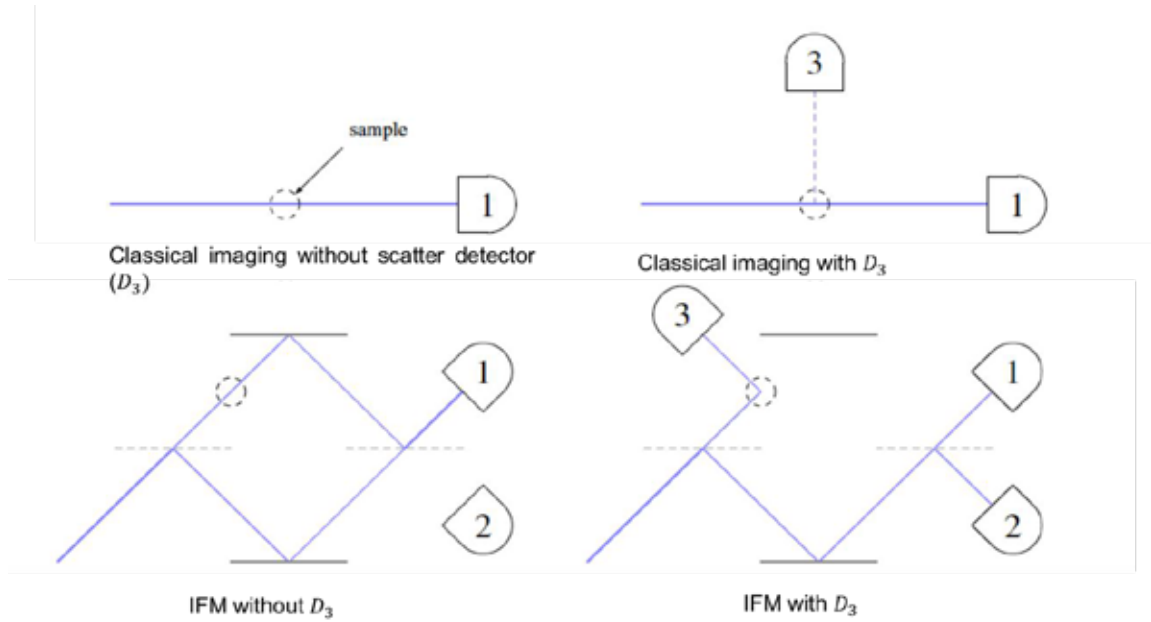


Figure 1 : The four imaging schemes considered in this work. 1, 2 and 3 indicate detectors D_1, D_2 (for transmitted electrons) and D_3 (for scattered electrons)

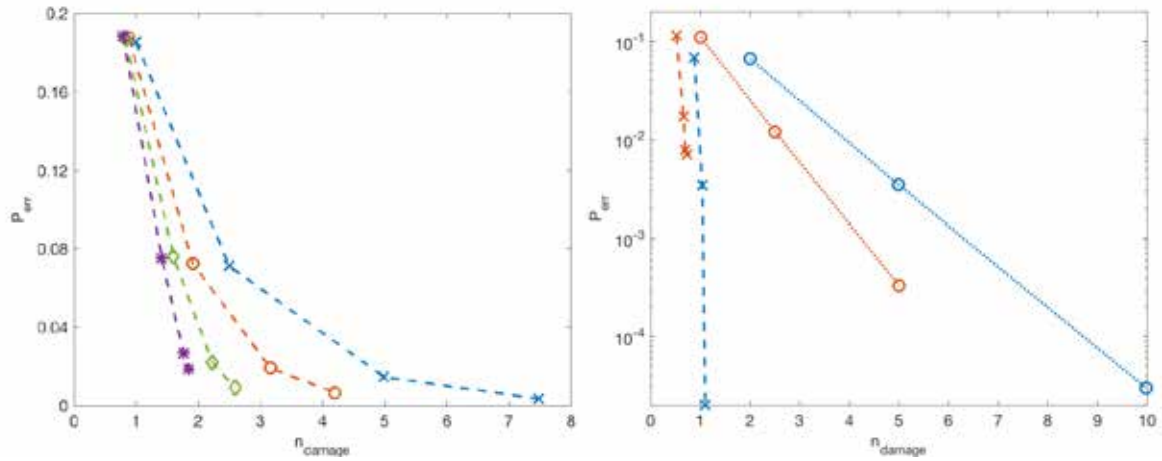


Figure 2 : Imaging with conditional re-illumination. (a) P_{err} vs \bar{n}_{damage} for IFM without D_3 for 1 (blue), 2 (orange), 10 (green) and 50 (purple) illuminations. As the number of illuminations increase, \bar{n}_{damage} reduces for the same P_{err} . (b) P_{err} vs \bar{n}_{damage} for classical (red) IFM (blue) with D_3 . Dotted lines with circles indicate values for single-stage illumination, and dashed lines with crosses indicate values for 50 illuminations. For both schemes, \bar{n}_{damage} reduced to 1 (classical) and 0.67 (IFM) for 50 illuminations as compared to single-stage.

Holography in Scanning Transmission Electron Microscopy

Tyler R. Harvey^{1,2}, Colin Ophus³, Fehmi S. Yasin¹, Jordan J. Chess¹, Jordan S. Pierce¹, and Benjamin J. McMorran¹

¹*Department of Physics, 1274 University of Oregon, Eugene, OR, 97403, USA*

²*Fourth Physical Institute, Georg-August-Universität Göttingen, Friedrich-Hund-Platz 1, Göttingen, Germany*

³*National Center for Electron Microscopy, Lawrence Berkeley National Laboratory, One Cyclotron Road, Building 72, Berkeley, CA 94720*

e-mail: tyler.harvey@uni-goettingen.de

Introduction

Off-axis electron holography, which uses an electrostatic biprism to interfere electrons transmitted through a specimen with a reference wave, has for many years been the premier technique for retrieving the phase of electrons. With holography, one can both reconstruct long-range electric and magnetic fields [1], and map the charge distribution in a nanowire [2]. However, the resolution of off-axis electron holography is fundamentally limited because interference fringes are recorded in real space; standard reconstruction of the phase has a resolution on the order of the fringe spacing [3].

A similar technique is possible in scanning transmission electron microscopy (STEM), where the transmitted beam and reference beam are focused, and holograms are recorded in diffraction as the beams are scanned. Resolution is limited only by the size of the focused beams at the specimen. This technique, called STEM holography, was pioneered several decades ago [4, 5, 6]. These early efforts worked around the slow speed of pixelated detectors at the time by using physical masks placed atop a monolithic detector to map fringe shifts onto intensity variations. As this method was technically challenging, the technique never found widespread use. Today, with fast direct electron detectors that allow rapid recording of a diffraction pattern at each position in STEM, and with nanofabricated diffraction gratings that can produce identical probe beams, STEM holography is an excellent technique for producing highly interpretable phase contrast. We show that phase retrieval is straightforward and intuitive and present a proof-of-principle demonstration.

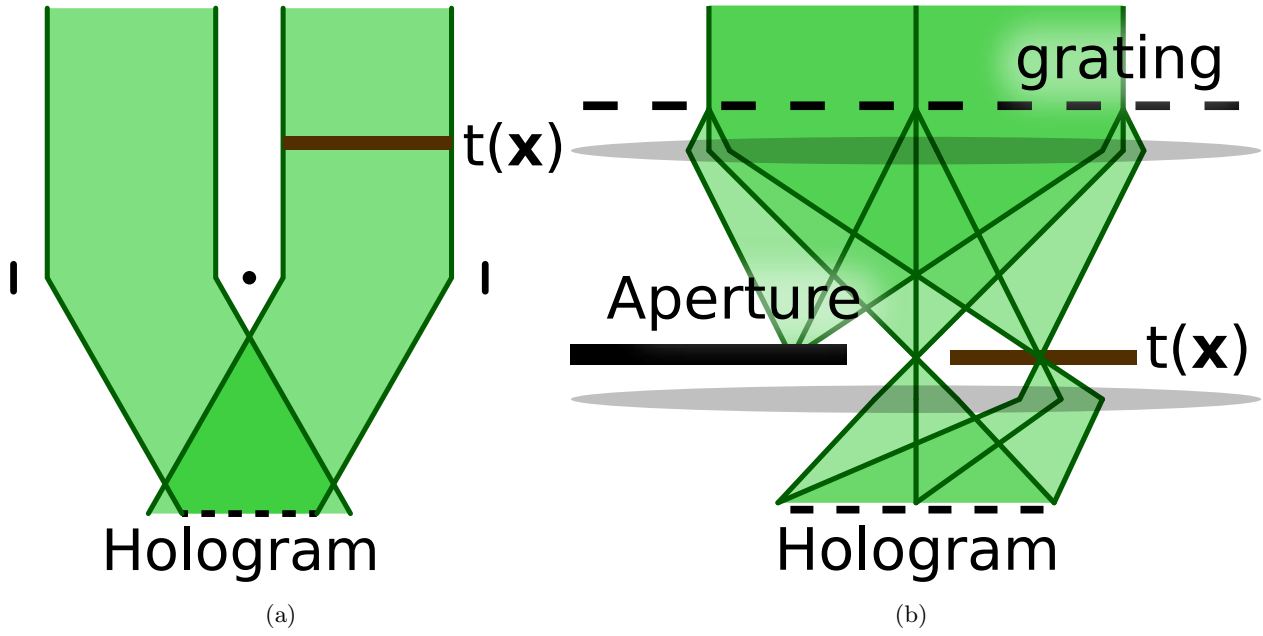


Figure 1: (a) Schematic of off-axis electron holography with a biprism. One plane wave is passed through the specimen (brown), and an electrostatic biprism (black dot) interferes this wave with a second plane wave passed through vacuum. (b) Schematic of STEM holography. A diffraction grating in the condenser system produces multiple beams at the specimen (brown). An aperture is used to pass only one beam that passed through the specimen and one passed through vacuum. The projector system combines these beams into a hologram.

Methods

We employ a nanofabricated diffraction grating [7] with a 150 nm pitch and 50 μm diameter placed in the second condenser aperture of the TEAM I instrument at the National Center for Electron Microscopy. In STEM mode with a 4 mrad convergence semi-angle, this grating produces beams separated by 120 nm at the specimen. With descans properly aligned, a selected area aperture passes only the two most intense beams without limiting the field of view. We scan the beams across a specimen and record one diffraction pattern per probe position.

To reconstruct the amplitude and phase of the specimen transfer function, we Fourier transform each diffraction pattern, select the first-order spot, multiply by a kernel (when aberrations are negligible, the complex conjugate of the first-order spot in vacuum is an appropriate choice), and integrate over the spot to retrieve the average phase at that probe position.

Results & Discussion

As a first demonstration of the technique, we imaged gold and semiconducting nanoparticles and an amorphous carbon substrate. The phase contrast provided by STEM holography provides high contrast on low-atomic-number materials; indeed, in Fig. 2a, we can clearly see a spot of

contamination in the upper left that is barely distinguishable in the simultaneously acquired ADF image (Fig. 2b).

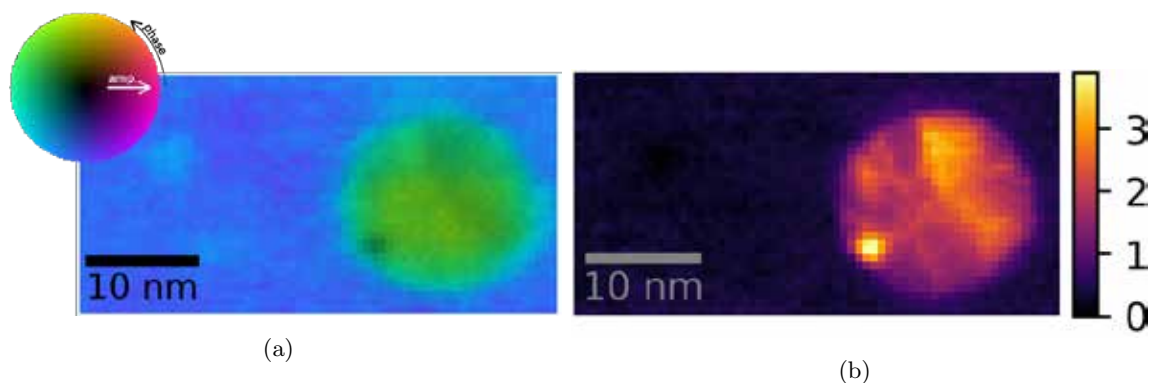


Figure 2: (a) Reconstructed phase (color) and amplitude (brightness) of a gold nanoparticle on an ultrathin carbon substrate. (b) Simultaneously acquired ADF signal.

STEM holography offers highly interpretable contrast on both high- and low-atomic-number materials. In addition, unlike any other phase contrast STEM technique, because of the vacuum reference for phase reconstruction, STEM holography can quantitatively electric and magnetic fields. Because resolution is limited only by the probe size and dose, atomic resolution should be achievable. STEM holography is a highly versatile tool and may become a workhorse tool for efficient, interpretable imaging in the electron microscope.

References

- [1] O. Matteucci, G.F. Missiroli, and G. Pozzi, *Advances in Imaging & Electron Physics* 99, 171 (1997).
- [2] Z. Gan, M. Gu, J. Tang, C.-Y. Wang, Y. He, K.L. Wang, C. Wang, D.J. Smith, M.R. McCartney, *Nano Letters* 16, 3748 (2016).
- [3] H. Lichte, *Advances in Optical and Electron Microscopy* 12, 25 (1991).
- [4] T. Leuthner, H. Lichte, and K.-H. Herrmann, *physica status solidi (a)* 116, 113 (1989).
- [5] Y. Takahashi, Y. Yajima, M. Ichikawa, and K. Kuroda, *Japanese Journal of Applied Physics* 33, L1352 (1994).
- [6] J. Cowley, *Ultramicroscopy* 96, 163 (2003).
- [7] T.R. Harvey, J.S. Pierce, A.K. Agrawal, P. Ercius, M. Linck, and B.J. McMorran, *New Journal of Physics* 16, 093039 (2014).

Maximizing contrast in cryo-transmission electron microscopy with physical phase plates

M. Obermair¹, S. Hettler¹, C. Hsieh², M. Marko² and D. Gerthsen¹

¹Laboratory for Electron Microscopy, KIT, Karlsruhe, Germany

²Wadsworth Center, New York State Department of Health, Albany, USA

E-mail: martin.obermair@kit.edu

The weak contrast of radiation-sensitive biological objects in (cryo-)transmission electron microscopy (TEM) poses a fundamental physical limit to their structure determination. By using physical phase plates (PPs) which induce a relative phase shift between the scattered and unscattered part of the electron wave and thus improve the phase contrast, the necessary dose to obtain the contrast required for structure determination is significantly decreased. In addition, when combined with a highly sensitive direct electron detector, the limit can be even pushed further.

Here, we compare two of the most promising PP types, namely the hole-free (HF) or Volta PP [1,2] and the electrostatic Zach PP [3] using a JEOL JEM-3200FSC/PP equipped with a Gatan K2 camera. Both types of PPs have in common, that they exhibit a smooth phase shift profile which is localized around the zero-order beam. This strongly reduces artifacts occurring for PPs with abrupt phase shift profiles. We acquired image series and electron tomograms of three cryo test samples to study the potential of the different PP types. Figure 1 shows a comparison of cryo-TEM images of a T4 bacteriophage sample obtained without PP (Fig. 1a), with HFPP (Fig. 1b) and with a Zach PP at a voltage of -2 V (Fig. 1c). The contrast enhancement generated by the PPs is clearly visible and is similar for both PP types. While the HFPP is easier to fabricate and use, its induced phase shift is difficult to control and changes under continuing application. An advantage of the Zach PP is the direct control of the induced phase shift allowing an object-wave reconstruction which comes at the expense of a complex fabrication and minor artifacts induced by the presence of the physical structure in the back focal plane.

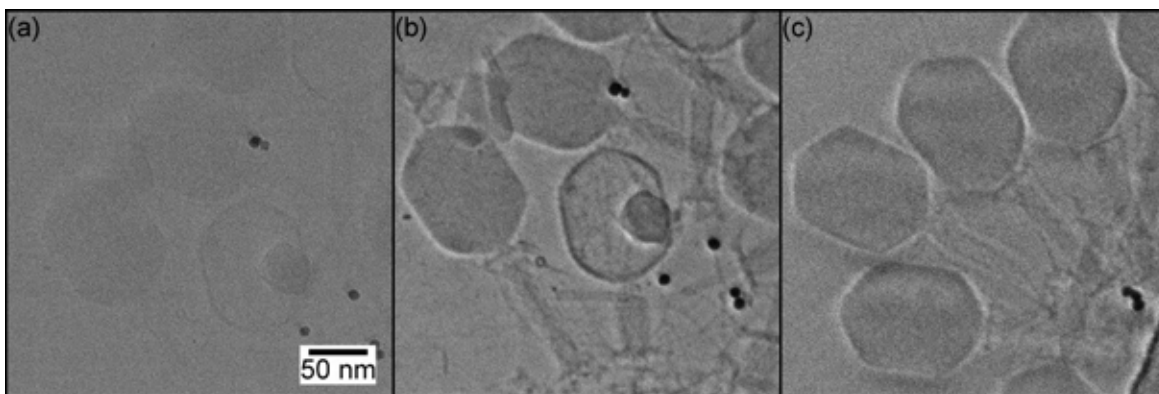


Fig.1 : Cryo-TEM images acquired (a) without PP, (b) with HFPP and (c) with Zach PP.

References

- [1] M. Malac et al., Ultramicroscopy **118**, 77-89 (2012).
- [2] R. Danev et al., PNAS **111**, 15635-15640 (2014).
- [3] Hettler et al., Microscopy and Microanalysis **18**, 1010-1015 (2012).

One nanoliter protein is sufficient to resolve near-atomic resolution structures; next generation sample preparation for fully automated cryo-EM analysis of macromolecular structures and cells

R.B.G. Ravelli, F. Nijpels, G. Weissenberger, R. Henderikx, A. Gijsbers, P. Huysmans, B. Beulen, C. Berger, C. Lopez-Iglesias, and P.J. Peters

*The Maastricht Multimodal Molecular Imaging institute
www.maastrichtuniversity.nl/m4i
Maastricht University, The Netherlands*

Cryo-EM is a rather cool technique for structural biology. Advances in detector technology and data processing have made tremendous impact, however, sample preparation remains one of the major bottlenecks of the process. The leading commercial device for sample preparation, the VitrobotTM was developed more than a decade ago within our lab in Maastricht. With the current process, more than 99.9% of precious sample is disposed upon application by blotting. Besides, mechanical stress can compromise the grid quality and the prolonged exposure to the air-water interface can induce partial protein unfolding and preferred molecular orientations. Many scientists new to cryo-EM are currently drawn to the field and face bottlenecks such as poor reproducibility and operator dependent results. Automated microscopes demand extra skills for the users to deal with mounting their precious samples in autogridTM rings in cryogenic conditions which also can induce damage.

We are developing the next generation vitrification machine which implement a number of radical different solutions. The device, named VitroJetTM, is fed by a cassette of pre-mounted autogrids, which are glow discharged inside the machine to enable a reproducible application of a thin layer. Subsequently, a sub-nanoliter amount of sample is pin-printed onto the grid while evaporation is mitigated by a dewpoint feedback loop. Directly after sample application, the sample is vitrified using liquid ethane jets. As the jets are directed to the center of the grid where the sample is located, superior cooling rates are obtained compared to traditional plunging methods. E.g., whereas pre-mounted autogrids cannot be properly vitrified within a Vitrobot, these assemblies can be successfully vitrified within the VitroJet. We will provide a status update of our developments, and present structures solved from samples prepared with this device.

Realization of the Feynman-Young thought experiment: Controlled electron interference in Fraunhofer and image space

**Amir H. Tavabi^{1,2}, Chris B. Boothroyd³, Emrah Yücelen⁴,
Stefano Frabboni^{5,6}, Gian Carlo Gazzadi⁵, Rafal E. Dunin-
Borkowski^{1,2}, Giulio Pozzi^{1,7}**

1. Ernst Ruska-Centre for Microscopy and Spectroscopy with Electrons, Forschungszentrum Juelich, 52425 Jülich, Germany
2. Peter Grünberg Institute, Forschungszentrum Jülich, 52425 Jülich, Germany
3. School of Materials Science and Engineering, Nanyang Technological University, 50 Nanyang Avenue, Singapore 639798
4. FEI Company, Achtseweg Noord 5, 5600 KA Eindhoven, The Netherlands
5. Department FIM, University of Modena and Reggio Emilia, via G. Campi 213/a, Modena 41125, Italy
6. CNR-Institute of Nanoscience-S3, Via G. Campi 213/a, Modena 41125, Italy
7. Department of Physics and Astronomy, University of Bologna, Viale B. Pichat 6/2, 40127 Bologna, Italy

The key features of quantum mechanics are illustrated by the Feynman-Young double-slit thought experiment, whose second part discusses the electron distribution when one of the two slits is partially or totally closed by an aperture and whose analysis leads to the idea of the probability amplitude. Although this experiment has been attempted previously [1,2], the presence of diffraction phenomena in the Fresnel regime meant that it was only an approximation to the ideal experiment. Here, we show how such shortcomings can be overcome in a modern electron microscope. We achieve an ideal Feynman-Young experiment, both in diffraction (Fraunhofer) space and in image space, by precisely tuning the microscope lenses to make use of conjugate plane(s) to the double slit plane.

Figure 1 shows the realisation of the controlled double slit experiment. The slits are in the object plane of the microscope, while a beam blocker (here, a Mollenstedt biprism) is placed exactly in a conjugate plane of the slits. The biprism is located in the image plane of an extra lens, which is just above the diffraction lens of the microscope. When the biprism covers one of the slits completely, the interference phenomena in the double slit regime transform into the diffraction envelope of a single slit. The experiment was carried out at 60 kV, in order to ensure that no electron could pass through the covered area of the slits or the beam blocker.

Figure 2 shows a controlled electron interference experiment performed in image space using two electron biprisms, with the lower biprism located close to the image plane of the diffraction lens. The upper biprism is tilted with respect to the slits, but is still in a conjugate plane. The lower biprism is slightly above the second conjugate plane and can be used to interfere the beams by applying a voltage to it. Changes in the spacing and direction of the interference fringes, which were observed when voltages were applied to one or both biprisms, will be discussed.

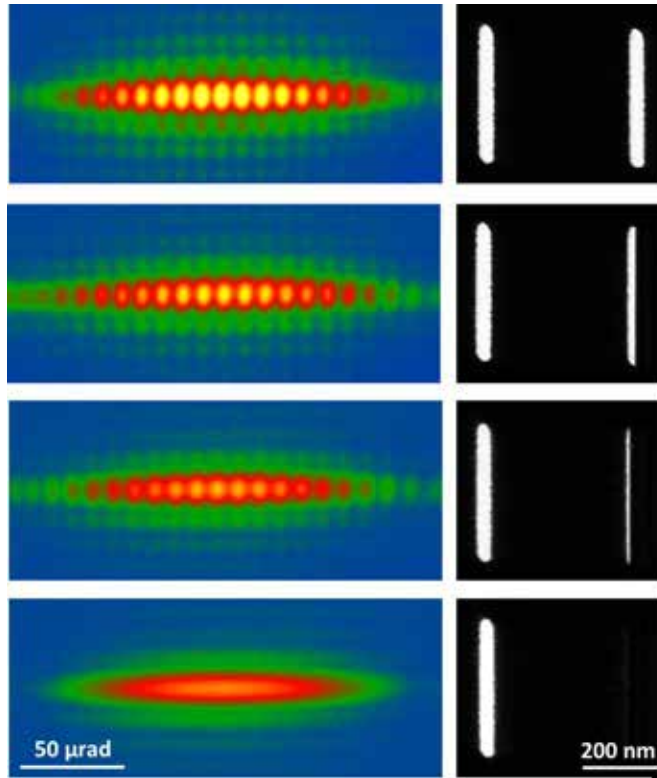


Figure 1: Double slit controlled electron beam experiment with a mask in a conjugate plane of the slits (right) and its effect on the corresponding Fraunhofer diffraction image (left).

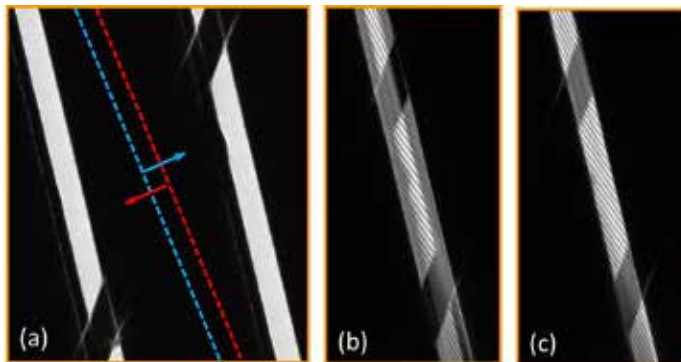


Figure 2: (a) Controlled electron interference experiments in image space performed using two electron biprisms. The lower biprism is located in the dark region between the two slits (and is positioned some distance above a conjugate image plane). Its edges are marked by dashed lines. The upper biprism is visible crossing the slits at an angle and is in a conjugate image plane. (b) Partial and (c) total overlap of the two slits was achieved when the bias applied to the lower biprism was increased, resulting in the formation of two-beam interference fringes.

References

- [1] G. Matteucci and G. Pozzi. Two further experiments on electron interference. Am. J. Phys., 46(6):619{623, 1978.
- [2] R. Bach, D. Pope, S.-H. Liou and H. Batelaan. Controlled double-slit electron diffraction. New J. Phys., 15(3):033018, 2013.

Fabrication of an e-beam OAM sorter via Electron Beam Lithography

Paolo Rosi ¹, Giacomo Medici ¹, Federico Venturi ¹, Claudia Menozzi¹, Gian Carlo Gazzadi², Stefano Frabboni ¹and Vincenzo Grillo ²

¹*Università di Modena e Reggio Emilia, Dipartimento FIM, Modena, Italy*

²*CNR Istituto Nanoscienze S3, Modena, Italy*

E-mail: paolo.rosi@unimore.it

Introduction

The discovery of the possibility to shape electron beam in a similar fashion as photon beams led to the generation of electron vortex beams carrying discrete quanta of Orbital Angular Momentum (OAM). This fact allowed vertical magnetic measurements [1] and opens the road to spin polarization and magnetic and plasmonic dichroism analysis.

While the generation of vortex beams has been the focus of many research groups for few years after the discovery, recently some research groups have started to take in consideration also the problem of how to efficiently analyze the OAM.

Phase holograms and electrostatic phase elements permit to introduce the most efficient method of OAM decomposition namely the OAM sorter based on the conformal mapping of the wavefunction. [2][3][4]

Our research group focused his efforts in the last years in producing increasingly difficult holograms by focused ion beam (FIB) nanofabrication, achieving satisfying results [5]. In the case of holographic production of an electron beam with very high OAM ($l=1000$) when the FIB reached its resolution limit we used electron beam lithography (EBL) to achieve better resolution. [6]

However, the production of the phase holograms via EBL is more complicated and requires to finely tune all the different steps to obtain satisfying results.

Here we present the early stage results for the production of sorting holograms via EBL which may lead to better results.

Methods

We started by depositing a thin layer ($\sim 50\text{nm}$) of a positive resist designed for electron beam lithography, CSAR6200/2 with a 4% concentration of polymer, on top of the Si_3N_4 substrate of the commercially available Si_3N_4 3mm TEM membranes.

The development of the resist has been done at $T_{\text{DEV}} \sim 5^\circ\text{C}$

The choice to use such resist has been made after realizing that the more commonly used PMMA was not as etch-resistant as hoped for.

In fact, after reproducing the pattern on the resist, it is necessary to transfer it on the Si_3N_4 membrane underneath. This step has been done utilizing Reactive Ion Etching (RIE). A gas mixture of $CF_4 + O_2$ was used to etch the Si_3N_4 membranes, such a mixture is commonly used to etch Si and its composites.

Results

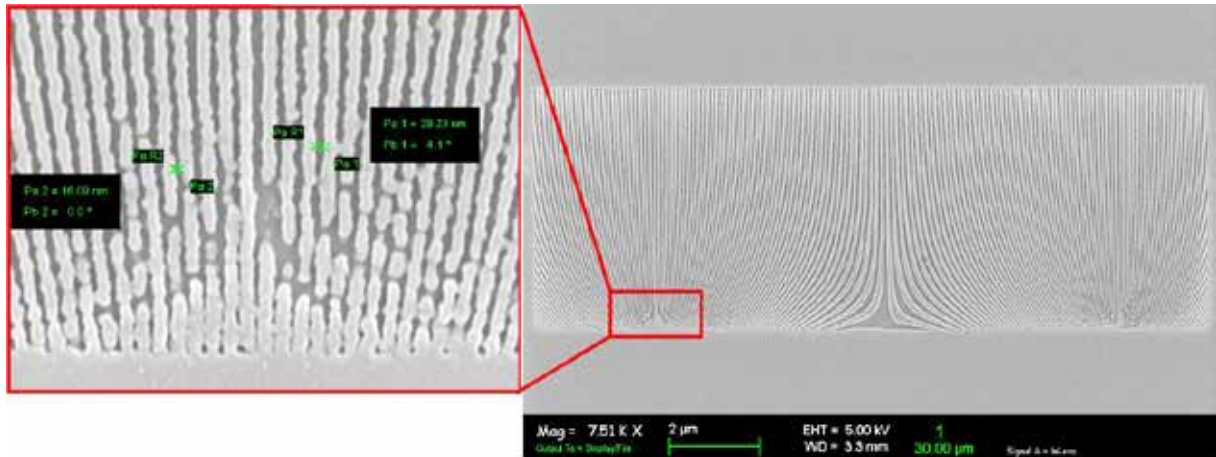


Figure 1: SEM images of part of the OAM sorter reproduced on the resist after development. The image has been obtained by C-metallization, which also enhances the contrast.

As it is possible to notice from Fig. 1 the results are quite satisfying, the pattern was almost perfectly reproduced on the resist, the smallest lines that can be found have a lateral dimension of $\sim 13nm$ and are $\sim 50nm$ deep (the depth was measured via Atomic Force Microscopy).

As anticipated in the Methods section, the next step has been transferring the pattern on the Si_3N_4 membrane underneath via RIE. The result of the transfer is shown in Fig.2.

The contrast in Fig.2 is not as crispy as in Fig.1, this is due to the fact that after the transfer we didn't perform a C-metallization, combined to the fact that Si_3N_4 is insulating.

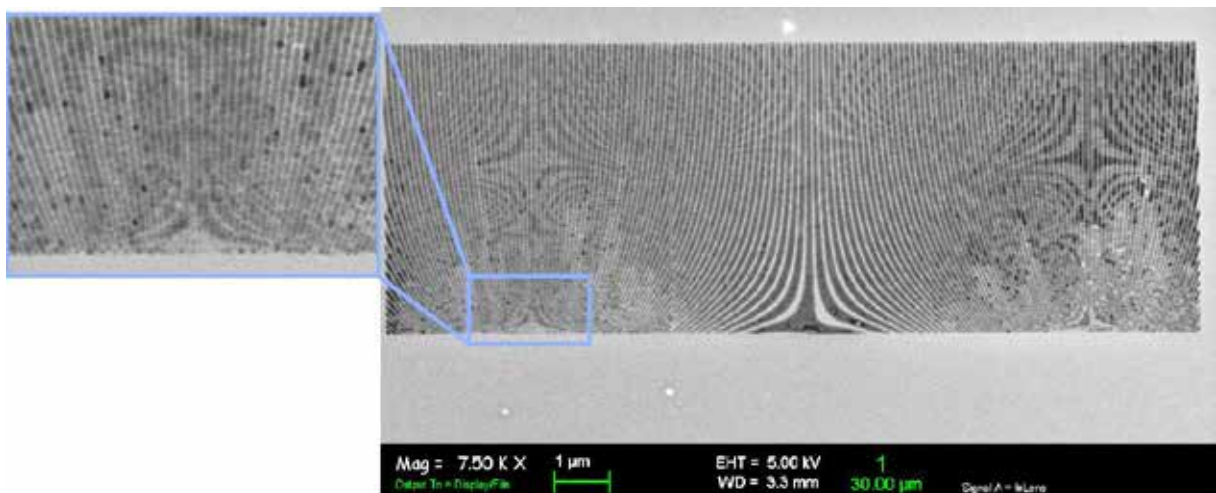


Figure 2: SEM image of the transferred pattern on the Si_3N_4 membrane via RIE.

From Fig.2 is possible to notice how the transfer of the pattern has not been perfect and the etching is uneven and has broadened the thinner lines. On the positive side, it is also possible to notice how most of the thinner lines have been transferred, which means that by further refining our recipe, we can obtain very satisfying results.

Discussion

We found how an almost perfect reproduction on the resist of the pattern of the e-beam OAM sorter is possible, and that the transfer to the underneath Si_3N_4 membrane is difficult and requires further experimenting.

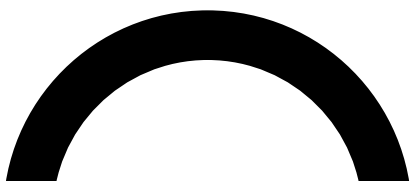
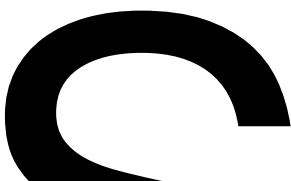
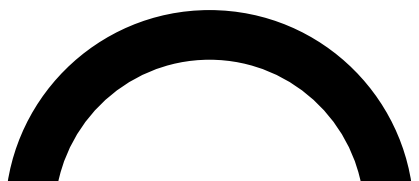
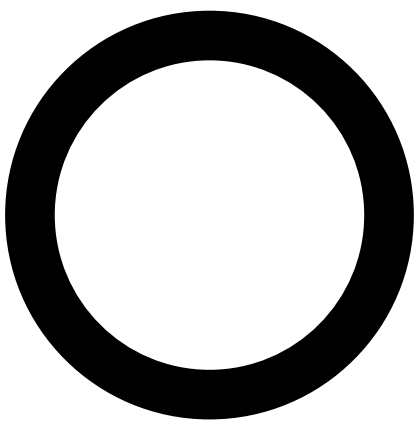
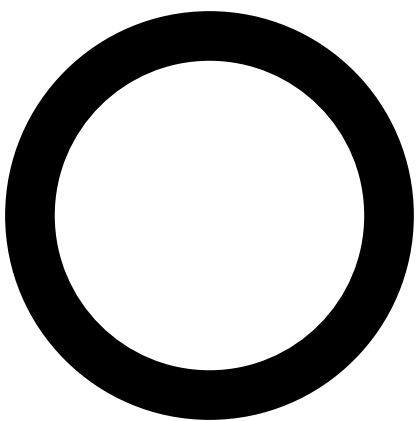
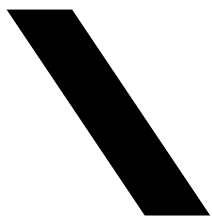
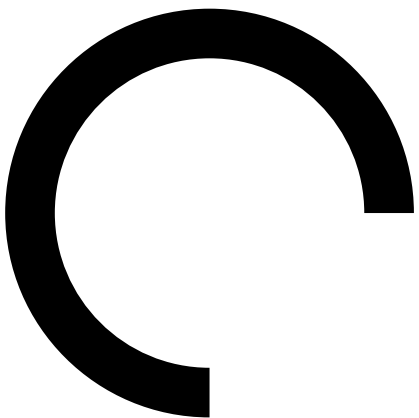
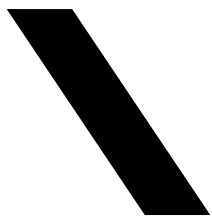
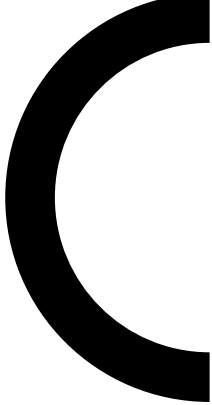
The unsatisfying results are probably due to the transfer process we used. Indeed RIE should uniformly etch a material surface removing a certain amount of substrate each second. With features that are in the order of tens of nanometers we observed that the etching rate depends on the exposed area of the material that needs to be etched. This introduces the problem that the membrane doesn't have grooves of the same height, which in return impacts the efficiency of the hologram.

Moreover, we also found out that the $CF_4 + O_2$ gas mixture was too aggressive on both the resist and the membrane, leading to a premature erosion of the resist. So for future experiments we will switch to a $CF_4 + CHF_3$ gas mixture, which allows a more controlled etching of Si_3N_4 and is less aggressive on the resist than the previous one.

Further studies are underway to find a way to mask the area around the patterned one with a thick layer of gold so that only the part of interest of the incoming beam is analyzed, and the superpositions are reduced.

References

- [1] V. Grillo et al. Nature Communications **8**. 689 (2017)
- [2] G.C.G Berkhout, et al. Phys.Rev.Lett.**105**,153601 (2010)
- [3] V.Grillo et al. Nature Communications **8**. 15536 (2017)
- [4] B.J.McMorran et al. New J.Phys. **19**, 023053 (2017)
- [5] H. Larocque et al. Contemporary Physics, doi: 10.1080/00107514.2017.1418046,1-19 (2018)
- [6] E. Mafakher et al. Appl. Phys. Lett. **110**, 093113 (2017)



List of participants

| First name | Family name | Institution | Department | City | Country | Email |
|------------------------|--------------------|--|-----------------------------------|-------------|---------|--|
| Juri | Barthel | ER-C 2 | | Jülich | DE | ju.barthel@fz-juelich.de |
| Armand | Béché | EMAT - University of Antwerp | | Antwerp | BE | armand.beche@uantwerpen.be |
| Marco | Beleggia | DTU | Danchip Cen | Kgs. Lyngby | DK | mb@cen.dtu.dk |
| Moritz | Carmesin | HZDR | Institut für Strahlenphysik | Dresden | DE | moritz.carmesin@uni-ulm.de |
| Jan | Caron | Forschungszentrum Jülich | ER-C | Jülich | DE | j.caron@fz-juelich.de |
| Thibaud | Denneulin | Forschungszentrum Jülich | | Jülich | DE | t.denneulin@fz-juelich.de |
| Martial | Duchamp | Nanyang Technological University | Materials Science and Engineering | Singapore | SG | mduchamp@ntu.edu.sg |
| Rafal | Dunin-Borkowski | Forschungszentrum Jülich | Ernst Ruska-Centre | Jülich | DE | rdb@fz-juelich.de |
| Maxim | Efremov | Institute of Quantum Physics | Ulm University | Ulm | DE | maxim.efremov@uni-ulm.de |
| Stefano | Frabboni | University of Modena and Reggio Emilia | FIM | Modena | IT | stefano.frabboni@unimore.it |
| Jim | Franssen | Eindhoven University | Applied physics | Eindhoven | NL | j.g.h.franssen@tue.nl |
| Bert | Freitag | Thermofisher Scientific | MS BU | Eindhoven | NL | Bert.Freitag@thermofisher.com |
| Luca Marco Carlo | Giberti | QED F&S Productions Ltd. | | Bristol | GB | lucamarcocarlogiberti@qedproductions.co.uk |
| Manuel | Goncalves | Ulm University | Institute of Experimental Physics | Ulm | DE | manuel.goncalves@uni-ulm.de |
| Avraham | Gover | Tel Aviv University | Physical Electronics | Tel Aviv | IL | gover@eng.tau.ac.il |
| Vincenzo | Grillo | CNR | Istituto Nanoscienze | Modena | IT | vincenzo.grillo@nano.cnr.it |
| Lukas | Grünewald | Karlsruher Institut für Technologie | Lab. für Elektronenmikroskopie | Karlsruhe | DE | lukas.gruenewald@student.kit.edu |
| Giulio | Guzzinati | University of Antwerp | Physics | Antwerp | BE | giulio.guzzinati@uantwerpen.be |
| Tyler | Harvey | University of Göttingen | Fourth Physical Institute | Göttingen | DE | tyler.harvey@uni-goettingen.de |
| Jonas | Heidler | Paul Scherrer Institut | LBR | Villigen | CH | jonas.heidler@psi.ch |
| Simon | Hettler | KIT - LEM | | Karlsruhe | DE | simon.hettler@kit.edu |
| Thomas | Juffmann | University of Vienna | Physics | Vienna | AT | thomas.juffmann@univie.ac.at |
| Ido | Kaminer | Technion | | Haifa | IL | ido.kaminer@gmail.com |
| Mark | Kasevich | Stanford University | | Stanford | US | kasevich@stanford.edu |
| Peter | Kling | Ulm University | Institute for Quantum Physics | Ulm | DE | peter.kling@uni-ulm.de |
| Stewart | Koppell | Stanford University | | Stanford | US | skoppell@stanford.edu |
| Christian | Kramberger | Technische Universität Wien | Solid State Physics | Vienna | AT | christian.kramberger-kaplan@tuwien.ac.at |
| Maurice | Krielaart | Delft University of Technology | Department of Imaging Physics | Delft | NL | m.a.r.krielaart@tudelft.nl |
| Hugo | Lourenço-Martins | Laboratoire Physique des Solides | | Orsay | FR | hugo.lourenco-martins@u-psud.fr |
| Peng-Han | Lu | Forschungszentrum Jülich | | Jülich | DE | p.lu@fz-juelich.de |
| Zheng | Ma | Forschungszentrum Jülich | ER-C | Jülich | DE | z.ma@fz-juelich.de |
| Sairam | Malladi | IIT Hyderabad | Materials Science & Met. Engg. | Hyderabad | IN | srkm@iith.ac.in |
| Ali | Mohammadi-Gheidari | Thermo Fisher Scientific | | Eindhoven | NL | Ali.Gheidari@fei.com |
| Yoshie | Murooka | Forschungszentrum Jülich | PGI-5/ER-C | Jülich | DE | y.murooka@fz-juelich.de |
| Devendra | Negi | Uppsala University | Dpt. Physics and Astronomy | UPPSALA | SE | dev.snegi1@gmail.com |

| | | | | | | |
|--------------------|---------------|---------------------------------------|-------------------------------|------------------|----|--------------------------------------|
| Eva | Olsson | Chalmers University of Technol | Department of Physics | Gothenburg | SE | eva.olsson@chalmers.se |
| Yiming | Pan | Tel Aviv University | Physical Electronics | Tel Aviv | IL | yimingpan@mail.tau.ac.il |
| Philipp | Pelz | Max Planck Institute | Atomically Resolved Dynamics | Hamburg | DE | philipp.pelz@mpsd.mpg.de |
| Dusko | Polovina | University of Belgrade | | Belgrade | RS | Eko.duki@gmail.com |
| Mina | Polovina | University of Belgrade | | Belgrade | RS | minamina1712@gmail.com |
| Peter | Peters | M4I | Nanoscopy | Maastricht | DE | peter.peters@maastrichtuniversity.nl |
| Enrico | Pomarico | EPFL | EPFL - SB - IPHYS - LUMES | Lausanne | CH | enrico.pomarico@epfl.ch |
| Ulrich | Poppe | CEOS/FZ-Jülich | PGI-5 | Jülich | DE | u.poppe@fzjuelich.de |
| Giulio | Pozzi | ER-C Jülich | | Jülich | DE | giulio.pozzi@unibo.it |
| MD Ashiqur | Rahman | University of Rome La Sapienza | Nanotechnology Engineering | Rome | IT | ashikbd89@yahoo.com |
| Achim | Raschka | Wikipedia | | Erfstadt | DE | achim.raschka@wikipedia.de |
| Raimond | Ravelli | Maastricht University | M4I | Maastricht | NL | rbg.ravelli@maastrichtuniversity.nl |
| Phila | Rembold | University of St Andrews | Physics | St Andrews | GB | pkmr@st-andrews.ac.uk |
| Roei | Remez | Tel Aviv University | | Tel Aviv | IL | roei.remez@gmail.com |
| Alberto | Roncaglia | CNR | | Bologna | IT | roncaglia@bo.imm.cnr.it |
| Paolo | Rosi | Università di Modena e Reggio | Physics, IT and Math | Fiorano Modenese | IT | paolo.rosi@unimore.it |
| Enzo | Rotunno | CNR-NANO | | Modena | IT | enzo.rotunno86@gmail.com |
| Georgi Gary Parham | Rozenman | Tel Aviv University | | Tel Aviv | IL | swamipremkeerti@gmail.com |
| | Sadooghi | University of Toronto | | Toronto | CA | parham.sadooghi@utoronto.ca |
| Raffaella | Santucci | QED Film and Stage Productions | | Bristol | GB | raffaella@qedproductions.co.uk |
| Wolfgang | Schleich | Ulm University | Institute of Quantum Physics | Ulm | DE | wolfgang.schleich@uni-ulm.de |
| Roy | Shiloh | Friedrich-Alexander University | Chair of Laser Physics | Erlangen | DE | roy.shiloh@fau.de |
| Helmut | Soltner | Research Center | ZEa-1 | Inden | DE | h.soltner@fz-juelich.de |
| Rolf | Speen | Forschungszentrum Jülich | | Jülich | DE | r.speen@fz-juelich.de |
| Daan | Stellinga | University of Glasgow | School of Physics & Astronomy | Glasgow | GB | daan.stellinga@glasgow.ac.uk |
| Andy | Stewart | University of Limerick | Physics | Limerick | IE | andy.stewart@ul.ie |
| Amir | Tavabi | Forschungszentrum Jülich | | Jülich | DE | a.tavabi@fz-juelich.de |
| Pooja | Thakkar | Paul Scherrer Insitut | | Villigen | CH | pooja.thakkar@psi.ch |
| Peter | Tiemeijer | R&D | | Eindhoven | NL | peter.tiemeijer@thermofisher.com |
| Ioannis | Tsiaoussis | Aristotle University | Physics Department | Thessaloniki | GR | tsiaous@auth.gr |
| Marco | Turchetti | Massachusetts Institute of Technology | | | US | turchett@mit.edu |
| Wouter | Van den Broek | Humboldt-Universität zu Berlin | Institut für Physik | Berlin | DE | vandenbroek@physik.hu-berlin.de |
| Jasper | van Rens | TU/e Eindhoven | Applied Physics | Eindhoven | NL | jaspervanrens@gmail.com |
| Yuri | van Staaden | Delft University of Technology | Imaging Physics | The Hague | NL | y.j.vanstaaden@student.tudelft.nl |
| Giovanni Maria | Vanacore | EPFL | Institute of Physics | Lausanne | CH | giovanni.vanacore@epfl.ch |
| Johan | Veerbeck | University of Antwerp | | Antwerp | BE | jo.verbeeck@uantwerpen.be |
| Dieter | Weber | Forschungszentrum Jülich | | Jülich | DE | d.weber@fz-juelich.de |
| Jun | Yuan | University of York | Physics | York | GB | jun.yuan@york.ac.uk |
| Xiaoyan | Zhong | Tsinghua University | | Beijing | CN | xyzhong@mail.tsinghua.edu.cn |
| Matthias | Zimmermann | Ulm University | | Ulm | DE | matthias.zimmermann@uni-ulm.de |

